Engineering Particles and Polymers to Improve Pulmonary Therapeutics

By

Christopher Andrew Arthur Kuehl

Submitted to the graduate degree program in Pharmaceutical Chemistry and the Graduate Faculty of the University of Kansas in partial fulfillment of the requirements for the degree of Doctor of Philosophy.

_____

Chairperson Dr. Cory Berkland

_____

Dr. Laird Forrest

_____

Dr. John Stobaugh

_____

Dr. Michael Wang

_____

Dr.Tom Prisinzano

Date Defended: August 5th, 2015

The Dissertation Committee for Christopher Andrew Arthur Kuehl

certifies that this is the approved version of the following dissertation:

Engineering Particles and Polymers to Improve Pulmonary Therapeutics

_____

Chairperson Cory Berkland

Date approved: August 5th, 2015

Acknowledgements

I would like to first express my deepest gratitude and sincerest appreciation to my advisor and mentor, Dr. Cory Berkland. Without his patience, understanding, guidance, and support, my time at KU would have gone very differently. He empowered me to approach challenges and analyze them critically; to take charge of my life and direct my own experiences. I appreciate all the conversations we had, both scientific and those that transcended science, as he taught me to apply what I constantly learned to all aspects of my life and future. Cory, thanks for all the time you have given me, and for showing me an example of what type of scientist and mentor I want to continuously strive to become.

I would like to thank my committee members: Dr. Laird Forrest, Dr. John Stobaugh, Dr. Michael Wang, and Dr. Tom Prisinzano. I appreciate all your helpful comments and suggestions as I progressed through my research. Without your guidance, my research and scientific development would not have progressed to allow me to be a critical scientist. I would also like to thank the other faculty members of the Pharmaceutical Chemistry department for numerous discussions, lectures, and meetings that contributed towards my increased understanding that provided me a necessary foundation of knowledge.

I would next like to thank all my colleagues and collaborators at the University of Kansas especially Dr. Teruna Siahaan, Dr. Nashwa El-Gendy, Dr. Joshua Sestak, Dr. Amir Fakhari, Dr. Parthiban Selvam, Dr. Jian Qian, Dr. Bradley Sullivan, Dr. Warangkana Pornputtapitak, Dr. Connor Dennis, Sharadvi Thati, Nabil Alhakamy, Laura Northrup, Brittany Hartwell, Lorena Antunez, Chad Pickens, Matt Christopher, Heather Shinogle, Dr. Prem Thapa, Dr. Justin Douglas, Dr. Todd Williams, Dr. Bob Drake, Dr. Ti Zhang, Dr. Qiuhong Yang, John Stewart, Dr. Jessica Bane, Dr. Justin Thomas, Dr. Barlas Buyuktimkin, Dr. Tamara Vasiljevic, Dr. Keith Anderson, Dr. John Haslem, Dr. Colleen Flynn, Dr. Michael McLeod, the Animal Care Unit, and Radiation Safety Services. I am incredibly grateful for your contributions, without which, who

knows how these projects would have ultimately turned out. I would like to acknowledge the staff of the Pharmaceutical Chemistry department including Nancy Helm, Nicole Brooks, and Karen Hall for all their assistance. I would like to thanks the staff of Higuchi Biosciences including Sandy Holland and Kathy Kiefer for all their help while I was on the Dynamic Aspects of Chemical Biology Training Grant. I would like to thank the Pharmaceutical Chemistry department and the Dynamic Aspects of Chemical Biology training grant especially Dr. Audrey Lamb and Dr. Paul Hanson for their generosity in funding, without which I would not have been able to achieve this research. Additionally, to all the other friends I have made in Lawrence especially those in Chemical Engineering, Medicinal Chemistry, and Molecular Biosciences as well as our basketball and softball crew, thanks for your friendship and making my time in Lawrence as fantastic as it has been.

To my mentors at previous institutions, including my high school teachers LeeAnn Steen and Diane Brudelie, thanks for nurturing my interest in science and putting me on my scientific path. To Dr. Chun Wang, Dr. David Odde, and Dr. Victor Barocas from the University of Minnesota, thanks for continuing my scientific growth and encouraging my pursuit of a scientific graduate degree. To Dr. Lisa Kaminskas and Dr. Chris Porter from Monash University, I appreciate your guidance and flexibility in allowing me to pursue an area that broadened my understanding. To my other Australia friends including Dr. Joseph Nicolazzo, Dr. Tri-Hung Nguyen, Dr. Gemma Ryan, Dr. Orlagh Feeney, Dr. Claire McEvoy, Dr. Erica Sloan, Dr. Hywel Williams, Victoria McLeod, and Matt Crum, thanks for making my experience in Melbourne unforgettable. To Dr. John Wang, Dr. Xanthe Lam, and Ada Hui at Genentech, I want to express my appreciation as their direction allowed me to expand my expertise and understanding. To my good friends, Nate Janssen, Taylor Nordstrom, and Jason Rosenberg, thanks for all your support and as you made me strive to continuously achieve.

Finally, and most importantly I would like to thank my family. To my parents, Ronald and Donna Kuehl, I could not have done this without your belief and support. Through all the years and trials, you had faith in me and continued to support me, even asking the tough questions. I know I was not always the easiest for you, but that makes me appreciate all your efforts that much more. To my sister, Sarah Kuehl, you have always employed a tough love approach and that has helped me in ways I cannot count. To my sister, Rebecca Kuehl-Hybbert, you constantly gave me an example to strive for. Thank you for all your early teaching as you provided me with so many gifts. To my brother-in-law, Adam Hybbert, you have provided silent encouragement and have been there to help me relax. To Cassie Sparks, you have made me reevaluate things and look at everything from a new perspective challenging me to be better and that means so much to me.

Table of Contents

Chapter 1: Introduction to Pulmonary Drug Delivery

1.1. Introduction
    1.1.1. Introduction to Pulmonary Drug Delivery
    1.1.2. Outline of Dissertation Chapters
1.2. Lung Physiology
    1.2.1. Lung Anatomy and Structure
    1.2.2. Lung Clearance Mechanisms
1.3. Advantages and Disadvantages of Pulmonary Delivery
1.4. Lung Drug Delivery Systems
1.5. Improving Local Lung Delivery
    1.5.1. Issues with Current Treatments
    1.5.2. Particle Engineering to Improve Local Pulmonary Deposition
1.6. Increasing Persistence of Pulmonary Therapies
    1.6.1. Drug Design
        1.6.1.1. Traditional Drugs and Progression to Current Molecules
    1.6.2. Other Approaches to Sustain Lung Delivery
1.7. Accessing Different Body Compartments from the Lungs
    1.7.1. Allergy Treatments and Antigen Specific Immunotherapy (ASIT) by Employing Pulmonary Drug Delivery
    1.7.2. Systemic Exposure After Pulmonary Delivery
    1.7.3. Lymphatic Exposure After Pulmonary Delivery
1.8. Pulmonary Delivery Needs

Chapter 2: NanoClusters Surface Area Allows Nanoparticle Dissolution with Microparticle Properties for Enhanced Lung Deposition

2.1. Introduction
2.2. Materials and Methods
    2.2.1. Materials
    2.2.2. NanoCluster Synthesis by Wet Milling
    2.2.3. NanoCluster Particle Size and Morphology
    2.2.4. Surface Area Determination Using BET.
    2.2.5. Determination of Degradation Using HPLC-UV
    2.2.6. NanoCluster Crystallinity Determination Using Powder X-ray Diffraction (PXRD)
    2.2.7. NanoCluster Analysis Using Differential Scanning Calorimetry (DSC)
    2.2.8. Dissolution of NanoCluster Dry Powder
2.3. Results and Discussion
    2.3.1. Wet Milling Created Nanoparticle Agglomerates
    2.3.2. Increase in Surface Area and Not a Change in Drug Properties Enhanced Dissolution
    2.3.3. NanoClusters Enhanced Dissolution Rate
2.4. Conclusion

Chapter 3: Hyaluronic Acid Molecular Weight Determines Lung Clearance and Biodistribution after Instillation

3.1. Introduction
3.2. Materials and Methods
    3.2.1. Materials
    3.2.2. Near Infrared Dye labeling of HA
    3.2.3. Radiolabeling of HA
    3.2.4. Sizing of HA
    3.2.5. Animals
    3.2.6. Intratracheal Instillation of HA
    3.2.7. Near Infrared Dye Ex Vivo Imaging
    3.2.8. Counting of Signal from Radiolabeled Tissue
    3.2.9. PK Analysis of Radiolabeled Tissue
3.3. Results

3.3.1. Size Characterization of HA
3.3.2. HA-Fluorescent Dye Conjugation Efficiency
3.3.3. Lung Distribution and Clearance of HA-IR Dye Conjugates
3.3.4. Radiolabeled HA Physiochemical Properties
3.3.5. Distribution and Clearance of HA-^{125}I Conjugates
3.4. Discussion
3.4.1. Characterization of HA and Labeled HA
3.4.2. Current Pulmonary HA Studies
3.4.3. Distribution and Clearance of Labeled HA
3.4.4. Lymphatic Transport of HA
3.5. Conclusion

Chapter 4: Using Soluble Antigen Arrays (SAgAs) for Immune Modulation after Pulmonary Administration
4.1. Introduction
4.2. Materials and Methods
4.2.1. Materials
4.2.2. Soluble Antigen Array (SAgA) Synthesis
4.2.3. Animals
4.2.4. Induction of Experimental Autoimmune Encephalomyelitis (EAE) and Time Course of Study
4.2.5. Treatment Schedule and Pulmonary Instillation of Compounds
4.3. Results
4.3.1. Characterization of SAgAs
4.3.2. Co-Delivery of Peptides via SAgAs Offers Improved Therapeutic Efficacy
4.4. Discussion
4.4.1. The Lungs and Immune Tolerance
4.4.2. Potential Licensing of Immune Cells in the Lungs for Immune Tolerance
4.4.3. Potential Immune Modulation Mechanism for SAgAs
4.5. Conclusion

Chapter 5: Conclusions and Future Directions
5.1. Conclusions and Future Directions
5.1.1. Potential Opportunities for Pulmonary Drug Delivery Challenges
5.1.2. Outline of Dissertation Chapters and Conclusions
5.1.3. Future Directions of Dissertation Chapters

Abstract

Pulmonary drug delivery has been an underutilized delivery space. Classically, pulmonary delivery has been employed for local delivery of small molecules for lung-centric respiratory diseases. The most typical example has been the application of corticosteroids as a treatment for asthma. There are multiple issues with this approach primarily focused on delivery as current formulations do not achieve a high amount of deposition into the lungs, which is countered by increased dose. To counter this, particle engineering strategies have been employed to improve delivery. By engineering our nanoparticle agglomerates, called NanoClusters, we have achieved increased deposition into the lungs. Corticosteroids are poorly water soluble and as such, dissolve slowly. There are lung clearance mechanisms that can clear these engineered NanoClusters before they dissolve, so the dissolution was assessed. It was observed that NanoClusters had enhanced dissolution making them an optimal system for lung delivery.

The lungs can be employed for regional and systemic delivery and not just local. The next study focused on delivery of a polymer, hyaluronic acid (HA) into the lungs. HA of different molecular weights was labeled, either fluorescently or with a radiolabel, and administered to mice. Labeled HA was tracked throughout the organs to determine the biodistribution of the polymer according to molecular weight along with determination of the pharmacokinetic parameters. The optimal size was determined to be between 67 and 215 kDa for HA to achieve increased persistence in the lungs. The lungs can be involved in the immune system as well in terms of systemic delivery. Recent research has shown that the lungs may contribute to profile switching in immune cells leading to different responses. By employing antigen presentation in a soluble antigen array for autoimmune diseases, there can be increased efficacy towards generating immune tolerance. By co-delivering two different antigens to the lungs, there is amelioration of the mouse model of multiple sclerosis suggesting the lungs may be a delivery space with increased possibilities in the future.

Chapter 1:

Introduction to Pulmonary Drug Delivery

1.1. Introduction

1.1.1. Introduction to Pulmonary Drug Delivery

Traditional pulmonary therapies have centered on inhalation of small molecules for local treatment of lung diseases. Multiple diseases including asthma, COPD, tuberculosis, and cystic fibrosis have classically been treated by simple small molecule formulations[1]. Newer treatments have focused on improving inhaled drug aerosols or designing molecules with improved efficacy or duration of effect[2]. For example, particle engineering has been employed to increase deposition into the lungs or to create advanced release profiles[3,4]. Medicinal chemistry has been implemented to develop new molecules with increased duration as a result of improved receptor binding affinity and persistence in lung tissue after inhalation. Even with continued development, there are still many challenges that remain in pulmonary drug delivery including poor patient outcomes and short duration of effect that will be described in further detail later in this chapter. These challenges present opportunities to provide increased efficacy, faster onset, longer duration, and fewer side effects by improving pulmonary drug delivery systems[5-8].

While traditional therapies for lung diseases continue to benefit from improvements in performance of inhaled medicines, the lungs are now being pursued for systemic drug delivery or for delivery to pulmonary lymphatics. Inhaled insulin was approved for delivery into the lungs with the target of systemic distribution and fast acting medicines for migraines and seizures are near approval[9]. There are some challenges with pulmonary delivery including proper administration and consistent dosing, but the lungs offer a novel administration route for compounds that are potentially challenging to deliver by other means or those that require rapid onset[9-11]. Also, lymph nodes that drain the lungs may facilitate access to immune cells and could allow localized immune modulation after inhalation of immunotherapies or antigens[12]. Thus, this dissertation investigates approaches to improve delivery of drugs to the lungs by engineering particles and polymers as drug carriers.

1.1.2. Outline of Dissertation Chapters

After an introduction to lung physiology, diseases, and treatments in Chapter 1, Chapter 2 investigated engineered drug particles designed to facilitate aerosolization and speed dissolution. Many of the small molecule drugs used in inhaled medicines are poorly water soluble, and there existed the potential for lung clearance mechanisms to remove the particles before they dissolve and produce an effect[13-26]. In addition, applications such as asthma rescue inhalers, may benefit from rapid onset[1,2]. The particle engineering strategy utilized here employs wet milling to create micron size particles comprised of nanoparticle agglomerates called NanoClusters. This chapter explored the characterization of the NanoClusters and assessed the dissolution of two poorly water soluble compounds that have been developed into NanoClusters[24-26]. Finally, this chapter utilized modeling to explain the dissolution phenomenon that was observed.

Chapter 3 focused on the biodistribution and pharmacokinetics of a polymer drug carrier hyaluronic acid (HA). HA has multiple available sites for chemical modification, is available in a wide range of molecular weights, and is naturally occurring[29-40]. HA has been investigated in multiple other administration routes (intravenous, subcutaneous, intralymph nodal) to determine its pharmacokinetics[30,39-49] and is beginning to gain acceptance in nebulized formulations to improve tolerance of the therapy[50-55]. By better understanding the distribution of HA based on molecular weight once it enters the lungs, formulations can be modified to have increased persistence or other desirable properties. This chapter explored the distribution of 5 molecular weights of HA (7, 30, 67, 215, and 741 kDa) labeled with either a fluorescent or radiolabel. HA distribution in major organs was assessed and pharmacokinetic parameters were calculated to correlate HA molecular weight with absorption, distribution, and elimination.

Chapter 4 explored HA as a carrier of peptides delivered into the lungs to treat experimental autoimmune encephalomyelitis (EAE). EAE is the mouse model of multiple

sclerosis, an autoimmune disease where immune cells attack the myelin sheath[55,56]. Strategies such as antigen specific immunotherapy have been developed to induce tolerance to foreign antigens (e.g. 'allergy shots')[57,58], but this chapter aimed to induce tolerance to myelin self-antigens[59-61]. The lungs have recently been highlighted as an important organ in the immune system, affecting the activation and trafficking of immune cells[62-67]. Thus, this chapter seeks to combine the ability to induce immune tolerance employing soluble antigen arrays (SAgA) that use HA to co-deliver a myelin antigen epitope and a peptide inhibiter of immune cell adhesion to the lungs[55,56]. Clinical disease was assessed in EAE mice treated with SAgAs compared to positive and negative controls. Finally, the dissertation concluded with some recommendations for future work and emerging opportunities in the field of pulmonary medicine.

1.2. Lung Physiology

1.2.1. Lung Anatomy and Structure

The lung is comprised of continually branching generations of airways ranging from 17 to 23 generations depending on physiological location starting with the trachea then proceeding into bronchi then bronchioles before terminating in alveoli. The trachea and initial bronchi have supporting cartilage in the form of rings to provide increased structural support. The bronchi are approximately 4 to 5 mm in diameter leading into the more terminal bronchioles diameter of approximately 1 mm, and finally, terminating in the alveoli that are 250 μm in diameter. The conducting portion of the lung consists of the uppermost airways that warm and moisten the air before it enters the respiratory bronchioles and the alveoli where gas exchange occurs typically in airway generations 20 to 23. The airways are comprised of an inner layer of epithelium surrounded by smooth muscle. The epithelium is covered in a mucus layer that is swept into the esophagus by cilia in the conducting airways. A thin layer of surfactant maintains the proper

surface tension for air exchange in the alveoli where macrophages patrol to remove any detrimental particles that are deposited in the deep lung. Figure 1.1 shows the tissue composition of the lung and how the different tissue layers transition in the lung. The airways also consist of a basement membrane that is composed of extracellular matrix as an attachment for the epithelial cells and is not a biological membrane[68,69]. The epithelial cells differ depending on their position in the lung. In the bronchi, the epithelial cells are approximately 60 μm in depth with up to 10 μm of mucous above the epithelial cells. In the next set of airways, the bronchioles, the epithelial cells are only 10 μm with 3 μm of solution terminating in the alveoli epithelial cells of only 0.1 μm with just 0.05 μm of solution[9].

Another important aspect of the lung is the different relationships it has with the other organ systems. The major intersection is with the cardiovascular system as gas exchange occurs in the lungs as red blood cells squeeze through the capillaries surrounding the terminal bronchioles and alveoli. The closeness of the cardiovascular system and the narrow barriers between the two allow for systemic delivery to occur. The other major organ system associated with the lungs is the lymphatic network in the upper thoracic cavity including the nodes around the alveoli[68,69]. As seen in Figure 1.8, lymph nodes form a network around the alveoli. The lymph nodes are adjacent to the terminal bronchioles with lymph vessels or capillaries wrapping around the alveoli. The lymph vessels can take macrophages that have exited the lungs and transport them to the lymph nodes to present encountered antigens to different immune cells[70].

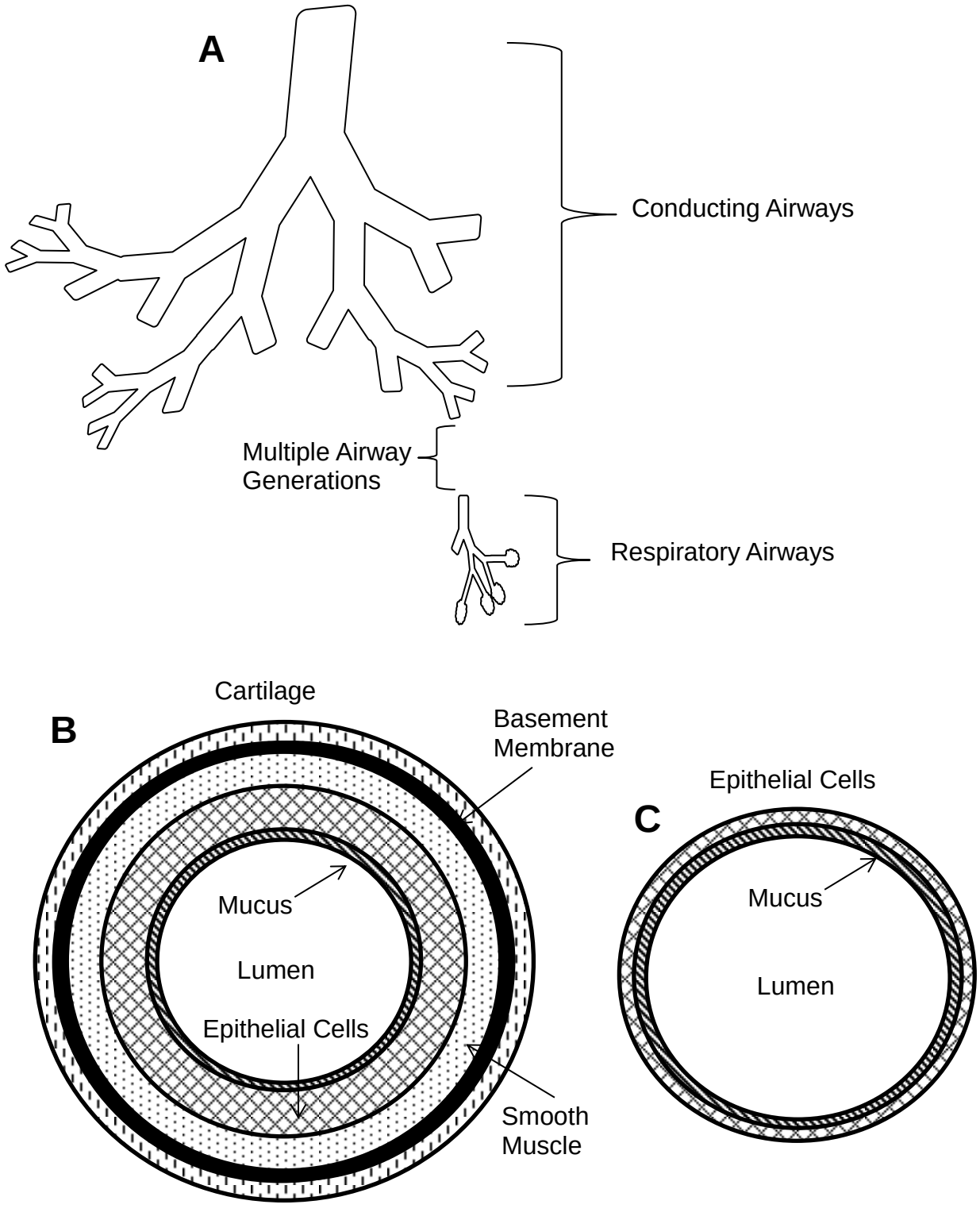

Figure 1.1: Tissue composition of the lungs and airways. Panel A depicts the branching and bifurcations that comprise the lungs down to the alveoli. Panel B shows the tissue composition in the upper airways (from the outside in – cartilage, basement membrane, smooth muscle, eptithelial cells, mucus, lumen), while Panel C shows the lower airways (eptithelial cells, mucus, lumen).

1.2.2. Lung Clearance Mechanisms

The lungs eliminate materials using active transport processes including mucociliary and macrophage clearance, as well as passive diffusion to the bloodstream or lymph. Mucociliary clearance occurs in the upper airways as ciliated cells sweep mucus up the trachea and into the oropharyngeal cavity, where it is typically swallowed. Residence time in the upper airways, therefore, would depend on the distance from the site of deposition to the oropharyngeal cavity. The rate of mucociliary clearance can also depend on viscosity. Slower and/or incomplete clearance of thick mucus is observed clinically, while expectorants facilitate mucus clearance. Further down the airways, macrophages can recognize molecules or particles in the conducting airways (terminal bronchioles and alveoli) below the mucociliary elevator. Macrophages that have bound or phagocytosed foreign particles can then actively transport to the lymphatics draining the pulmonary bed. Finally, compounds can dissolve into the fluid layer lining the lung epithelium and then absorb into the bloodstream. Systemic absorption is typically fastest in the alveolar region, where the tissue barriers are as thin as a few hundred nanometers. Passive diffusion can also provide access into the lymphatic network draining the lungs as a possible clearance mechanism depending on the particle or molecular size[9,69].

In terms of achieving systemic delivery from the lungs, there are several challenges that must first be overcome. The first issue is that there are several layers of physiological barriers after a therapy has been delivered to the lung. Mucus presents a surface gel phase and underlying sol phase. A compound must dissolve and diffuse through the mucus (or lung surfactant in the alveolar region), then partition into and across the cell layer, before ultimately diffusing into the systemic circulation through the capillary bed. These multiple barriers can maintain therapies in the lungs to achieve a high local concentration to increase therapeutic efficacy in the lungs. These barriers compete with the multiple clearance mechanisms

mentioned above, which can remove these treatments from the lungs before they have a chance to provide efficacy[9-11].

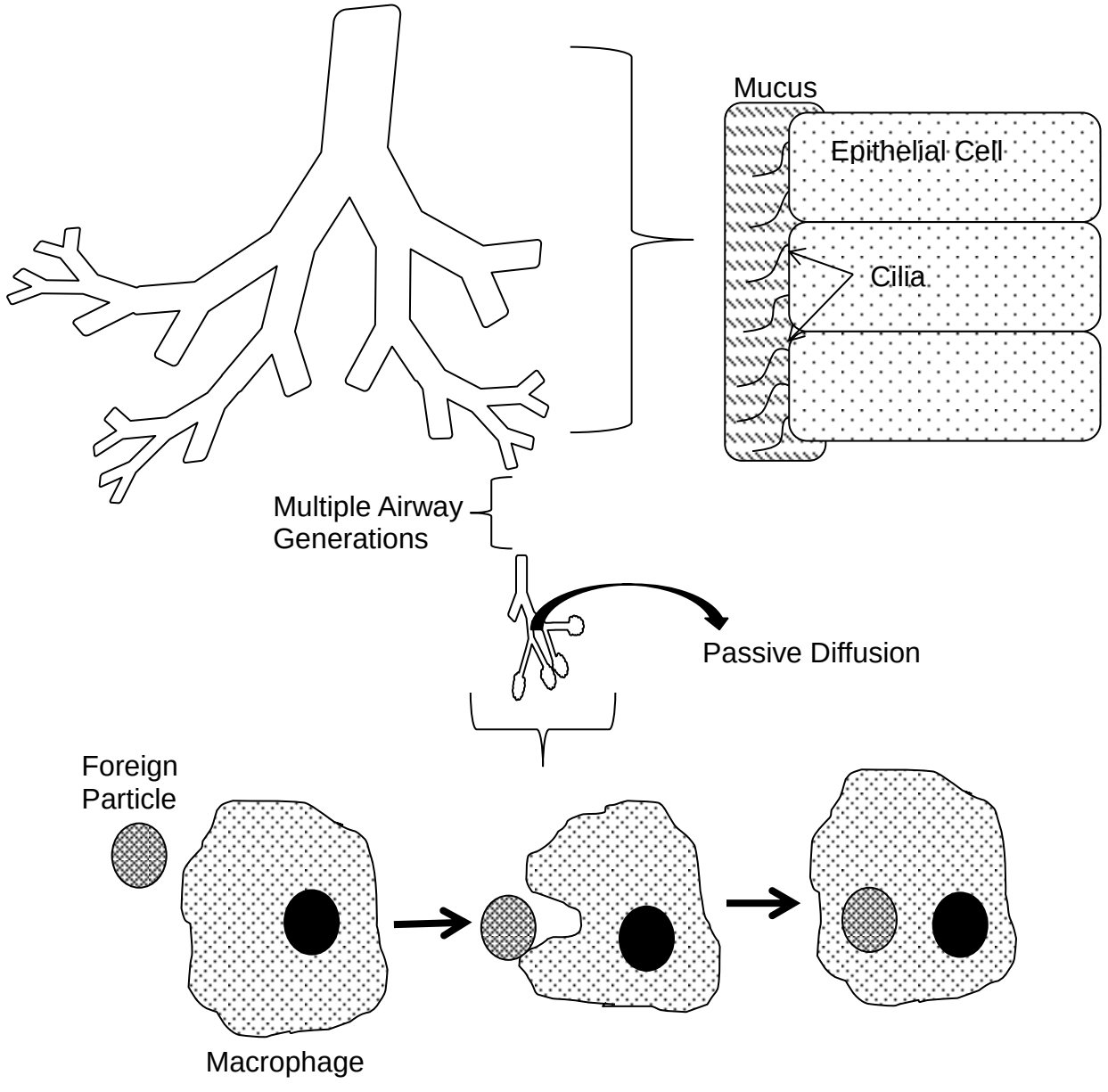

Figure 1.3: Lung clearance mechanisms based on position in the lungs. Mucociliary clearance occurs in the upper airways, where ciliated epithelial cells propel mucus from the airways into the oropharynx to be swallowed. Macrophage uptake occurs in the lower airways and alveolar region as does an increased portion of passive diffusion, which can occur in the upper airways but to a lesser degree.

1.3. Advantages and Disadvantages of Pulmonary Delivery

There are several advantages to pulmonary delivery of therapies that have made it an enticing administration route. As discussed above, the lungs provide a large and accessible target for local delivery of therapies. Molecules have been designed to persist in the lungs or undergo rapid metabolism if absorbed systemically, which is an attractive approach to improve drug safety and efficacy. The lungs possess up to 140 m^2 of accessible surface area for absorption of compounds and ample blood supply, which provides an attractive portal for systemic drug delivery. Delivery to the lungs helps to circumvent one potential major issue with systemic therapies, as pulmonary delivery avoids first pass metabolism that occurs in the liver, which can remove much of the active compound from the body[71,72]. The lungs have a low level of enzymatic activity, mainly phosphodiesterase activity, especially compared to that in the liver during systemic administration (Table 1.1)[69].

There are some potential disadvantages with pulmonary drug delivery that have hampered this area, which require continued improvement and research. There is the challenge of the conditions of the respiratory system specifically the increased humidity, which can alter the aerosol performance of the formulation, and amplify the challenge of maneuvering through the airways to reach the deep lung. Most marketed formulations suffer from extremely poor delivery largely due to the particle or droplet size of the aerosolized dose, which can be manipulated using different synthesis strategies and devices. Only approximately 20 – 30% of current formulations typically reach the lungs and most is deposited into the oropharynx and upper conducting airways. Particles larger than 5 um tend to deposit into the oropharynx and upper airways, while particles smaller than 1 um tend to be exhaled. Poor and inconsistent delivery is one possible explanation for inadequate control of diseases such as in asthma, where up to 50% of patients have poorly controlled symptoms. Due to the various different delivery systems available, each one requires a different breathing profile. These different

profiles can be challenging for patients, leading to incorrect use and reduced efficacy of the therapy (Table 1.1)[71,72].

Table 1.1: Advantages and disadvantages of pulmonary drug delivery.

Advantages	***Disadvantages***
Large surface area	Different breathing profiles needed for different delivery systems
Avoids first pass metabolism	Low delivery efficiency of devices
Thin physiological barrier for systemic delivery	Multiple tissue barriers to prevent systemic exposure of local therapies

1.4. Lung Drug Delivery Systems

There are three major drug delivery systems for inhalations products: nebulizers, pressurized metered dose inhalers (pMDI), and dry powder inhalers (DPI)[73]. Nebulizers utilize a liquid formulation that is dispersed by gas or sonic waves. Nebulizers have advantages of typically being easy to use by utilizing only normal tidal breathing, can be adapted for high and low doses, and may be used to deliver combination therapies (Table 1.2). Nebulizer disadvantages include a lack of portability, typically needing longer treatment times of approximately 10 to 20 minutes, and do not efficiently aerosolize formulations, although recent advances in vibrating mesh nebulizers are improving efficiency[73-77]. pMDIs act by utilizing a propellant to aerosolize a dose from a liquid drug reservoir, which is then inhaled by the patient. The advantages of pMDIs include a short treatment duration, small containers so they are portable, no drug preparation is necessary, and dose reproducibility is high. The disadvantages

of pMDIs include coordination of breathing and actuation necessary for delivery, which may lead to improper use, upper limits for dose, insufficient means to track the amount of dose left in reservoir, and high oropharynx deposition when using a pMDI without a spacer. Besides these drawbacks, the propellants initially used were chlorofluorocarbons (CFCs), which due to their depletion of ozone, have been switched to hydrofluoroalkanes (HFAs). HFAs have different properties necessitating reformulation, and even now HFAs are being phased out in Europe[73,78-84]. DPIs work differently from pMDI and nebulizers, delivering a dry powder aerosol that utilizes the patient's breathing to disperse and deliver the formulation. DPI advantages are that they are small and easy to use with breathe actuation devices, portable, do not require spacers, offer short treatment duration, and have many different device forms (single and multiple doses). The disadvantages of DPI include requiring a high inspiratory flow rate, typically high deposition in the oropharynx, and not all formulations have been developed to be dry powders (Table 1.2)[73,85-92].

Table 1.2: Discussion of different pulmonary drug delivery systems and their potential advantages and disadvantages.

Delivery System	***Advantages***	***Disadvantages***
DPI	1. No propellants 2. Dose counters 3. Multiple device forms	1. Can have high oropharynx deposition 2. High flow rate required
pMDI	1. Short treatment time 2. High dose-dose reproducibility	1. Needs breath coordination 2. Need spacer for optimal delivery
Nebulizer	1. Easy to use 2. Dose modifications	1. Time consuming treatment and not portable 2. Poor aerosolization of suspensions

1.5. Improving Local Lung Delivery

1.5.1. Issues with Current Treatments

The development of inhaled treatments has focused on two areas: device and formulation design. In terms of device design, DPIs have gained increased prevalence due to the more desirable properties discussed above; however, DPIs are difficult for children to use as high inspiratory flow rates are required to achieve optimum delivery efficiencies. For example, only approximately 20% of an inhaled steroid dose is delivered into the lungs (Figure 1.4). The remaining 80% is deposited in the mouth and oropharynx, where it is swallowed and enters systemic circulation. Many steroid drugs have been selected because of their high first pass metabolism, which removes them from systemic circulation leaving only 1-10% of active ingredient in the blood. Chronic use may elicit unwanted side effects, however, which can be a particular issue in children as systemic exposure of steroids has been linked to issues in bone development[93].

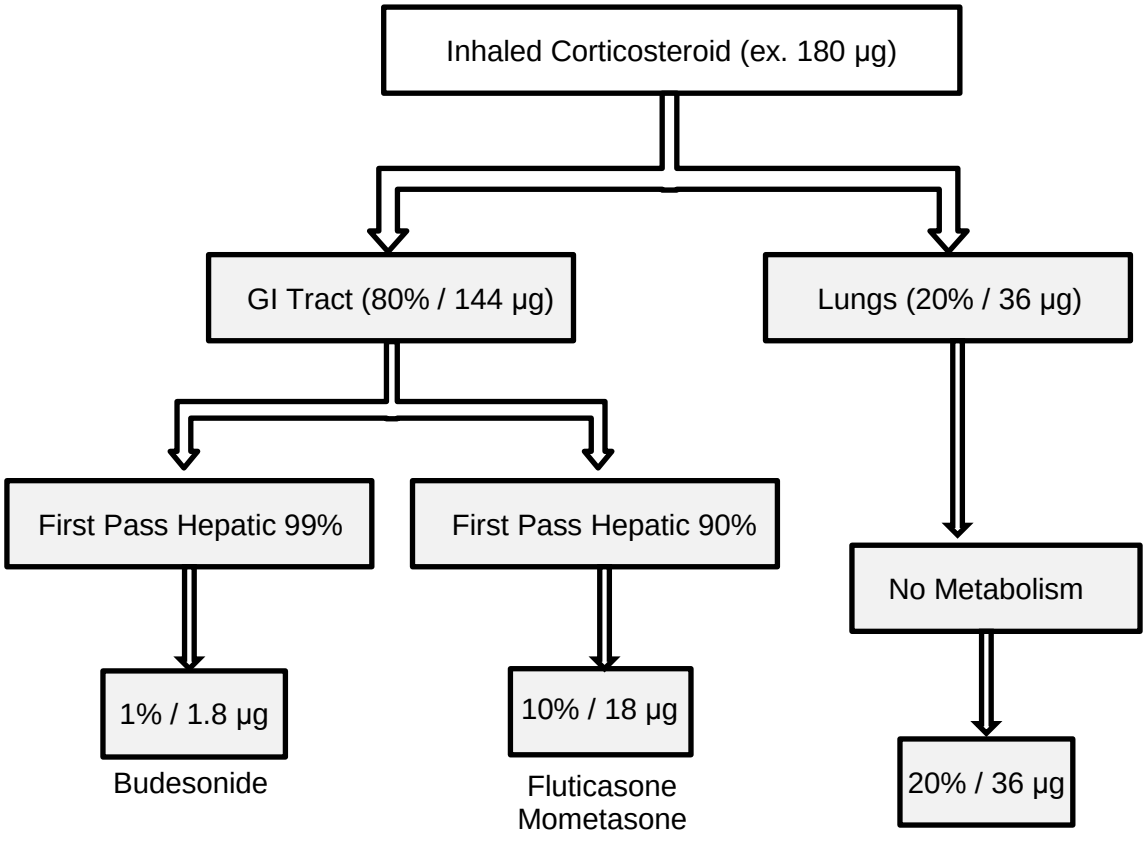

Figure 1.4: Deposition of corticosteroids from inhaled devices. A majority enters the GI tract and a small percentage accesses the lungs to elicit therapeutic effect.

There is the complicating factor of poor patient compliance in many of these inhaled therapies. Previous therapies have required multiple doses, between 2-4 doses, to be taken a day for control therapies to maintain symptom control. When patients skip treatments, they can fall out of the therapeutic window. Also, some asthma types do not respond to steroids and up to 50% of patients have poorly controlled asthma symptoms by just steroids[94-96].

The other issue with current inhaled therapies focuses on the challenge of formulation. The first line treatment of therapies for local lung diseases such as asthma is corticosteroids. Corticosteroids are processed into micron sized particles, which are subsequently blended with lactose carrier particles so the corticosteroids are physically associated on the surface of the

lactose (Figure 1.5). A high inspiratory flow rate is needed to achieve enough shear to separate the drug particles from the carrier lactose so the drug particles can follow the air flow for deposition into the lungs, while the much larger lactose particles deposit in the mouth and throat and are swallowed[97-99]. DPIs are fundamentally different in their formulation when compared to pMDIs and nebulizers as both of these are wet formulations, delivering drugs in droplets. Today, many therapies are combination therapies to achieve 24 hour duration or a once daily formulation. There are new challenges of co-formulating multiple drugs and improving deposition (Table 1.3)[3,73].

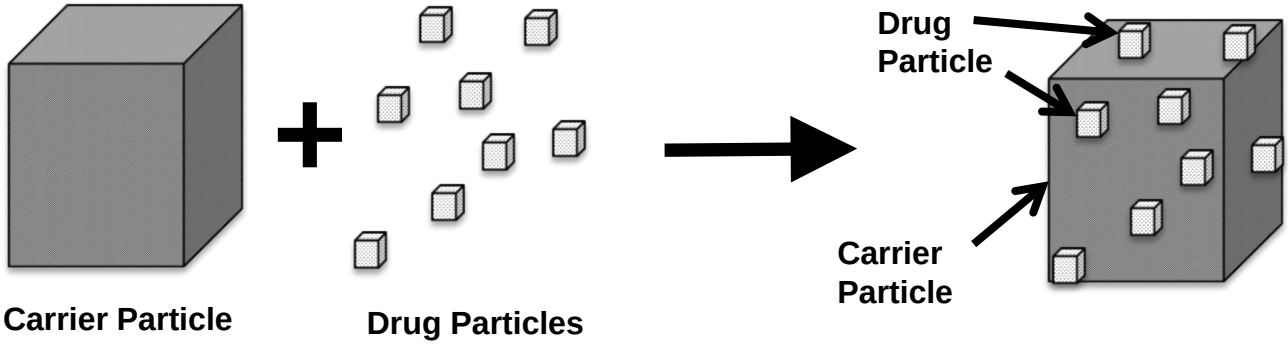

Figure 1.5: Current inhalation formulation strategy comprised of large carrier particles (typically lactose >10 µm and typically >50 µm) and blended with smaller drug particles (~1-5 µm).

Table 1.3: Current marketed therapies for local treatment of lung inflammatory diseases (asthma and COPD) including their active compound and indication.

Product	***Active Ingredients***	***Indication***	***Description***
Symbicort	Budesonide and Formoterol	Asthma and COPD – control	Combination therapy
Advair	Fluticasone and Salmeterol	Asthma and COPD – control	Combination therapy for years 4+
Dulera	Mometasone and Formoterol	Asthma – control	Combination therapy
Breo Ellipta	Fluticasone and Vilanterol	Asthma and COPD - control	Once daily combination therapy
Pulmicort	Budesonide	Asthma – control	Corticosteroid only formulation
Flovent	Fluticasone	Asthma – control	Corticosteroid only formulation for years 4+
Singulair	Montelukast	Asthma – Control	Treats exercise induced constriction
Xolair	Omalizumab	Asthma (allergic) – control	Effective treatment for allergic asthma subset and 2-4 week duration

1.5.2. Particle Engineering to Improve Local Pulmonary Deposition

Several particle engineering strategies have been employed to control deposition into the lung as well as alternative sustained release approaches to increase lung exposure and persistence or to target a specific area of the lung. Particle engineering strategies have employed multiple techniques to achieve the different morphologies that provide particles with their improved properties including spray drying, spray freeze drying, emulsification, supercritical precipitation, as well as traditional micronization and blending (Figure 1.6)[3,4].

Spray drying involves atomizing the solution into a spray followed by drying and separation of the dried product. Each of these steps can have different operating parameters

creating different particle morphologies. Spray drying can produce particles that are amorphous and the process is fairly straightforward and simple, but degradation can occur due to the heat used in the process. For example, spray drying has been of interest for biomolecules but can lead to protein denaturation or aggregation for degradation. Spray drying has been employed as PulmiSphere™ technology to create low density hollow particles. Spray drying has also been employed to form aggregates of crystalline drug with amorphous excipients. Finally, spray drying has been utilized for sustained release as different polymers have been sprayed creating different properties in the particles. Spray freeze drying has also been used to create amorphous or crystalline particles and this approach can be used for compounds that are more heat sensitive to reduce degradation. Spray freeze drying can modulate the morphology of the particles in a manner that is similar, but more expensive than spray drying.

Emulsions can be used to precipitate solid composite particles with a narrow size distribution that can be utilized for controlled release micro- and nanoparticle suspensions. Emulsions have traditionally been employed for biodegradable PLGA particles with double and triple phases of oil and water, but it can be difficult to scale up and remove residual solvents. The phases can be adjusted to create different particle morphologies. Similarly, precipitation into supercritical antisolvent can create crystalline particles that are typically stable and non-cohesive but control of the particle size can be difficult[3,4].

Micronization of drug and blending with excipient 'carrier' particles (e.g. lactose) is a proven industry standard to deal with drug crystals that are cohesive and have poor flowability due to electrostatic forces. Micronization is conducted by milling (dry, wet, jet) and has produced a majority of the marketed inhaled products. It can be employed for small molecules and has been adapted for some biomolecules, but since it is a grinding technique, it is less adaptable for more complex particle engineering structures including porous particles or composites[25,26].

All of these particle engineering methods plus other methods allow for many different particle morphologies and compositions to be created. There are large porous particles, aggregates, rods, fibers, solid particles and combinations of these that aim to facilitate particle access to the lungs. One disadvantage is that many of particle engineering strategies were first employed for oral dosage forms and the solvents and excipients to create some of these interesting morphologies have not been tested for their pulmonary safety (Figure 1.6)[3,4].

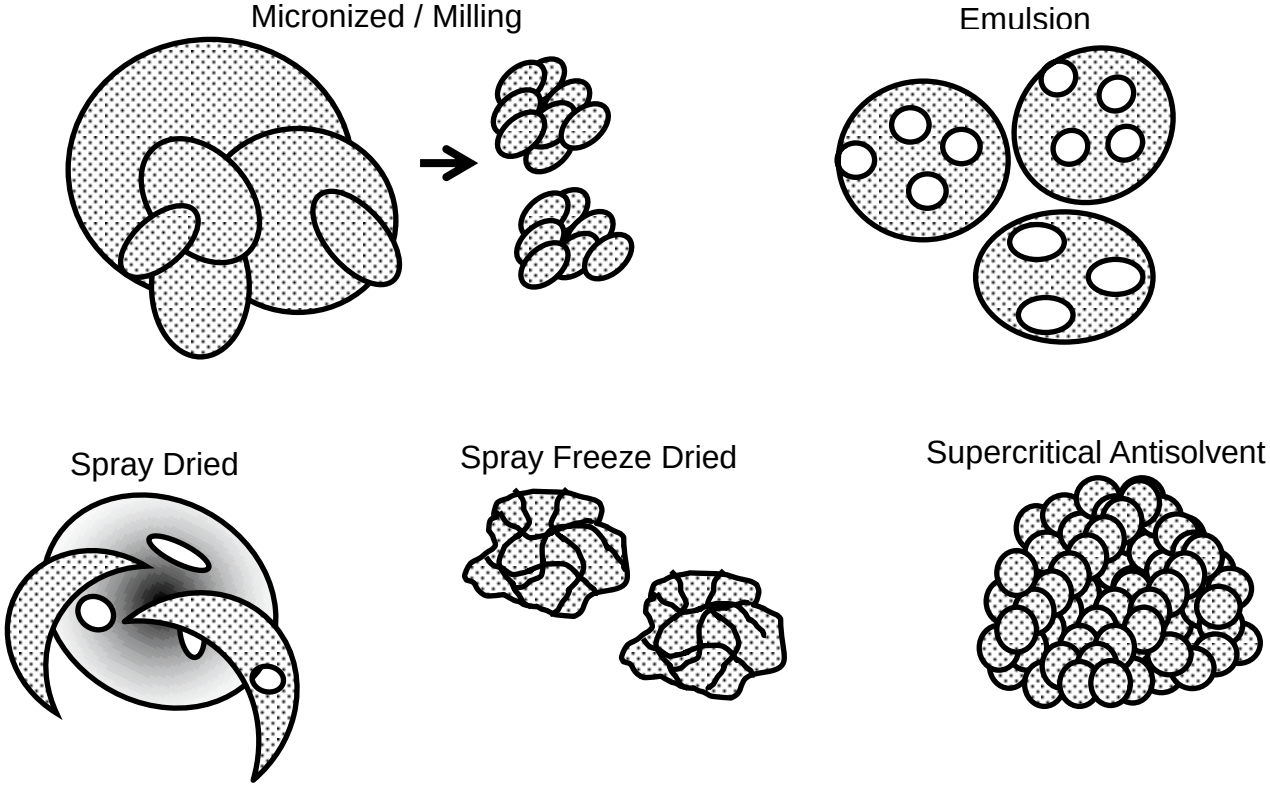

Figure 1.6: Particles created by different particle engineering techniques generating different particle morphologies. Micronizing can produce smaller particles; emulsion can create hollow spherical particles; spray dried can generate large porous and irregularly shaped particles; spray freeze dried can produce dried raisin particles; supercritical antisolvent can generate large agglomerates of small partcles.

Many of the particle engineering techniques have focused on increasing the aerodynamic properties of the particles, while decreasing the density of the particles. The typical method introduces porosity into the starting solid particles either by making hollow

particles or irregular surfaces[3,4]. An alternative approach is to utilize the small drug particles as building blocks to generate larger, low density particles. NanoClusters are a composition particle made by agglomerating solid nanoparticles into microparticles (Figure 1.7)[25,26]. These particles have void spaces present, which allow them to act smaller aerodynamically. NanoClusters can increase delivery into the lungs without carrier particles (Figure 1.5), while minimizing delivery to the GI tract by swallowing as seen with current formulations (Figure 1.6). This dissertation explores the advantages of NanoClusters for rapidly dissolving steroid formulations (Chapter 2).

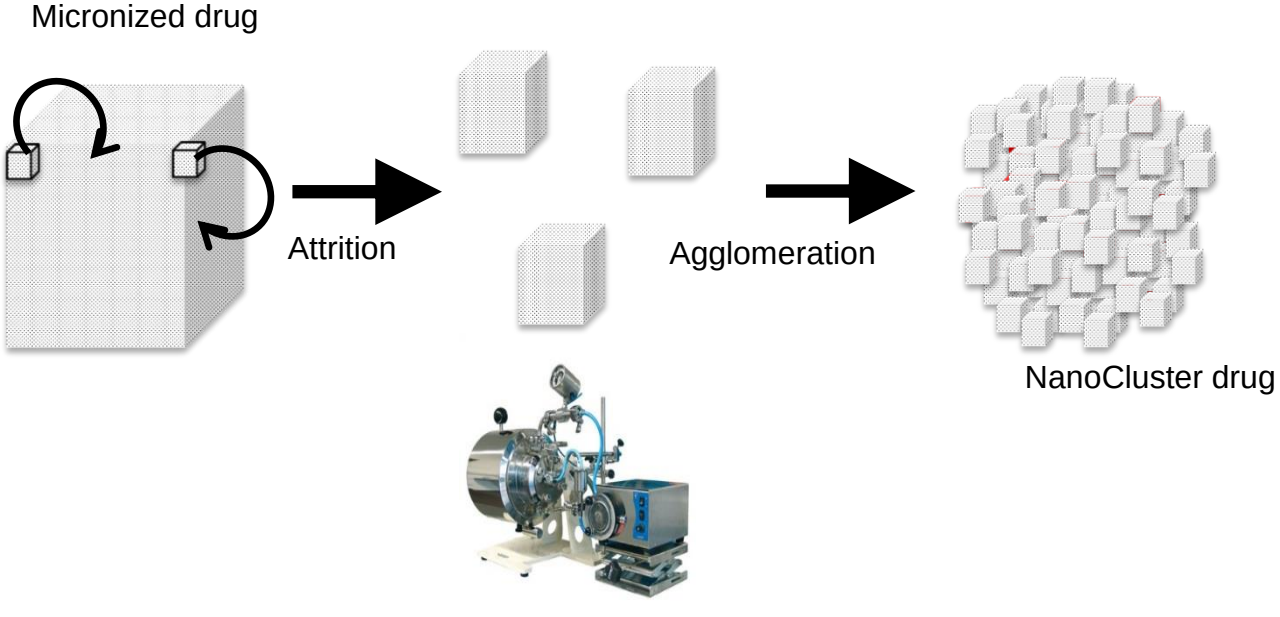

Figure 1.7: Synthesis and composition of NanoClusters. Large particles are reduced in size to nanoparticles and agglomerate to produce excipient free microparticles.

1.6. Increasing Persistence of Pulmonary Therapies

1.6.1. Drug Design

The NanoCluster formulations explored in this dissertation have the potential to enable rapid onset. On the other hand, many current inhaled therapies have a limited duration of effect requiring multiple doses per day. The requirement of frequent dosing can discourage patient compliance, which can lead to poor patient outcomes[95,96]. To counter this trend, there has been a drive for once-daily therapies, and to achieve this, chemistry has been utilized primarily focusing on three particular drug classes: corticosteroids[11], muscarinic antagonists[5], and beta-2 agonists[6,7]. In this section, medicinal chemistry approaches to prolong the effect of inhaled drugs then transitions to current physical chemistry approaches, motivating the exploration of hyaluronic acid delivery to the lungs explored in this dissertation (Chapter 3).

Medicinal chemistry approaches for inhalation have focused on some common molecular motifs adapted from oral compounds. Lipinski's, Gleeson's, and Waring's rules are based on molecular weight, hydrophobicity, and heteroatoms related to hydrogen bond donors and acceptors. By looking at these molecular properties, there is a certain desirable range of characteristics to achieve optimal oral delivery of the molecule. By comparison, approved inhaled therapies exhibit a slightly higher molecular weight and are less hydrophobic, although this data is thought to be skewed since a large number of inhaled drugs are thought to be a by-product of selection bias toward traditional oral compounds. These design criteria have been extrapolated to create more effective and persistent compounds for inhaled therapy[100-104].

1.6.1.1. Traditional Drugs and Progression to Current Molecules

Corticosteroids including budesonide, mometasone, and fluticasone, have been the standard treatment option for asthma to locally reduce inflammation in the airways. Steroids are able to enter the cells in the airways as they have high lipophilic character and can permeate

the cell membrane. Corticosteroids, once in the cell, bind to the glucocorticoid receptor present on the nucleus, which is then taken into nucleus. The internalized receptor-ligand complex binds upstream of the target genes and modifies protein transcription and reduces inflammatory gene expression and increases anti-inflammatory gene transcription. Steroids typically act on the epithelial cells reducing inflammation and hyperresponsiveness though they do little in terms of treating the underlying condition. Since inflammation and hyperresponsiveness are hallmarks of both asthma and COPD, corticosteroids are effective treatments for both diseases[105,106].

Beta-2 agonists (BA) have been utilized since the 1960s with the first use of albuterol. BAs act as bronchodilators as they stimulate β2 receptors in the smooth muscle layer of the airways. As BAs bind with the receptors, adenylyl cyclase becomes activated through stimulatory G protein. The activated G protein causes an increase in cAMP levels leading to bronchodilation[6,107].

BAs have been developed now into 3 different categories: short acting BAs (SABAs), long acting (LABAs), and ultra-long acting (ULABAs). SABAs including albuterol were the first generation of BAs that were developed in the 1960s typically working 3 to 4 hours but potentially working up to 6 hours. Due to their physicochemical properties and binding ability, they have a quick onset of activity typically on the order of 5 minutes. They are more effective for treating asthma brought on by exercise, cold air, and allergens. LABAs such as formoterol and salmeterol are the second generation and typically have 12 hour duration. LABAs have an increased binding constant compared to SABAs combined with a decreased dissociation constant, which is a reason for their improved efficacy and longer duration. In addition, to the improved binding, their physicochemical properties are such that they can form a depot in the cell membrane allowing the drug to diffuse continuously to the receptor further increasing its duration of effect. Formoterol has similar onset to albuterol, while salmeterol has a slightly longer onset time of approximately 30 minutes. LABAs have been continually refined for

increased efficacy and duration leading to ultra long acting BAs such as indacaterol and vilanterol. These ULABAs have duration of 24 hours again due to increased binding affinity between the drug and the beta 2 receptor[6,108-111].

Table 1.3: Progression of β2 agonists from short acting to long acting to ultra-long acting and their associated chemical structure.

Name	***Classification***	***Chemical Structure***
Albuterol	Short acting	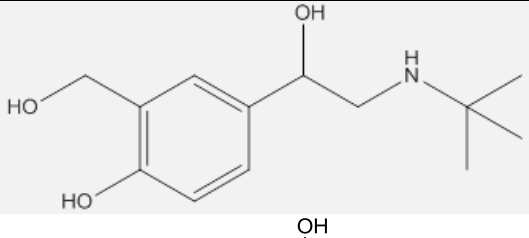
Epinephrine	Short acting	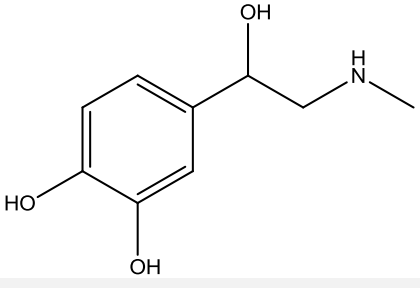
Formoterol	Long acting	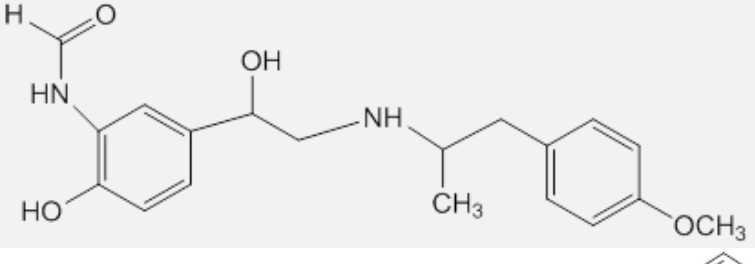
Salmeterol	Long acting	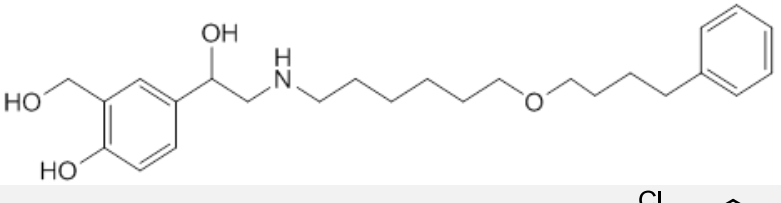
Vilanterol	Ultra long acting	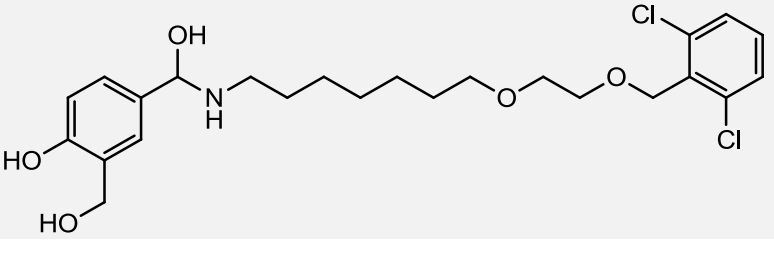

Carmoterol	Ultra long acting	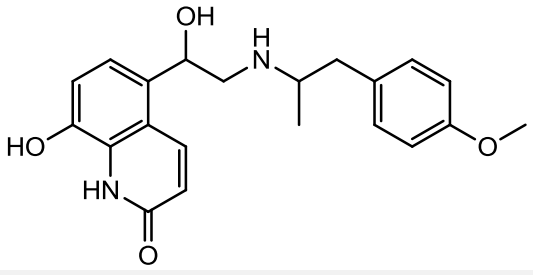
Indacaterol	Ultra long acting	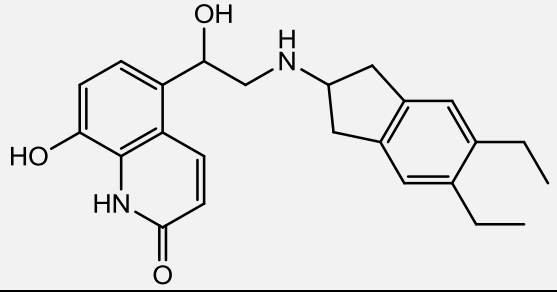

There are some common motifs found throughout BAs. The design criteria included in newer generations in development includes the use of benzylic hydroxyl groups to improve potency, intrinsic activity, and selectivity. The next criteria for rational design included the use of another basic motif in the chain, which increased plasma half-life. Half-life was continually refined by altering lipophilicity to achieve high plasma half-life that corresponded to high lung half-life. The progression of BAs has followed the molecular design rules by increasing in molecular weight and increasing the number of heteroatoms, oxygen and nitrogen, to decrease lipophilicity[3,110]. There have been further structure elucidations to improve delivery including the addition of sulfonamide headgroups[112,113] or building off of procaterol by utilizing the carbostyril skeleton[114].

Table 1.4: Some common molecular motifs in β2 agonists that elicit therapeutic effect and their associated chemical structure. The column on the right depicts the aromatic group (Ar) off the skeletal structure.

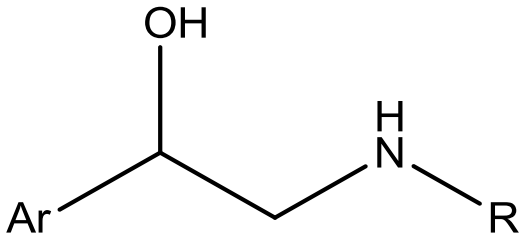	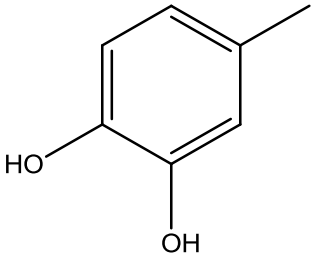
	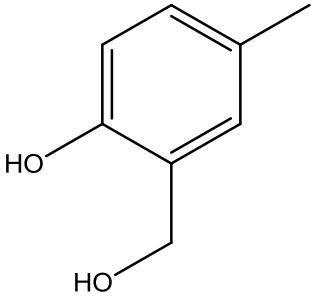
	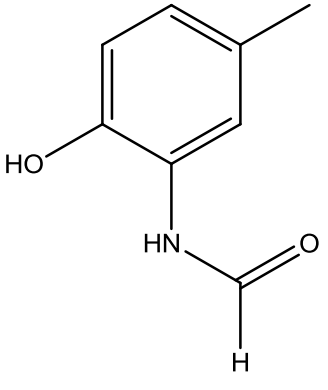

Muscarinic antagonists (or anticholinergics) are another class of bronchodilators that are used more often in COPD compared to asthma due to their lower efficacy in treating asthma then BAs. Muscarinic antagonists including tiotropium and ipratropium are specific antagonists

for muscarinic receptors to reduce cholinergic nerve related bronchoconstriction. Muscarinics inhibit the action of the cholinergic nerve but have no direct action on inflammatory mediators such as histamine and leukotrienes. They are typically less effective for treating asthma brought on by allergen and exercise by treating airway narrowing, which is currently the only reversible symptom of COPD[5,115]. Muscarinic optimization has followed the approach taken for BAs. Ipratropium was first developed and has a duration of up to 6 hours, while the latest drug, tiotropoum, has a duration of 24 hours[116]. Many of the muscarinic antagonists employ a quaternary amine, which due to the permanent positive charge inhibits transport across the cell layers from the lung to enter systemic circulation. Another advantage of the quaternary amine, is that any drug entering systemic circulation is rapidly metabolized and then cleared helping to reduce unwanted side effects[5].

Table 1.5: Progression of muscarinic agonists from short acting to long acting to ultra-long acting and their associated chemical structure.

Name	***Classification***	***Chemical Structure***
Atropine	Short acting	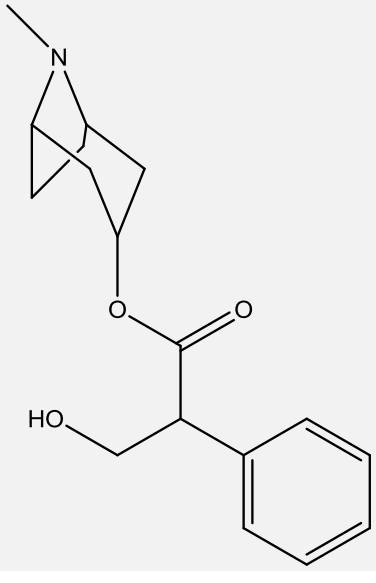

Ipratropium Bromide	Long acting	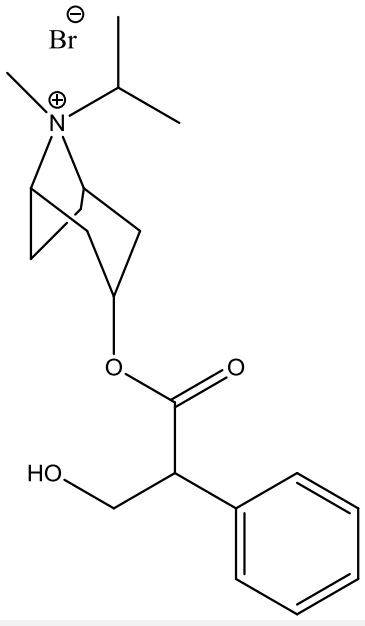
Tiotropium Bromide	Ultra long acting	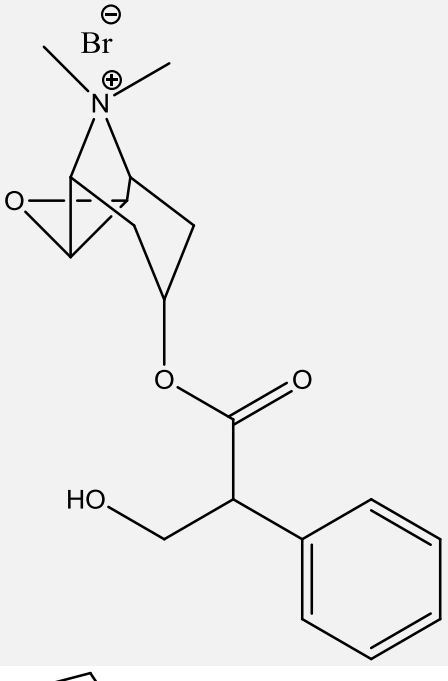
Glycopyrrolate	Ultra long acting	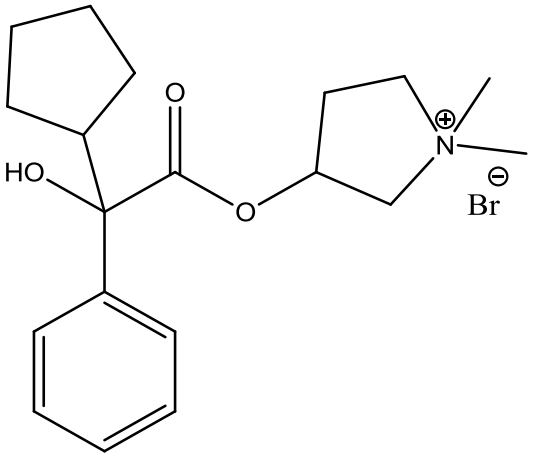

Aclidinium Bromide	Ultra long acting 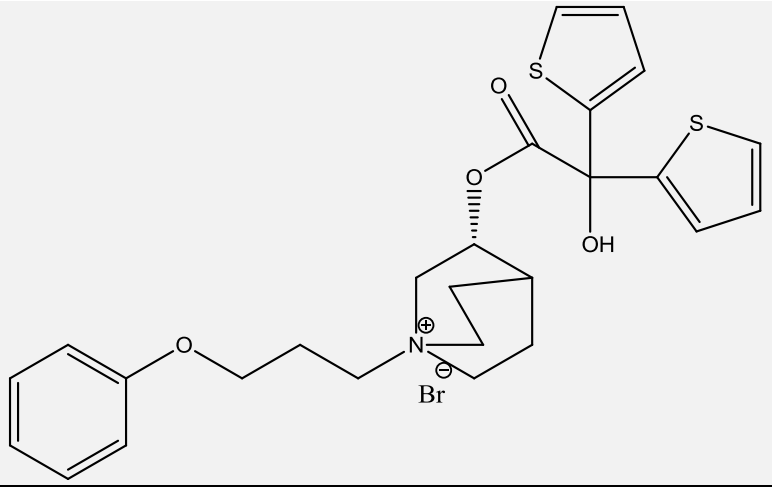

BAs are now being combined with other therapeutics including steroids and muscarinic antagonists to create a complete therapy for both controlling and relief to improve patient compliance in the desire to achieve a once daily formulation. There are several different options that have been employed as combination therapies which are typically corticosteroids with BAs (budesonide with formoterol, Symbicort, fluticasone with salmeterol, Advair, mometasone with formoterol, Dulera, and fluticasone with vilanterol, Ellipta) and corticosteroids with muscarinic antagonists. Both of these treatments work in synergistic forms as the steroids reduce the inflammation in the airways and the beta 2 agonists and muscarinic agents cause bronchodilation. Combination therapies have improved efficacy over single therapies with fluticasone/salmeterol having fewer asthma symptom days and exacerbations. Budesonide/formoterol combination had more days with asthma control, increased time between exacerbations, higher volume of air expelled from the lungs, and a lower dose of steroids compared to just budesonide[94,117-119].

1.6.2. Other Approaches to Sustain Lung Delivery

Besides medicinal chemistry approaches to increase duration, there have been new drug delivery strategies employed to achieve increased lung deposition and persistence. There have been numerous examples of engineered polymeric particles[120]. Polymeric microparticles and porous particles have been utilized as carriers especially with poly lactic glycolic acid (PLGA) given its ability to have a modulated degradation. Porous PLGA particles loaded with budesonide had a better performance in terms of reduced inflammation compared to nonporous PLGA budesonide loaded particles[121]. Hydroxypropyl-β-cyclodextrin has been incorporated as an excipient to reduce insulin release and to modulate powder aerodynamic properties. These particles had increased deposition into the deep lung and alveoli, which allowed rapid systemic onset compared to an insulin solution[123,124]. Nanoparticle medicines using similar excipients have also been explored to increase persistence in the lung. Nanoparticles typically utilize a different delivery strategy such as liquid formulations via nebulization or encapsulation in carrier particles[120]. Tobramycin PLGA nanoparticles have been embedded in lactose particles with alginate, polyvinyl alcohol, and chitosan used to modulate the size and release properties of tobramycin from the nanoparticles to increase persistence to 1 month[124]. Studies on PLGA particles coated in chitosan reported increased lung persistence and residence time potentially due to increased mucoadhesiveness. Chitosan is a permeation enhancer and as such, is not recommended for use in inhalation as it can alter the tight junctions in the lung. Other excipients including chitosan, alginate, and lipids have been employed to sustain delivery. PLGA has been extensively studied as an excipient in other products, but not for inhalation, and it has yet to be incorporated into an approved inhalation product[120].

Liposomes have been explored for sustained pulmonary delivery of drugs as well. Naturally occurring lipids in lung surfactant and tissue have been employed and appear to be well accepted in the lung. Multiple drug classes have been encapsulated within liposomes

including antibiotics, bronchodilators, anticancer agents, and proteins[120]. Arikace®, amikacin encapsulated in liposomes, is in clinical trials for cystic fibrosis patients with infections and are comprised of cholesterol and dipalmitoylphosphatidylcholine in a 1:2 ratio. The liposome formulation provided slow sustained release, while free amikacin was found to interact with mucus decreasing efficacy and requiring higher dosing[125,126]. Pulmaquin®, a ciprofloxacin liposome formulation in clinical trials, provides a combination effect of burst release and sustained release over 24 hours to avoid some of the irritant reactions resulting from free drug exposure[127].

The final method of sustained delivery utilizes conjugation to polymers via PEGylation and dendrimers. Different molecular weights of PEG have shown different clearance properties from the lungs. PEG 2 to 5 kDa in length has mucus penetrating abilities, while increased PEG size (10 kDa) was reported to stick in the mucus. Mutliple PEGylation sites on the same protein and longer PEG chains, 5-12 kDa, was also reported to slow absorption from the lungs[128,129]. PEGylation of proteins including insulin and rhG-CSF also appears to slow absorption from the lungs, extending the plasma half-life[130-132]. PEGylation increases hydrophilicty and steric hindrance, which may decrease degradation rates, since PEGylation has been used to protect peptides from proteases in the lung and increase systemic absorption after delivery to the lungs. Calcitonin PEGylation using 1 to 5 kDa PEG increased stability in the lungs by 1000 times, which increased systemic bioavailability 8 fold[120]. PEG has also been conjugated to antibodies to increase their residence time in the lungs. IL-17A Fab and anti-IL-17A had 40 kDa PEG conjugated, which increased their persistence from 1 day to 2 days. The PEG antibodies remained stable in the lung lumen and also reduced associated inflammation compared to the native proteins[133]. By conjugating PEG, one hypothesis is that there is increased adhesion to mucus and decreased macrophage uptake instead of larger sizes or decreased enzymatic activity. Small molecule drugs have undergone PEGylation as well including prednisolone that utilized a hydrolysable ester bond. By conjugating 2 kDa PEG, the prednisolone absorption rate

dropped almost 8 times across the lung tissue barrier, which was thought to result from an increase in molecular size[134].

Dendrimers have also been investigated as a means to extend the persistence of drugs in the lungs. Drugs can be encapsulated or conjugated to the surface of dendrimers using the unique chemistry groups or through electrostatic interactions. Polyamidoamine dendrimers had methylprednisolone conjugated that reduced lung inflammation by remaining in the lungs for one week[135]. Dendrimers conjugated with PEG (11, 22, and 78 kDa) had differential access to different body compartments based on their molecular weight. The smaller molecular weights had increased systemic exposure compared to larger dendrimers as facilitated by the more rapid transport into the blood from the lungs. The 78 kDa dendrimer had lung persistence up to 7 days and remained relatively intact in the lungs[136]. Other work has utilized a 56 kDa PEGylated polylysine dendrimer with doxorubicin conjugated, which sustained drug levels over the course of one week compared to the free drug, which was rapidly removed. These conjugates yielded complete remission of lung tumors compared with high levels of toxicity with the free drug[137].

Hyaluronic acid (HA) is another polymer besides dendrimers and PEG that has been employed to improve pulmonary delivery. Cisplatin-hyaluronan conjugates have been utilized to increase local concentrations of drug in the lung compared to cisplatin delivered intravenously[138]. HA has been employed in nebulized formulations as well to decrease lung inflammation and improve patient outcomes[50-54]. HA is available in many varied molecular weights and is a natural biopolymer, making it an attractive candidate for sustained lung delivery. Thus, Chapter 3 of this dissertation explores the effect of HA molecular weight on lung retention and subsequent biodistribution. HA is then used as a carrier molecule for delivering peptides to the lungs that alter immune response (Chapter 4).

1.7. Accessing Different Body Compartments from the Lungs

1.7.1. Allergy Treatments and Antigen Specific Immunotherapy (ASIT) by Employing Pulmonary Drug Delivery

As mentioned earlier, the lungs play a significant role in immune disease resulting from both exogenous and endogenous antigens[62-67]. Antigen specific immunotherapies (ASIT) have been explored recently as a strategy for restoring immune tolerance in autoimmune diseases. Classically, subcutaneous injections of allergens has been employed to gradually desensitize the immune system (e.g. 'allergy shots')[58,139]. A similar type of ASIT has been tried for autoimmune diseases as well. Different antigenic peptides are being employed in an attempt to desensitize the autoimmune response in diseases such as rheumatoid arthritis, type-1 diabetes, and lupus[60-62].

The lungs are exposed to the outside environment and have mucosal membranes lining the surface, which offers a first line of defense as protection from foreign antigens. The lungs also contain a mucosal immune system capable of processing foreign antigens and introducing them to the effector cells to elicit the appropriate response. The mucosal immune system includes the mucosa-associated lymphoid tissue (MALT). MALT encounters a large number of foreign antigens, and it functions to prevent damage to surrounding native cells. MALT is distinct from the systemic immune system, and the immune cells between these two systems are believed to have separate populations with limited crossover to decrease unwanted immune responses[140-142].

Classically, the spleen and lymph nodes have been considered secondary lymphoid organs, where immune cells traffic to become activated and primed. The lungs have recently been implicated in a 'Hub and Spoke' model for the immune system. The 'Hub and Spoke' hypothesis proposes that systemic immune cells or those present in secondary lymphoid organs

including the lymph nodes and spleen have to be activated before eliciting a response[62,63,65]. Next, immune cells are imprinted with a tissue 'zip code' enabling their migration to target organs, which is proposed to happen in the lungs. This process is called 'licensing'. The immune cells transport from the hub (lungs) to the different spokes depending on the autoimmune disease, such as the brain for MS, pancreas for type-1 diabetes, and the large intestine for irritable bowel disease[67]. One study tracked the injection of activated immune cells specific to CNS antigens. Depending on the site of injection there was a difference seen in symptoms and onset of symptoms. Cells administered intravenously did not produce central nervous system (CNS) symptoms until 5 days post dose. When these same cells were administered directly into the CNS, there were no observable symptoms. Finally, if these cells were administered into the lungs (hub), it took approximately 1 day for the CNS symptoms to be elicited[66].

T cells have been implicated as primary players in the 'Hub and Spoke' hypothesis. T cells must become 'licensed', expressing correct integrins, which are key components directing T cell migration. In experimental autoimmune encephalomyelitis (EAE), there is minimal direct evidence of licensing of immune cells though evidence is increasing. If licensing is in fact occurring in the lungs as a 'hub', drug delivery to the lungs offers the potential for crosstalk between the mucosal immune system and systemic immunity via the 'Hub and Spoke' hypothesis. Regardless of the mechanism, the lungs offer an interesting opportunity to shift immune profiles, leading to modification of the immune response throughout the body[65-67].

There are practically no reports of ASIT pulmonary delivery. The closest applications to pulmonary ASIT have primarily focused on cancer treatments and treatment of type-1 diabetes, but are not specifically ASIT. Several previous products for inhaled insulin for type-1 diabetes (Exubera and now Afrezza®) will be described in more detail in the following section[143]. These are not classical ASIT as they do not induce hyposensitization of the immune system by

applying an antigen but serve to replace loss of endogenous insulin production by pulmonary administration. The recent literature suggests ASIT delivered to the lungs may have increased efficacy compared to standard delivery routes when treating autoimmune disease.

1.7.2. Systemic Exposure After Pulmonary Delivery

There are different design criteria to consider when attempting systemic delivery through the lungs. Small molecule compounds compared to large molecule compounds will have different clearance and ability to cross the physiological barriers in the lung as discussed previously. The molecular weight, charge, and hydrophobic character of molecules often dictate the rate of passage through the lungs into systemic circulation. Even large proteins, however, can be delivered to bloodstream after inhalation and the understanding these dynamics is essential to drug delivery.

For small molecule drugs, there is one major property to consider which increases systemic absorption. Increased hydrophilicity corresponds with an increased half-life in terms of absorption of the initial dose. Drugs with a lipophilicity of approximately 0 – 4 for a log P (and more so a log P of 1-3) corresponds to a half-life on the order of a few minutes. Drugs with a log P of -2 - -4 that correlates with fairly hydrophilic compounds have a half-life of approximately 70 minutes. The other property that one might consider for systemic absorption is molecular weight. However, when looking at the molecular weight range of 100 – 1000 Da, the typical size for small molecules, there is no correlation besides lipophilicity. Again, the lipophilic drugs have a shorter half-life compared to hydrophilic compounds. There are only a few compounds actively transported, so there are not enough data points to determine the important properties[10].

For inhaled systemic peptides and proteins, there are several factors to take into account. The exact mechanism of large molecule absorption is not known but there are several theories. With peptides, there is the possibility that they could pass through the cells via the tight junctions even including molecules up to 2 nm in size, which includes insulin in the upper airways. Another possibility in the alveolar region is that a vesicle forms in the fluid that enters into the cell. The vesicle can pass through the cell to the interstitium where the process happens again allowing access to the blood. Molecules can potentially access the lymph from the interstitium depending on their size. There are two major examples of systemic absorption of large molecules, insulin and human growth hormone (HGH). Insulin Inhaled insulin has faster pharmacokinetics than subcutaneous injected insulin both in terms of absorption and clearance. Insulin has a narrow therapeutic window, which complicates the aerosol delivery of it besides the earlier issues with the delivery device. Insulin also had some issues with stimulating cellular growth in the lungs, which had a slight detrimental effect on breathing. HGH had a lower bioavailability when inhaled compared to subcutaneous injection (only ~10%), but it achieved increased growth in rats without seeing abnormal histology in the lungs for up to 28 days. An example of an inhaled peptide is leuprolide acetate that stimulates the pituitary gland. It had a bioavailability between 35 – 55% and had levels in the lungs over 12 hours. Inhaled insulin, which is approximately 5 times larger in size reached a maximum in only 15 minutes. This may have been a by-product of the formulation as it was a pMDI[143].

1.7.3. Lymphatic Exposure After Pulmonary Delivery

The final compartment of interest that may be accessible through the lungs is the lymphatics. Research has suggested that in the alveolar region, vesicles can form in the fluid layer lining the cells for passive transport across this tissue barrier (Figure 1.8). Once the vesicle transverses the cell and releases cargo into the interstitium, molecular weight can

determine its ultimate end point as molecules larger than 25 kDa may avoid absorption into the blood stream and enter the lymphatics. In the lungs, the interstitium is a passageway where the lymph is transported around a bundle of alveoli leading to a lymph node higher up in the respiratory tree. This transport mechanism has been observed with labeled polymers that have been investigated, especially for cancer therapies[143].

The alveolar region also has macrophages patrolling to remove foreign particles and antigens that can participate in active transport to the lymphatics. The macrophages in the alveolar region have closer access to the lymphatic network with ducts and nodes just outside the alveolar sacs. There is also less of a tissue barrier in the alveolar region as the epithelium layer is <1 μm in thickness compared to >10 μm in the upper airways with the addition of fibrous and smooth muscle tissue[9]. Solid lipid nanoparticles have been shown to access the lymphatics as potential treatments for cancer and metastases and (<200 nm) can rapidly access different areas of the pulmonary lymphatic network[144].

There are multiple nodes that can be accessed from the lungs including the hilar, mediastinal, carinal, and aortic nodes. Liposomal formulations for the treatment of cancer have gained particular interest as the lymphatics are implicated in metastases. Pulmonary delivery and associated lymph drainage can by-pass some of the problems with conventional chemotherapeutic delivery namely off-target toxicity and poor penetration into the lymphatics. For example, pulmonary delivery of a liposomal formulation of paclitaxel and a vitamin E analog resulted in decreased mammary tumor burden, fewer cells were positive for CD31 and Ki67 suggesting an inhibition of lymphatic metastases. Other work has focused on liposomal delivery of this vitamin E analog with another chemotherapy drug, which resulted in prolonged survival rate by a decreased tumor progression. Liposomes have also been combined with radioactive markers to improve diagnostics. These radioliposomes were administered to wild boars and provided information on the deep lung and associated lymphatics that was unavailable from

conventional diagnostic methods. Similarly, radiolabeled SLNs accumulated in the inguinal node of rats and remained in the lungs after 4 hours whereas free radiolabel was mainly cleared by systemic circulation and showed minimal lymph node signal[145].

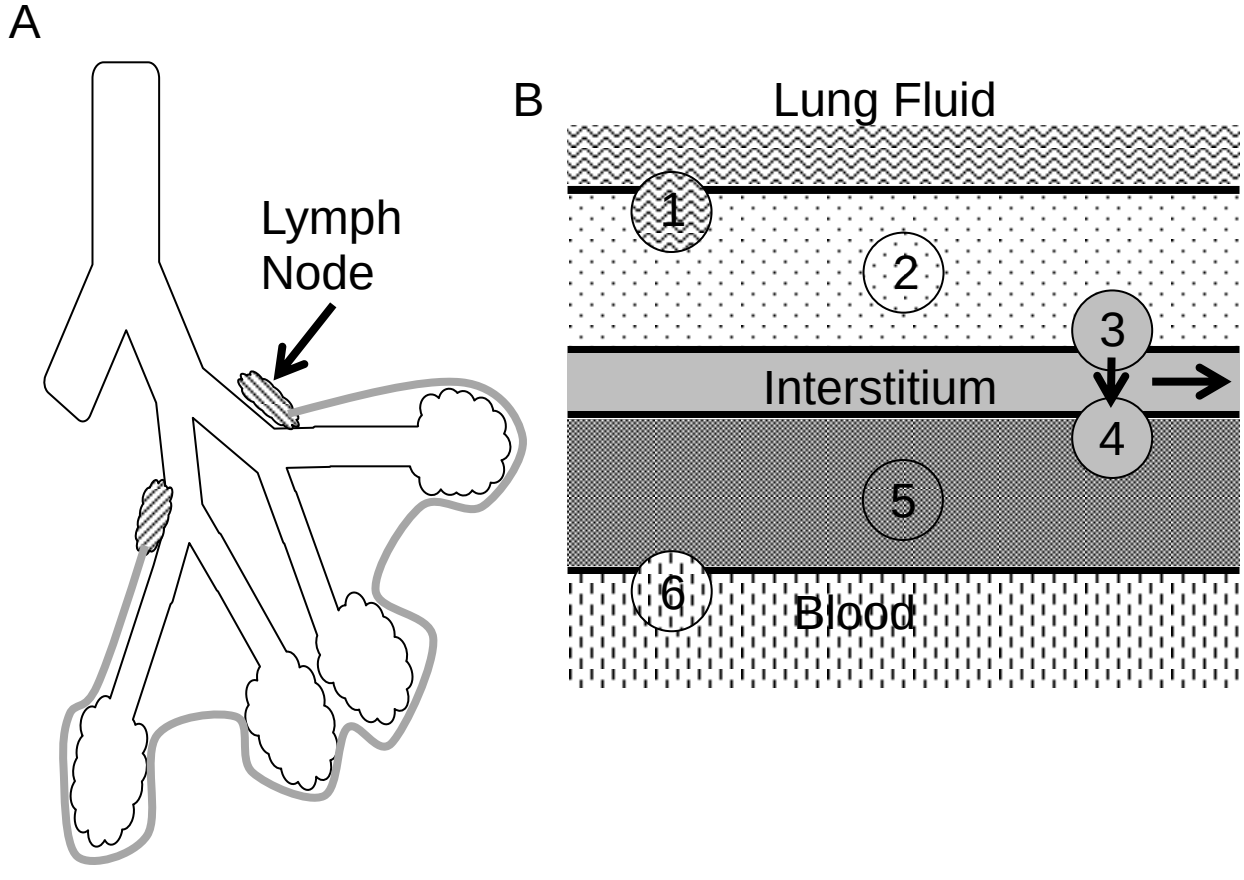

Figure 1.8: Structure of the lung lymphatics. A depicts the lymph nodes around the alveoli. B shows a close-up of the conducting airway and accessing the lymph. 1 is a vesicle forming from the lung fluid passing through the epithelial cell (2) before entering the interstitium. At 4 the molecule enters the cells surrounding the blood vessel before passing through it (5) and depositing into systemic circulation. Between 3 and 4, molecules >25 kDa or having high lipophilicity may enter the lymphatics though the interstitium.

1.8. Pulmonary Delivery Needs

There are many different areas for improving pulmonary delivery. The lung is not a stand-alone organ but is tied into multiple organs and systems in the body. This dissertation focuses on physical approaches to address specific pulmonary delivery needs. Particle engineering is explored in Chapter 2 to improve aerosol deposition and provide an increase in dissolution by harnessing microparticles comprised of agglomerated nanoparticles (NanoClusters). In Chapter 3, the molecular weight of the polymer hyaluronic acid (HA) is explored as a physical approach to achieve sustained exposure in the lung. Finally, since the lungs have recently been implicated in the immune system, Chapter 4 of this dissertation investigates pulmonary ASIT therapy applied to an autoimmune disease, experimental autoimmune encephalomyelitis (EAE) in an effort to induce antigen-specific immune tolerance. Physical approaches to improving delivery of pulmonary therapeutics offer new treatment paradigms, which are discussed as the culmination of this dissertation.

References

1. Barnes, Peter. “Drugs for airway disease.” Medicine. 36(4):181-190. 2008

2. Barnes, Peter. “New therapies for asthma: is there any progress?” Trends in Pharmacological Sciences. 31(7):335-343. 2010

3. Chow, Albert, Henry Tong, Pratibhash Chattopadhyay, and Boris Shekunov. “Particle Engineering for Pulmonary Drug Delivery.” Pharmaceutical Research. 24(3):411-437. 2007

4. Healy, Anne Marie, Maria Inês Amaro, Krzysztof J. Paluch, and Lidia Tajber. “Dry powders for oral inhalation free of lactose carrier particles.” Advanced Drug Delivery Reviews. 75:32-52. 2014

5. Busch-Petersen, Jakob, and Dramane Laine. “Inhaled long-acting muscarinic antagonists in chronic obstructive pulmonary disease.” Future Medicinal Chemistry. 3(13):1623-1634. 2011

6. Jacobsen, John. “Third-generation long-acting β2-adrenoceptor agonists: medicinal chemistry strategies employed in the identification of once-daily inhaled β2-adrenoceptor agonists.” Future Medicinal Chemistry. 3(13):1607-1622. 2011

7. Cazzola, Mario, Luigino Calzetta, and Maria Gabriella Matera. “β2-adrenoceptor agonists: current and future direction.” British Journal of Pharmacology. 163(1):4-17. 2011

8. Tashkin, Donald P, Leonardo M Fabbri. “Long-acting beta-agonists in the management of chronic obstructive pulmonary disease: current and future agents.” Respiratory Research. 11:149-152. 2010

9. Patton, John and Peter Byron. “Inhaling medicines: delivering drugs to the body through the lungs.” Nature Reviews: Drug Discovery. 6(1):67-74. 2007

10. Patton, John, C. Simone Fishburn, and Jeffry G. Weers. “The Lungs as a Portal of Entry for Systemic Drug Delivery.” Proceedings of the American Thoracic Society. 1:338-334. 2004

11. Winkler, Julia, Guenther Hochhaus, and Hartmut Derendorf. “How the Lung Handles Drugs Pharmacokinetics and Pharmacodynamics of Inhaled Corticosteroids.” Proceedings of the American Thoracic Society. 1:356-363. 2004

12. Kaminskas, Lisa M., Christopher J.H. Porter. “Targeting the lymphatics using dendritic polymers (dendrimers).” Advanced Drug Delivery Review. 63(10-11):899-900. 2011

13. Burapapadh, Kanokporn, Hirofumi Takeuchi, Pornsak Sriamornsak. “Novel pectin-based nanoparticles prepared from nanoemulsion templates for improving in vitro dissolution and in vivo absorption of poorly water-soluble drug.” European Journal of Pharmaceutics and Biopharmaceutics. 82(2):250-2612012

14. Raseneck and Muller. “Dissolution Rate Enhancement by in Situ Micronization of Poorly Water Soluble Drugs.” Pharmaceutical Research. 19(12):1894-1900. 2002

15. Vogt, Markus, Klaus Kunath, Jennifer B. Dressman. “Dissolution improvement of four poorly water soluble drugs by cogrinding with commonly used excipients.” International Journal of Pharmaceutics and Biopharmaceutics. 68(2):330-338. 2008

16. Edlund, U., A.-C. Albertsson. “Degradable Polymer Microspheres for Controlled Drug Delivery.” Advances in Polymer Science. 157:67-112. 2002

17. Maulvi, Furqan A., Sonali J. Dalwadi, Vaishali T. Thakkar, Tejal G. Soni, Mukesh C. Gohel, Tejal R. Gandhi. “Improvement of dissolution rate of aceclofenac by solid dispersion technique.” Powder Technology. 207(1-3):47-54. 2011

18. Hu, Jiahui, Keith P. Johnston, Robert O. Williams, III. “Rapid dissolving high potency danazol powders produced by spray freezing into liquid process.” International Journal of Pharmaceutics. 271(1-2):145-154. 2004

19. Chen, Xiaoxia, Jason Vaughn, Miguel Yacaman, Robert Williams III, Keith Johnston. “Rapid Dissolution of High-Potency Danazol Particles Produced by Evaporative Precipitation into Aqueous Solution.” Journal of Pharmaceutical Sciences. 93(7):1867-1878. 2004

20. Rogers, True, Keith P. Johnston, and Robert O. Williams III. “Physical Stability of Micronized Powders Produced by Spray-Freezing into Liquid (SFL) to Enhance the Dissolution of an Insoluble Drug.” Pharmaceutical Development and Technology. 8(2):187-197. 2003.

21. Hu, Jiahui, True L. Rogers, Judith Brown, Tim Young, Keith P. Johnston, and Robert O. Williams III “Improvement of Dissolution Rates of Poorly Water Soluble APIs Using Novel Spray Freezing into Liquid Technology.” Pharmaceutical Research. 19(9):1278-1284. 2002

22. Li, Chan, Caixia Li, Yuan Le, Jian-Feng Chen. “Formation of bicalutamide nanodispersion for dissolution rate enhancement.” International Journal of Pharmaceutics. 404(1-2):257-263. 2011

23. Rogers, True L., Andrew C. Nelsen, Marazban Sarkari, Timothy J. Young, Keith P. Johnston, and Robert O. Williams, III. Enhanced Aqueous Dissolution of a Poorly Water Soluble Drug by Novel Particle Engineering Technology: Spray-Freezing into Liquid with Atmospheric Freeze-Drying.” Pharmaceutical Research. 20(3):485-493. 2003

24. Aillon, Kristin L., Nashwa El-Gendy, Connor Dennis, Jeffrey P. Norenberg, Jacob McDonald, and Cory Berkland. Iodinated NanoClusters as an Inhaled Computed Tomography Contrast Agent for Lung Visualization.” Molecular Pharmaceutics. 7(4):1274-1282. 2010

25. El-Gendy, Nashwa, Shan Huang, Parthiban Selvam, Pravin Soni, Cory Berkland. “Development of Budesonide NanoCluster Dry Powder Aerosols: Formulation and Stability.” Journal of Pharmaceutical Sciences. 101(9):3445-3455. 2012

26. El-Gendy, Nashwa, Shan Huang, Parthiban Selvam, Pravin Soni, Cory Berkland. Development of Budesonide NanoCluster Dry Powder Aerosols: Processing." Journal of Pharmaceutical Sciences. 101(9):3425-3433. 2012

27. Kuo, JW. Practical Aspects of Hyaluronan Based Medical Products. Crc Press, Boca Raton, Florida. 2006

28. Schanté, Carole, Guy Zuber, Corinne Herlin, Thierry Vandamme. "Chemical modifications of hyaluronic acid for the synthesis of derivatives for a broad range of biomedical applications." Carbohydrate Polymers. 85(3):469-489. 2011

29. Motokawa, Keiko, Sei Kwang Hahn, Teruo Nakamura, Hajime Miyamoto, Tsuyoshi Shimoboji. "Selectively crosslinked hyaluronic acid hydrogels for sustained release formulation of erythropoietin." Journal of Biomedical Materials Part A. 78(3):459-465. 2006

30. Fakhari, Amir. "Biomedical Application of Hyaluronic Acid Nanoparticles." Dissertation from University of Kansas. 2012

31. Allison DD, Grande-Allen KJ. "Hyaluronan: a powerful tissue engineering tool." Tissue Engineering. 12(8):2131-2140. 2006

32. Necas, J, L Bartosikova, P Brauner, J Kolar. "Hyaluronic Acid (Hyaluronan): a Review." Veterinarni Medicina. 53(8): 397-411. 2008

33. Jiang, Dianhua, Jiurong Liang, Paul Noble. "Hyaluronan as an Immune Regulator in Human Diseases." Physiological Reviews. 91(1):221-264. 2011

34. Jiang, Dianhua, Jiurong Liang, and Pau lW. Noble. "Hyaluronan in Tissue Injury and Repair." Annual Review of Cell and Developmental Biology. 23:435-461. 2007

35. Laurent, Torvard, Ulla BG Laurent, J Robert Fraser. "The Structure and Function of Hyaluronan: an Overview." Immunology and Cell Biology. 74(2):A1-A7. 1996

36. Laurent, Torvard and J Robert Fraser. "Hyaluronan." The Journal of the Federation of American Societies for Experiental Biology." 6(7):2397-2404. 1992

37. Laurent, Torvard. "Biochemistry of Hyaluronan." Acta Oto-laryngologica. 104(s442):7-24. 1987

38. Hascall, Vincent. "Hyaluronan, a common thread." Glycoconjugate Journal. 17(7-9):607-616. 2000

39. Brown, MB, SA Jones. "Hyaluronic acid: a unique topical vehicle for the localized delivery of drugs to the skin." Journal of the European Academy of Dermatology and Venereology. 19(3):308-318. 2005

40. Burdick, Jason A. and Glenn D. Prestwich. "Hyaluronic Acid Hydrogels for Biomedical Applications." Advanced Materials. 23(12):H41-H56. 2011

41. Reed, R, U Laurent, S King, J Fraser, T Laurent. “Effect of Increased Interstitial Fluid Flux on Fractional Catabolic rate of High Molecular Weight [3H]Hyaluronan Injected in Rabbit Skin.” Acta Physiologica Scandinavica. 156(2):93-98. 1996

42. Reed, Rolf and Ulla Laurent. “Removal rate of [3H] hyaluronan injected subcutaneously in rabbits.” American Journal of Physiology. 259(2 Pt 2):H532-5. 1990

43. Laurent, Ulla, Lauritz Dahl, and Rolf Reed. “Catabolism of Hyaluronan in Rabbit Skin Takes Place Locally, in Lymph Nodes and Liver.” Experimental Physiology. 76(5):695-703. 1991

44. Allen, Steven, Robert Fraser, Ulla Laurent, Rolf Reed, and Torvard Laurent. “Turnover of hyaluronan in the rabbit pleural space.” Journal of Applied Physiology. 73(4):1457-1460. 1992

45. Laznicek, Milan, Alice Laznickova, Dagmar Cozikova, Vladimir Velebny. “Preclinical pharmacokinetics of radiolabelled hyaluronan.” Pharmacological Reports. 64(2):428-437. 2012

46. Balogh, Lajos, Andras Polyak, Domokos Mathe, Reka Kiraly, Juliana Thuroczy, Marian Terez, Gyozo Janoki, Yaoting Ting, Luke Bucci, Alexander Schauss. “Absorption, Uptake and Tissue Affinity of High-Molecular-Weight Hyaluronan after Oral Administration in Rats and Dogs.” Journal of Agricultural and Food Chemistry. 56(2):10582-10593. 2008

47. Fraser, R, T Laurent, A Engstrom-Laurent, and U Laurent. “Elimination of Hyaluronic Acid From the Blood Stream in the Human.” Clinical and Experimental Pharmacology and Physiology. 11(1): 17-25. 1984

48. Fraser, Robert, Torvard Laurent, Hakan Pertoft, and Elsmaree Baxter. “Plasma clearance, tissue distribution and metabolism of hyaluronic acid injected intravenously in the rabbit.” Biochemical Journal. 200(2):415-424. 1981

49. Gustafson, Stefan, Tomas Bjorkman, Jan-Erik Westlin. “Labelling of high molecular weight hyaluronan with 1251-tyrosine: studies in vitro and in vivo in the rat.” Glycoconjugate Journal. 11(6):608-613. 1994

50. Gavina, Manuela, Alessandro Luciani, Valeria R. Villella, Speranza Esposito, Eleonora Ferrari, Ilaria Bressani, Alida Casale, Emanuela M. Bruscia, Luigi Maiuri, and Valeria Raia. “Nebulized Hyaluronan Ameliorates Lung Inflammation in Cystic Fibrosis Mice.” Pediatric Pulmonology. 48(8):761–771. 2013

51. Buonpensiero, Paolo, Fabiola De Gregorio, Angela Sepe, Antonio Di Pasqua, Pasqualina Ferri, Maria Siano, Vito Terlizzi, and Valeria Raia “Hyaluronic Acid Improves “Pleasantness” and Tolerability of Nebulized Hypertonic Saline in a Cohort of Patients with Cystic Fibrosis.” Advanced Therapeutics. 27(11):870-878. 2010

52. Casale, Manuele, Lorenzo Sabatino, Valeria Frari, Francesco Mazzola, Rosa Dell’Aquila, Peter Baptista, Ranko Mladina, Fabrizio Salvinelli. “The potential role of hyaluronan in minimizing symptoms and preventing exacerbations of chronic rhinosinusitis.” American Journal of Rhinology and Allergy. 28(4):345-348. 2014

53. Furnari, Maria Lucia, Lisa Termini, Gabriella Traverso, Stefania Barrale, Maria Rita Bonaccorso, Giuseppina Damiani, Caterina Lo Piparo and Mirella Collura. "Nebulized hypertonic saline containing hyaluronic acid improves tolerability in patients with cystic fibrosis and lung disease compared with nebulized hypertonic saline alone: a prospective, randomized, double-blind, controlled study." Therapeutic Advances in Respiratory Disease. 6(6):315-322. 2012

54. Nenna, Raffaella, Paola Papoff, Corrado Moretti, Daniela De Angelis, Massimo Battaglia, Stefano Papasso, Mariangela Bernabucci, Giulia Cangiano, Laura Petrarca, Serena Salvadei, Ambra Nicolai, Marianna Ferrara, Enea Bonci, and Fabio Midulla. "Seven Percent Hypertonic Saline—0.1% Hyaluronic Acid in Infants With Mild-To-Moderate Bronchiolitis." Pediatric Pulmonology. 49(9):919-925. 2014

55. Sestak, Joshua, Bradley P Sullivan, Sharadvi Thati, Laura Northrup, Brittany Hartwell, Lorena Antunez, M Laird Forrest, Charlotte M Vines, Teruna J Siahaan, and Cory Berkland. "Codelivery of antigen and an immune cell adhesion inhibitor is necessary for efficacy of soluble antigen arrays in experimental autoimmune encephalomyelitis." Nature Molecular Therapy — Methods & Clinical Development. 1:1-9. 2014

56. Thati, Sharadvi, Christopher Kuehl, Brittany Hartwell, Joshua Sestak, Teruna Siahaan, M Laird Forrest, and Cory Berkland. "Routes of Administration and Dose Optimization of Soluble Antigen Arrays in Mice with Experimental Autoimmune Encephalomyelitis." Journal of Pharmaceutical Sciences. 10(2)4:714–721. 2015

57. Sabatos-Peyton, Catherine, Johan Verhagen, and David C Wraith. "Antigen-specific immunotherapy of autoimmune and allergic diseases." Current Opinion in Immunology. 22(5):609–615. 2010

58. Aasbjerg, K., V. Backer, G. Lund, J. Holm, N. C. Nielsen, M. Holse, V. R. Wagtmann, and P. A. Wurtzen. "Immunological comparison of allergen immunotherapy tablet treatment and subcutaneous immunotherapy against grass allergy." Clinical and Experimental Allergy. 44(3):417–428. 2014

59. Thrower, SL, James L, Hall W, Green KM, Arif S, Allen JS, Van-Krinks C, Lozanoska-Ochser B, Marquesini L, Brown S et al. "Proinsulin peptide immunotherapy in type 1 diabetes: report of a first-in-man Phase I safety study." Clinical and Experimental Immunology. 155(2):156-165. 2009

60. Muller, S, Monneaux F, Schall N, Rashkov RK, Oparanov BA, Wiesel P, Geiger JM, Zimmer R "Spliceosomal peptide P140 for immunotherapy of systemic lupus erythematosus: results of an early phase II clinical trial." Arthritis and Rheumatology. 58(12):3873-3883. 2008

61. Koffeman EC, Genovese M, Amox D, Keogh E, Santana E, Matteson EL, Kavanaugh A, Molitor JA, Schiff MH, Posever JO et al. "Epitope-specific immunotherapy of rheumatoid arthritis: clinical responsiveness occurs with immune deviation and relies on the expression of a cluster of molecules associated with T cell tolerance in a double-blind, placebo-controlled, pilot phase II trial." Arthritis and Rheumatology. 60(11):3207-3216. 2009

62. Steinman, Lawrence. “A molecular trio in relapse and remission in multiple sclerosis.” Nature Reviews of Immunology. 9(6):440-447. 2009

63. Steinman, Lawrence. “Immunology of Relapse and Remission in Multiple Sclerosis.” Annual Review of Immunology. 32:257–81. 2014

64. Rayamajhi, Manira, Elizabeth F. Redente, Tracy V. Condon, Mercedes Gonzalez-Juarrero, David W.H. Riches, and Laurel L. Lenz. “Non-surgical intratracheal instillation of mice with analysis of lungs and lung draining lymph nodes by flow cytometry.” Journal of Visualized Experiments – NIH Public Access. 51:2702. 2012

65. Steinman, Lawrence. “‘Hub-and-spoke’ T cell traffic in autoimmunity.” Nature Medicine. 19(2):139-141. 2013

66. Odoardi, Francesca, Christopher Sie, Kristina Streyl, Vijay K. Ulaganathan, Christian Schlager, Dmitri Lodygin, Klaus Heckelsmiller, Wilfried Nietfeld, Joachim Ellwart, Wolfgang E. F. Klinkert, Claudio Lottaz, Mikhail Nosov, Volker Brinkmann, Rainer Spang, Hans Lehrach, Martin Vingron, Hartmut Wekerle, Cassandra Flugel-Koch, Alexander Flugel. “T cells become licensed in the lung to enter the central nervous system.” Nature. 488(7413):675-682. 2012

67. Ransohoff, Richard. “Licensed in the Lungs.” Nature Research News and Views. 488(7413):595-596. 2012

68. Ross, Michael, and Wojciech Pawlina. Histology, a Text and Atlas. 6th ed. Wolters Kluwer, Alphen aan den Rijn, Netherlands. 589:Table 18.1

69. Smyth, H.D.C. and A.J. Hickey. Controlled Pulmonary Drug Delivery. Springer Publishing, New York, New York. 2011

70. Prokop, Ales. Intracellular Delivery – Fundamentals and Applications. Springer Publishing, New York, New York. 2011

71. Rau, Joseph. “The Inhalation of Drugs: Advantages and Problems.” Respiratory Care. 50(3):367-382. 2005

72. Smaldone, Gerald, Cory Berkland, Igor Gonda, Jolyon Mitchell, Omar Usmani, Andy Clark. “The benefits and challenges of pulmonary drug delivery.” Therapeutic Delivery. 4(8):905-913. 2013

73. Kleinstreuer, C, Z. Zhang, and J.F. Donohue. “Targeted Drug-Aerosol Delivery in the Human Respiratory System.” Annual Review of Biomedical Engineering. 10:195–220. 2008

74. Gradon, L, Marijnissen J. Optimization of Aerosol Drug Delivery. Kluwer Academic, Boston, Massachusetts. 2003

75. Hickey, AJ. Pharmaceutical Inhalation Aerosol Technology. Marcel Dekker, New York, New York. 2004

76. Finlay, WH. The Mechanics of Inhaled Pharmaceutical Aerosols: An Introduction. Academic Press, Waltham, Massachusetts. 2001

77. Bissgard, H, O'Callaghan C, Smaldone G. Drug Delivery to the Lungs. Marcel Dekker, New York, New York. 2002

78. Kwok, PCL, Collins R, Chan HK. "Effect of spacers on the electrostatic charge properties of metered dose inhaler aerosols." Journal of Aerosol Science. 37(12):1671–1682. 2006

79. Newman SP. "Spacer devices for metered dose inhalers." Clinical Pharmacokinetics. 43(6):349–360. 2004

80. Cheng YS, Fu CS, Yazzie D, Zhou Y. "Respiratory deposition patterns of salbutamol pMDI with CFC and HFA-134a formulations in a human airway replica." Journal of Aerosol Medicine. 14(2):255–266. 2001

81. Rahmatalla, MF, Zuberbuhler PC, Lange CF, Finlay WH. "In vitro effect of a holding chamber on the mouth-throat deposition of QVAR® (Hydrofluoroalkane-beclomethasone dipropionate)." Journal of Aerosol Medicine. 15(4):379–385. 2002

82. Asmus MJ, Coowanitwong I, Kwon SH, Khorsand N, Hochhaus G. "In vitro performance of two common valved holding chambers with a chlorofluorocarbon-free beclomethasone metered-dose inhaler." Pharmacotherapy 23(12):1538–1544. 2003

83. Kleinstreuer C, Shi H, Zhang Z. 2007. Computational analyses of a pressurized metered dose inhaler and a new drug-aerosol targeting methodology. J. Aerosol Med. 20(3):294–309

84. Canadian Medical Association Journal. "Inhalation devices." Canadian Medical Association Journal. 173(6):S39–45. 2005

85. Coates MS, Chan HK, Fletcher DF, Raper JA. "Influence of air flow on the performance of a dry powder inhaler using computational and experimental analyses." Pharmaceutical Research. 22(9):1445–1453. 2005

86. Chan HK. "Dry powder aerosol delivery systems: current and future research directions." Journal of Aerosol Medicine. 19(1):21–27. 2006

87. Edwards DA, Dunbar C. "Bioengineering of therapeutic aerosols." Annual Review of Biomedical Engineering. 4:93–107. 2002

88. Dolovich MB, Ahrens RC, Hess DR, Anderson P, Dhand R, Rau JL, Smaldone GC, Guyatt G. "Device selection and outcomes of aerosol therapy: evidence-based guidelines." Chest 127(1):335–371. 2005

89. Smyth HDC, Leach CL. "Alternative propellant aerosol delivery systems." Critical Reviews in Therapeutic Drug Carrier Systems. 22(6):493–534. 2005

90. Brocklebank D, Wright J, Cates C. “Systematic review of clinical effectiveness of pressurised metered dose inhalers versus other hand held inhaler devices for delivering corticosteroids in asthma.” British Medical Journal. 323(7318):896–900. 2001

91. O’Connor BJ. “The ideal inhaler: design and characteristics to improve outcomes.” Respiratory Medicine. 98(SA):S10–16. 2004

92. Telko MJ, Hickey AJ. “Dry powder inhaler formulation.” Respiratory Care. 50(9):1209–1227. 2005

93. Lipworth and Jackson. “Safety of Inhaled and Intranasal Corticosteroids.” Drug Safety. 23(1):11-33. 2000

94. Zhou, Qi, Patricia Tang, Sharon Shui Yee Leung, John Gar Yan Chan, Hak-Kim Chan. “Emerging inhalation aerosol devices and strategies: Where are we headed?” Advanced Drug Delivery Reviews. 75:3-17. 2014

95. Restrepo, Ruben, Melissa T Alvarez, Leonard D Wittnebel, Helen Sorenson, Richard Wettstein, David L Vines, Jennifer Sikkema-Ortiz, Donna D Gardner, and Robert L Wilkins. “Medication adherence issues in patients treated for COPD.” International Journal of COPD. 3(3):371-384. 2008

96. Sumino, Kaharu, and Michael Cabana. “Medication adherence in asthma patients.” Current Opinion in Pulmonary Medicine. 19(1):49-53. 2013

97. Ooi, Jesslynn, Daniela Traini, Susan Hoe, William Wong, Paul M. Young. “Does carrier size matter? A fundamental study of drug aerosolisation from carrier based dry powder inhalation systems.” International Journal of Pharmaceutics. 413(1-2):1-9. 2011

98. Kaialy, Waseem, Amjad Alhalaweh, Sitaram P. Velaga, Ali Nokhodchi. “Effect of carrier particle shape on dry powder inhaler performance.” International Journal of Pharmaceutics. 421(1):12-23. 2011

99. Donovan, Martin J. and Hugh D.C. Smyth. “Influence of size and surface roughness of large lactose carrier particles in dry powder inhaler formulations.” International Journal of Pharmaceutics. 402(1-2):1-9. 2010

100. Hann, Michael, and Gyorgy Keseru. “Finding the sweet spot: the role of nature and nurture in medicinal chemistry.” Nature Reviews: Drug Discovery. 11(5):355-365. 2012

101. Waring, M. “Lipophilicity in drug discovery.” Expert Opinion on Drug Discovery. 5(3):235–248. 2010

102. Waring, M. “Defining optimum lipophilicity and molecular weight ranges for drug candidates — molecular weight dependent lower logD limits based on permeability.” Bioorganic and Medicinal Chemistry Letters. 19(10):2844–2851. 2009

103. Gleeson, M. P. “Generation of a set of simple, interpretable ADMET rules of thumb.” Journal of Medicinal Chemistry. 51(4):817–834. 2008

104. Gleeson, M. P., Hersey, A., Montanari, D. and Overington, J. “Probing the links between in vitro potency, ADMET and physicochemical parameters.” Nature Reviews Drug Discovery. 10(3):197–208. 2011

105. Newton, Robert. “Molecular mechanisms of glucocorticoid action: what is important?” Thorax. 55(7):603-613. 2000

106. Barnes, Peter. “Anti-inflammatory actions of glucocorticoids : molecular mechanisms.” Clinical Science. 94:557-572. 1998

107. Johnson, M. “Beta2-adrenoceptors: mechanisms of action of beta2-agonists.” Pediatric Respiratory Reviews. 2(1):57-62. 2001

108. Cazzola, M and MG Matera. “Novel long-acting bronchodilators for COPD and asthma.” British Journal of Pharmacology. 15(5):291-297. 2008

109. Düringer, Caroline, Gunilla Grundström, Eylem Gürcan, Ian A Dainty, Mandy Lawson, Solange H Korn, Anders Jerre, Hanna Falk Håkansson, Elisabet Wieslander, Karin Fredriksson, Carl Magnus Sköld, Magnus Löfdahl, Claes-Göran Löfdahl, David J Nicholls, and David S Silberstein. “Agonist-specific patterns of b2-adrenoceptor responses in human airway cells during prolonged exposure.” British Journal of Pharmacology. 158(1):169-179. 2009

110. Anderson, GP, A. Lindén, K.F. Rabe. “Why are long-acting beta-adrenoceptor agonists long-acting?” European Respiratory Journal. 7(3):569-578. 1994

111. Bouyssou, T, P. Casarosa, E. Naline, S. Pestel, I. Konetzki, P. Devillier, and A. Schnapp. “Pharmacological Characterization of Olodaterol, a Novel Inhaled 2-Adrenoceptor Agonist Exerting a 24-Hour-Long Duration of Action in Preclinical Models.” The Journal of Pharmacology and Experimental Therapies. 334(1):53-62. 2010

112. Glossop, Paul, Charlotte A. L. Lane, David A. Price, Mark E. Bunnage, Russell A. Lewthwaite, Kim James, Alan D. Brown, Michael Yeadon, Christelle Perros-Huguet, Michael A. Trevethick, Nicholas P. Clarke, Robert Webster, Rhys M. Jones, Jane L. Burrows, Neil Feeder, Stefan C. J. Taylor, and Fiona J. Spence. “Inhalation by Design: Novel Ultra-Long-Acting β2-Adrenoreceptor Agonists for Inhaled Once-Daily Treatment of Asthma and Chronic Obstructive Pulmonary Disease That Utilize a Sulfonamide Agonist Headgroup.” Journal of Medicinal Chemistry. 53(18):6640-6652. 2010

113. Perez, Daniel, Maribel Crespo, Laia Solé, Maria Prat, Carla Carcasona, Elena Calama, Raquel Otal, Amadeu Gavaldá, Mireia Gómez-Angelats, Montserrat Miralpeix, and Carles Puig. “Discovery of substituted phenyl urea derivatives as novel long-acting b2-adrenoreceptor agonists.” Bioorganic and Medicinal Chemistry Letters. 21(5):1545-1548. 2011

114. Connolly, Stephen, Lilian Alcaraz, Andrew Bailey, Elaine Cadogan, Jadeen Christie, Anthony R. Cook, Adrian J. Fisher, Stephen Hill, Alexander Humphries, Anthony H. Ingall, Zoe Kane, Stuart Paine, Garry Pairaudeau, Michael J. Stocks, and Alan Young. "Design-driven LO: The discovery of new ultra long acting dibasic b2-adrenoceptor agonists." Bioorganic and Medicinal Chemistry Letters. 21(15):4612-4616. 2011

115. Cazzola, Mario, Clive Page, and Maria Gabriella Matera. "Long-acting muscarinic receptor antagonists for the treatment of respiratory disease." Pulmonary Pharmacology and Therapeutics. 26(3):307-317. 2013

116. Donohue, James F, Charles Fogarty, Jan Lotvall, Donald A. Mahler, Heinrich Worth, Arzu Yorgancioglu, Amir Iqbal, James Swales, Roger Owen, Mark Higgins, and Benjamin Kramer. "Once-Daily Bronchodilators for Chronic Obstructive Pulmonary Disease: Indacaterol Versus Tiotropium." American Journal of Respiratory and Critical Care Medicine. 182(2):155-162. 2010

117. Kim, Dennis, Mark Glaum, and Richard Lockey. "Evaluation of combination long-acting beta2 agonists and inhaled corticosteroids for treatment of asthma." Expert Opinion on Drug Metabolism and Toxicology. 5(8):933-940. 2009

118. Mansfield, Lyndon. "The future of the long-acting beta-adrenergic bronchodilators in the treatment of asthma." Allergy and Asthma Proceedings. 29(2):103-108. 2008

119. Hughes, Adam, and Lyn Jones. "Dual-pharmacology muscarinic antagonist and β2 agonist molecules for the treatment of chronic obstructive pulmonary disease." Future Medicinal Chemistry. 3(13):1585-1605. 2011

120. Loira-Pastoriza, Cristina, Julie Todoroff, Rita Vanbever. "Delivery strategies for sustained drug release in the lungs." Advanced Drug Delivery Reviews. 75:81-91. 2014

121. Y.J. Oh, J. Lee, J.Y. Seo, T. Rhim, S.H. Kim, H.J. Yoon, K.Y. Lee. "Preparation of budesonide-loaded porous PLGA microparticles and their therapeutic efficacy in a murine asthma model." Journal of Controlled Release. 150(1):56–62. 2011

122. F. Ungaro, R. d'Emmanuele di Villa Bianca, C. Giovino, A. Miro, R. Sorrentino, F. Quaglia, M.I. La Rotonda. "Insulin-loaded PLGA/cyclodextrin large porous particles with improved aerosolization properties: in vivo deposition and hypoglycaemic activity after delivery to rat lungs." Journal of Controlled Release. 135(1):25–34. 2009

123. G. De Rosa, D. Larobina, M. Immacolata La Rotonda, P. Musto, F. Quaglia, F. Ungaro. "How cyclodextrin incorporation affects the properties of protein-loaded PLGA based microspheres: the case of insulin/hydroxypropyl-β-cyclodextrin system." Journal of Controlled Release. 102(1):71–83. 2005

124. F. Ungaro, I. d'Angelo, C. Coletta, R. d'Emmanuele di Villa Bianca, R. Sorrentino, B. Perfetto, M.A. Tufano, A. Miro, M.I. La Rotonda, F. Quaglia. "Dry powders based on PLGA nanoparticles for pulmonary delivery of antibiotics: modulation of encapsulation efficiency,

release rate and lung deposition pattern by hydrophilic polymers." Journal of Controlled Release. 157(1):149–159. 2012

125. J.P. Clancy, L. Dupont,M.W.Konstan, J. Billings, S. Fustik, C.H.Goss, J. Lymp, P.Minic,A. L.Quittner, R.C. Rubenstein, K.R. Young, L. Saiman, J.L. Burns, J.R.W. Govan, B. Ramsey, R. Gupta. "Phase II studies of nebulised Arikace in CF patients with Pseudomonas aeruginosa infection." Thorax. 68(9):818–825. 2013

126. P. Meers, M. Neville, V. Malinin, A.W. Scotto, G. Sardaryan, R. Kurumunda, C. Mackinson, G. James, S. Fisher,W.R. Perkins. "Biofilm penetration, triggered release and in vivo activity of inhaled liposomal amikacin in chronic Pseudomonas aeruginosa lung infections." Journal of Antimicrobial Chemotherapy. 61(4):859–868. 2008

127. D.J. Serisier, D. Bilton, A. De Soyza, P.J. Thompson, J. Kolbe, H.W. Greville, D. Cipolla, P. Bruinenberg, I. Gonda. "Inhaled, dual release liposomal ciprofloxacin in non-cystic fibrosis bronchiectasis (ORBIT-2): a randomised, double-blind, placebo-controlled trial." Thorax 68(9):812–817. 2013

128. Y.S. Youn, M.J. Kwon, D.H. Na, S.Y. Chae, S. Lee, K.C. Lee. "Improved intrapulmonary delivery of site-specific PEGylated salmon calcitonin: optimization by PEG size selection." Journal of Controlled Release. 125(1):68–75. 2008

129. K.C. Lee, S.Y. Chae, T.H. Kim, S. Lee, E.S. Lee, Y.S. Youn. "Intrapulmonary potential of polyethylene glycol-modified glucagon-like peptide-1s as a type 2 anti-diabetic agent." Regulatory Peptide. 152(1-3):101–107. 2009

130. C. Leach, M. Kuo, B. Bueche, S. Fishburn, T. Viegas,M. Bossard, L. Guo,M. Bentley, C. Hobbs, A. Cherrington. "Modifying the pulmonary absorption and retention of proteins through PEGylation." Respiratory Drug Delivery. IX 1:69–77. 2004

131. R.W. Niven, K.L.Whitcomb, L. Shaner, L.D. Ralph, A.D. Habberfield, J.V. Wilson. "Pulmonary absorption of polyethylene glycolated recombinant human granulocyte-colony stimulating factor (PEG rhG-CSF)." Journal of Controlled Release. 32(2):177–189. 1994

132. R.W. Niven, K.L.Whitcomb, L. Shaner, A.Y. Ip, O.B. Kinstler. "The pulmonary absorption of aerosolized and intratracheally instilled rhG-CSF and monoPEGylated rhG-CSF." Pharmaceutical Research. 12(9):1343–1349. 1995

133. S.J. Koussoroplis, G. Paulissen, D. Tyteca, H. Goldansaz, J. Todoroff, C. Barilly, C.Uyttenhove, J. Van Snick, D. Cataldo, R. Vanbever. "PEGylation of antibody fragments greatly increases their local residence time following delivery to the respiratory tract." Journal of Controlled Release 187:91–100. 2014

134. F.J.C. Bayard, W. Thielemans, D.I. Pritchard, S.W. Paine, S.S. Young, P. Bäckman, P. Ewing, C. Bosquillon. "Polyethylene glycol-drug ester conjugates for prolonged retention of small inhaled drugs in the lung." Journal of Controlled Release. 171:234–240. 2013

135. R. Inapagolla, B.R. Guru, Y.E. Kurtoglu, X. Gao, M. Lieh-Lai, D.J.P. Bassett, R.M. Kannan. “In vivo efficacy of dendrimer-methylprednisolone conjugate formulation for the treatment of lung inflammation.” International Journal of Pharmaceutics. 399(1-2):140–147. 2010

136. Ryan, Gemma, Lisa M. Kaminskas, Brian D. Kelly, David J. Owen, Michelle P. McIntosh, and Christopher J. H. Porter. “Pulmonary Administration of PEGylated Polylysine Dendrimers: Absorption from the Lung versus Retention within the Lung Is Highly Size-Dependent.” Molecular Pharmaceutics. 10(8):2986-2995. 2013

137. L.M. Kaminskas, V.M. McLeod, G.M. Ryan, B.D. Kelly, J.M. Haynes,M.Williamson, N. Thienthong, D.J. Owen, C.J. Porter. “Pulmonary administration of a doxorubicin conjugated dendrimer enhances drug exposure to lung metastases and improves cancer therapy.” Journal of Controlled Release. 183:18–26. 2014

138. Xie, Yumei, Kristin L. Aillon, Shuang Cai, Jason M. Christian, Neal M. Davies, Cory J. Berkland, M. Laird Forrest. “Pulmonary delivery of cisplatin–hyaluronan conjugates via endotracheal instillation for the treatment of lung cancer.” International Journal of Pharmaceutics. 392(1-2):156-163. 2010

139. Sabatos-Peyton, Catherine, Johan Verhagen, and David C Wraith. “Antigen-specific immunotherapy of autoimmune and allergic diseases.” Current Opinion in Immunology. 22(5):609–615. 2010

140. Holmgren, Jan and Ceecil Czerkinsky. “Mucosal Immunity and Vaccines.” Nature Medicine. 11(4):545-553. 2005

141. Mestecky, J., Michael E. Lamm, Jerry R. McGhee, John Bienenstock, Lloyd Mayer and Warren Strober. Mucosal Immunology 3rd edition. Academic Press, San Diego. 2005

142. Mowat, A.M. “Anatomical basis of tolerance and immunity to intestinal antigens.” Nature Reviews Immunology. 3(4):331−341. 2003

143. Patton, John and Robert Platz. “Routes of Delivery: Case Studies: Pulmonary delivery of peptides and proteins for systemic action.” Advanced Drug Delivery Reviews. 8(2-3):179-196. 1992

144. Khan, Arshad, Jahanzeb Mudassir, Noratiqah Mohtar, Yusrida Darwis. “Advanced drug delivery to the lymphatic system: lipid-based nanoformulations.” International Journal of Nanomedicine. 8(1):2733-2744. 2013

145. Cai, Shuang, Qiuhong Yang, Taryn R. Bagby, and M. Laird Forrest. “Lymphatic drug delivery using engineered liposomes and solid lipid nanoparticles.” Advanced Drug Delivery Reviews. 63(10-11):901-908. 2011

Chapter 2

NanoClusters Surface Area Allows Nanoparticle Dissolution with Microparticle Properties for Enhanced Lung Deposition

2.1. Introduction

Corticosteroids are the first treatment option for several particular respiratory diseases including asthma as they treat the associated airway inflammation. With the prevalence of asthma increasing throughout the United States from 20 to 30 million patients over the past decade and expected to increase to almost 400 million patients worldwide in the next decade, improvements need to be made to continue to treat this growing patient population[1-3]. Another compounding factor is that a significant portion of patients (almost 50% of both children and adults) have poorly controlled asthma symptoms[1]. Improvements are necessary in the delivery of corticosteroids. The delivery methods include dry powder inhalers (DPIs), pressurized metered dose inhalers (pMDIs), and nebulizers. DPIs are increasing in usage as pMDIs use environmentally harmful propellants and nebulizers require long dosing times of 10 – 20 minutes.[4]

In current DPI corticosteroid formulations, only approximately 20% of the delivered dose reaches the lung where it elicits its therapeutic effect. The remaining 80% is deposited in the mouth, oropharynx, and throat where it is swallowed and enters systemic circulation. To counter the decreased delivery efficiency of corticosteroids, higher doses are administered to elicit the therapeutic effect and treat the patient's symptoms. The 80% that encounters first pass metabolism through the liver has 90 – 99% of the plasma levels removed, but there still remains a significant portion present that can provoke unwanted side effects[5]. These side effects and systemic delivery are of especial importance when these medications are used for children. Children have a slightly higher prevalence of asthma than adults (10% to 8%), and systemic corticosteroids are more harmful in their developing bodies. Corticosteroids influence the developing skeletal structure potentially leading to decreased bone mass, suppression of the adrenal glands, and increased bruising of the skin all of which are a major concern in children[5,6].

Aerosol delivery from DPIs depends on the particle size of the drug. Particles larger than 5 microns in diameter are typically deposited in the mouth, oropharynx, and throat due to inertial impaction, while particles smaller than 1 micron are more prone to exhalation after delivery. Only particles between 1 and 5 microns in size have the necessary properties to reach the bronchial tree and lung periphery to improve patient response[7]. There have been multiple particle engineering technologies employed to manipulate the size of drug particles to improve delivery[8-13]. There are bottom-up methods including precipitation, solid dispersions[14-16], spray drying and spray freezing into liquid[14,17-21] as well as top-down methods such as homogenization and milling[18,21-23]. Some bottom-up methods using precipitation can involve solvents[24], which add the burden of solvent removal and disposal after processing and before use by patients[25]. Spray drying allows more precise control of particle size but may be an issue if the product is thermally labile[17] or insoluble in the desired processing media. Bottom-up methods including some precipitation methods and spray freezing into liquids can produce amorphous compounds. Amorphous compounds tend to be less stable than crystalline forms and can spontaneously revert to a lower energy crystalline form. Of course, changes in drug morphology over time are not desirable and may alter the properties of the drug performance[19]. Finally, bottom-up methods can be more difficult to scale up to the large amounts needed in the pharmaceutical industry[23].

Top-down approaches include methods such as milling[21] and homogenization[23]. Milling can be further broken down into dry and wet milling[26]. Dry milling includes jet milling, which has the tendency to create surface defects, potentially increasing powder electrostatics[27]. Wet milling can reduce surface defects by allowing some recrystallization to occur[28]. One such top down technology is called NanoCrystal®, where the drug compound is milled with surfactants to create and maintain individual nanoparticles in an effort to achieve more rapid dissolution[29-31]. The strategy behind many of these techniques is to decrease particle size to increase surface

area[18,32]. One potential issue with using surfactants in aerosol formulations is that surfactants can have side effects in the lungs of patients[32].

Corticosteroids have another delivery challenge as they are poorly water soluble drugs. There are multiple clearance mechanisms in the lung that can remove the drug particles before they can elicit their effect. Mucocilliary clearance can remove undissolved particles from the upper airways as the ciliated cells lining these airways escalate the mucus lining the airways to the mouth. Macrophages patrol the alveoli region engulfing microparticles that could potentially harm these delicate cells. Increased surface area of corticosteroids should accelerate drug dissolution into the solution phase lining the lung allowing the drug to diffuse to target receptors and elicit their effect before they are removed by clearance mechanisms[33-35].

This work will analyze two poorly water soluble steroids, budesonide[36] and danazol[37] as model compounds to test increased dissolution by particle engineering by forming nanoparticle agglomerates, called NanoClusters through wet milling. Since they are agglomerates, NanoClusters[38-40] offer both micronized particle and nanoparticle properties. NanoClusters could, therefore, provide an excipient free alternative to strategies such as NanoCrystal® technology[30,31] Here, we investigate if increased surface area of NanoClusters improves dissolution of poorly water soluble compounds in comparison to micronized drug particles.

2.2. Materials and methods

2.2.1. Materials

Budesonide micronized stock (Bud) was obtained from Sicor de Mexico (Lerma, Mexico). Danazol micronized stock (Dan) was purchased from Voigt Global Distribution Inc (Lawrence, Kansas). Pluronic® F-68 was obtained from BASF (Florham, New Jersey). All

water used was deionized (DI) water from a Labconco Pro PS system. All other chemicals and materials including acetonitrile, sodium lauryl sulfate, 0.1 µm pore size Whatman nylon filters, and Beckton Dickinson 3 mL plastic syringes, were purchased from Fisher Scientific.

2.2.2. NanoCluster Synthesis by Wet Milling

Budesonide and danazol NanoCluster suspensions were synthesized using a Netzsch MiniCer Media Mill (NETZSCH Fine Particle Technology, LLC, Exton, PA). The mill was run with several predetermined process parameters including a grinder speed of 2772 rpm, a chiller unit temperature between 6 and 8°C, a mill temperature of 18°C, and a mill pressure of under 2 bar. The drug suspensions were milled using 200 µm YTZ® (yttrium treated zirconium) grinding media from Tosoh Corp., Tokyo, Japan.

Budesonide and danazol micronized stock were each suspended in nitrogen purged DI water to reduce the likelihood of oxidation during milling. Either drug (3.25 g) was added to 390 mL of nitrogen-flushed DI water. The powder was wetted by introducing drug slowly, while continuously stirring, and NanoClusters were produced by grinding with no added excipients. Both budesonide and danazol samples were collected at 5, 10, and 15 hours. Thirty mL of the suspension was collected at each time point with 10 mL deposited into three 20 mL antistatic vials. Upon completion, the remaining suspension was collected into 20 to 25 antistatic vials. Nanoparticle suspension samples were produced by milling in 0.1% (w/v) Pluronic® F-68 solution[30,31] until a mean diameter of 150 to 200 nm was achieved. Samples were immediately frozen in liquid nitrogen and maintained at a temperature of -80 °C. Samples were lyophilized for 72 hours at a temperature of -72 °C at a vacuum of <300 millitorr (VirTis Feezemobile-12XL, The Virtis Company, NY).

2.2.3. NanoCluster Particle Size and Morphology

A LEO 1550 field emission scanning electron microscope (SEM) was used to evaluate the particle size and morphology of the NanoCluster powder compared to the micronized stock and to the nanoparticle suspension[43]. Samples were sputter-coated with gold for 3 min. Dynamic light scattering (DLS) (Brookhaven Instruments Corp., ZetaPALS, Holtsville, NY) was performed to determine individual particle size comprising the agglomerates[43]. To better estimate the size of the nanoparticles and not the agglomerates, 0.5 mL of the milled suspension was diluted to 10 mL with 0.1% (w/v) Pluronic® F-68 solution. The suspension was then sonicated for 30 s at an amplitude of 20% with a microtip probe sonicator (Fisher Scientific, Sonic Dismembrator, Pittsburgh, PA) prior to analysis. The agglomerated NanoClusters were sized using micro flow imaging (MFI) (DPA 4100/4200 from Brightwell Technologies, Inc. Ottawa Canada) with Flow Microscope MVSS version 2 software. Samples were suspended in 0.01% sodium lauryl sulfate to ensure particles did not stick in the flow cell while maintaining a particle concentration of approximately 900000 counts/mL.

2.2.4. Surface Area Determination Using BET

Surface area was determined via the BET (Brunauer, Emmett and Teller) Theory using a TriStar 3000, Micrometrics Gemini 2375 V 5.01, Norcross, GA connected to a computer running Star Driver (version 2.03). The surface area for the NanoClusters was measured for all powders by nitrogen adsorption and compared to that of the micronized stock drug and nanoparticle suspension. Prior to surface area measurement, a known mass of the sample powder (120 ± 30 mg) was placed in a sample tube. Another reference tube filled with 3 mm spherical glass beads was used as a reference. Liquid nitrogen was used to maintain the sample and reference tube at low temperature to yield an accurate determination of surface area[44].

2.2.5. Determination of Degradation Using HPLC-UV

The chemical stability of the NanoCluster powder was determined by chromatographic analysis. The HPLC-UV system consisted of a Shimadzu CBM-20A system controller, LC-10AT solvent delivery pump, SPD-10A UV detector, and SIL-10AxL autoinjector. Chromatograms were acquired and analyzed using Shimadzu Class vp 7.4 software. A Kromasil C8 column (100 x 4.6 mm) was used for budesonide separation, while a Hypersil C18 (100 x 4.6 mm) was used for danazol. The powders used an isocratic system with a mobile phase of 55/45 acetonitrile/water at a flow rate of 1.1 mL/min. Detection was performed at 244 nm for budesonide, and danazol was detected at 288 nm. Samples of NanoClusters and micronized stock powder were made at a concentration of 250 µg/mL in acetonitrile and 30 µL was injected. The spectra showed a characteristic budesonide peak with a retention time of 4.55 min and a degradant peak with a retention time of 2.72 min. Danazol had a retention time of 9.2 min and a degradation peak at 6.35 min. Percent degradation was determined using the peak area of the degradant relative to the total peak area[40,41,43].

$$Degradation\ Percent = \frac{AUC\ of\ degradant}{AUC\ of\ parent\ compound}\ X\ 100$$

2.2.6. NanoCluster Crystallinity Determination Using Powder X-ray Diffraction (PXRD)

PXRD was used to determine the relative crystallinity of the NanoClusters compared to the miconized stock material. PXRD was performed using a monochromated CuKα radiation (λ= 1.54178 Å) on a Bruker Proteum Diffraction System equipped with Helios multilayer optics, an APEX II CCD detector or a Platinum 135 CCD detector and a Bruker MicroStar microfocus rotating anode x-ray source operating at 45 kV and 60 mA. The powder sample was suspended in Paratone N oil then loaded on a nylon loop. The loop was then loaded on the goniometer

where either 3 or 2, 180° 1 minute scans (based on the detector) were taken using the Bruker Apex2 V2010.3-0 software package. Scans were taken at 30°, 60° and 90° with the detector 50.0 mm away. The patterns were analyzed using the Bruker EVA powder diffraction software package version 13.0[43].

2.2.7. NanoCluster Analysis Using Differential Scanning Calorimetry (DSC)

DSC was performed to determine any thermal transitions of the NanoClusters compared to the micronized drug. DSC was performed on a Q100 DSC (TA Instruments). Approximately 3 to 5 mg of each sample was loaded into an aluminum hermetic pan. DSC was performed from 40 °C to 300 °C using a ramp of 10 °C per min for both budesonide and danazol[43].

2.2.8. Dissolution of NanoCluster Dry Powder

Dissolution was performed using a Distek 2100A dissolution tester with temperature control system. Dissolution medium was 900 mL of 0.25% sodium lauryl sulfate solution. Approximately 25 mg of powder was wetted then added to the dissolution vessels mimicking the USP Type II paddle method (37 °C $\pm$ 0.5 °C, paddle speed of 75 rpm, and paddle depth of 2.5 mm from the bottom of the vessels). Three mL samples were taken at 5, 10, 15, 20, 30, 45, and 60 minutes with dissolution medium added to replace the sample volume. Samples were immediately filtered using a 0.1 µm nylon filter to remove any undissolved drug particles and were then analyzed using HPLC-UV under the same conditions specified to determine chemical degradation[27,45].

2.3. Results and discussion

2.3.1. Wet Milling Created Nanoparticle Agglomerates

The wet milling process created nanoparticle agglomerates, called NanoClusters, which were confirmed using SEM[43]. There was a definitive decrease in particle size due to milling when compared to the stock micronized drug particles (Fig 2.1 and 2.2). The NanoClusters were in the size range of 1 to 4 µm and were composed of agglomerated drug nanoparticles approximately 200 nm in size. The micronized stock drugs were approximately 2 to 10 µm for both budesonide and danazol and were solid crystals. MFI confirmed that the typical median size or D50 of the NanoClusters was between 1 and 2 microns and decreased with milling time. The micronized stock was over 2 microns in size, slightly larger than both budesonide and danazol NanoClusters (Table 2.1 and 2.2). Samples were tested over a period of two years with a negligible change in particle size in both DLS and MFI to confirm physical stability (Table 2.1 and 2.2).

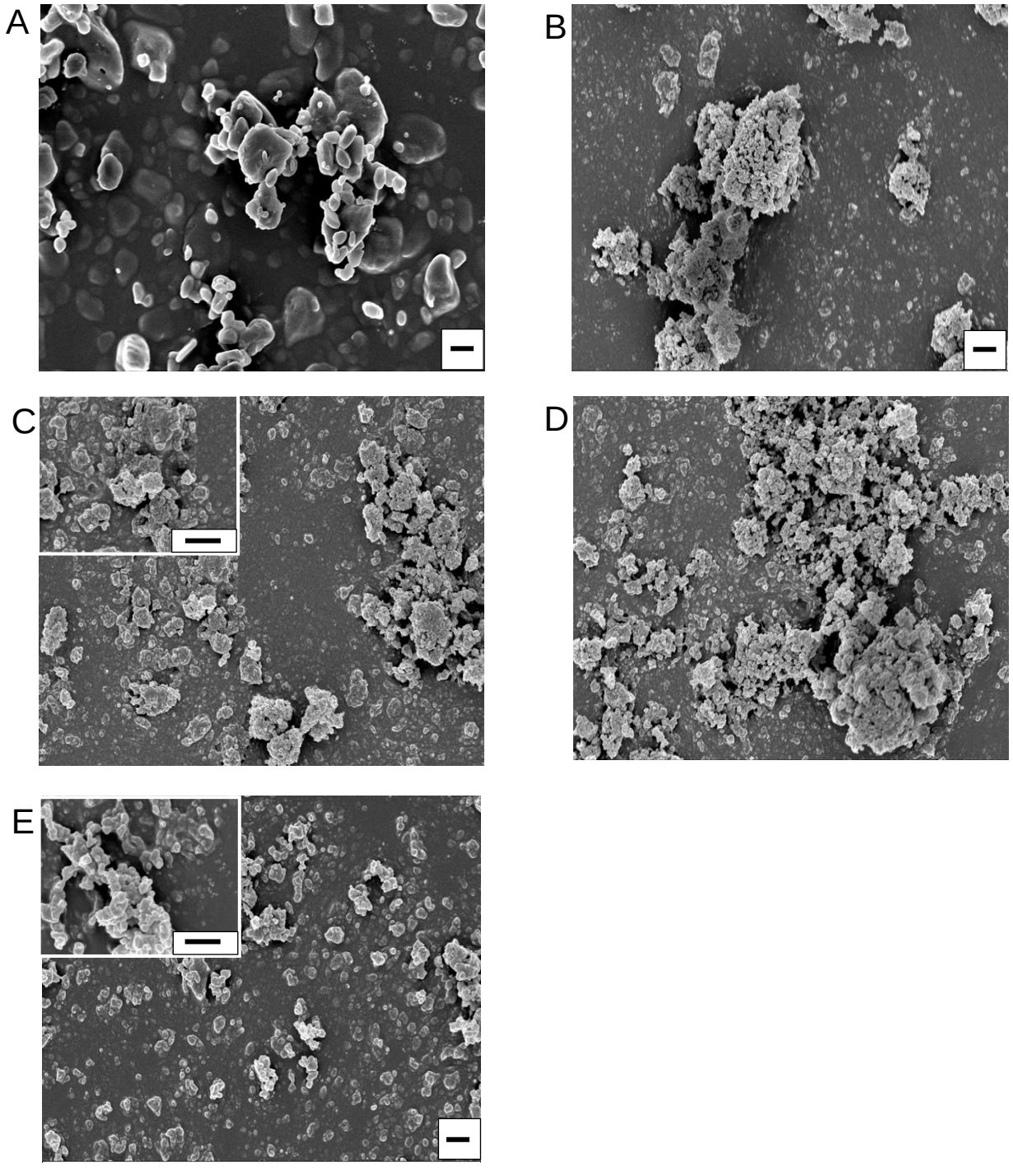

Figure 2.1: SEM images of A) micronized stock budesonide, B) NanoCluster powder milled for 5 hours, C) NanoCluster powder milled for 10 hours, D) NanoCluster powder milled for 15 hours, E) nanoparticle suspension powder milled in 0.1% (w/v) Pluronic® F-68 solution. Magnification in all is 15000x while insets in C and E are 50000x. All scale bars are 1 µm.

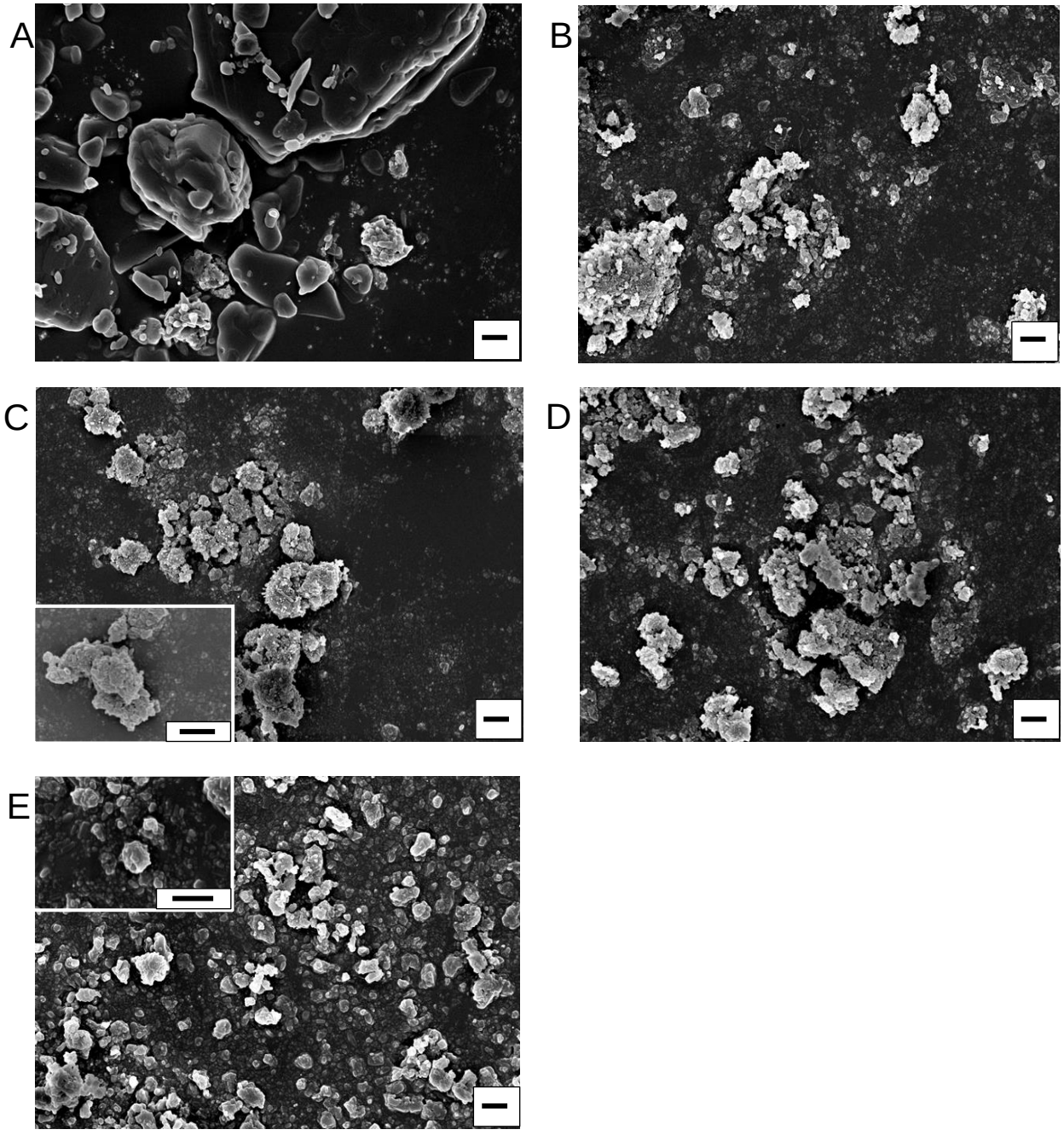

Figure 2.2: SEM images of A) micronized stock danazol, B) NanoCluster powder milled for 5 hours, C) NanoCluster powder milled for 10 hours, D) NanoCluster powder milled for 15 hours, E) nanoparticle suspension powder milled in 0.1% (w/v) Pluronic® F-68 solution, Magnification in all is 15000x while insets in C and F are 50000x. All scale bars are 1 µm.

Table 2.1: Budesonide Powder Characteristics (*Calculated from BET; **Calculated from particle size[46]). Particle size was determined using DLS while MFI was used to determine NanoCluster D50 size. NA – was not applicable.

Sample	***Degradation***	***Particle Size***	***NanoCluster D50 Size***	***BET Surface Area***	***DSC Melting Temperature***
Stock Budesonide	NA	1.7 um*	2.2 um	4.12±0.06 m^2/g	261.54 ºC
5 Hour Milled	0.20±0.02%	352.5±2.2 nm	1.5 um	33.92±0.23 m^2/g	254.03 ºC
10 Hour Milled	0.51±0.05%	373.0±5.1 nm	1.1 um	33.59±0.28 m^2/g	251.26 ºC
15 Hour Milled	0.88±0.08%	420.7±11.5 nm	1.0 um	32.42±0.12 m^2/g	248.75 ºC
Nanoparticle Suspension	NA	236.3±2.6 nm	NA	35.55 m^2/g**	254.17 ºC

Table 2.2: Danazol Powder Characteristics (*Calculated from BET; **Calculated from particle size[46]). Particle size was determined using DLS while MFI was used to determine NanoCluster D50 size. NA – was not applicable.

Sample	***Degradation***	***Particle Size***	***NanoCluster D50 Size***	***BET Surface Area***	***DSC Melting Temperature***
Stock Danazol	NA	2.5 um*	2.5 um	3.28±0.03 m^2/g	227.49 ºC
5 Hour Milled	0.39±0.20%	341.2±8.6 nm	2.0 um	25.86±0.10 m^2/g	223.82 ºC
10 Hour Milled	0.90±0.48%	354.5±10.0 nm	1.8 um	36.75±0.14 m^2/g	222.08 ºC
15 Hour Milled	1.23±0.06%	412.8±11.8 nm	1.6 um	47.65±0.26 m^2/g	220.89 ºC
Nanoparticle Suspension	NA	234.8±1.9 nm	NA	34.07 m^2/g**	224.78 ºC

The NanoClusters had a different particle morphology compared to the other samples (Fig 2.1B-D and 2.2B-D). The NanoClusters were somewhat spherical or irregular microparticles formed by agglomerated 200 – 400 nm nanoparticles with some cavities and voids left between the nanoparticles. The nanoparticle suspension samples were mostly individual nanoparticles stabilized by Pluronic® F-68 during synthesis (Fig 2.1E and 2.2E). Small agglomerates in the nanoparticle sample formed as a result of the drying process during lyophilization. The nanoparticle suspension samples had particle distribution mainly below 1 µm with a mean size of 250 nm with some reversible agglomeration occurring after lyophilization.

After an initial period of size reduction, the particles in the agglomerated NanoClusters slightly increased in size by approximately 70 nm with increasing milling time (Table 2.1 and 2.2). There are a couple of possible explanations for this increase in particle size. One would be that even though the agglomerates are sonicated in 0.1% (w/v) Pluronic® F-68 for sizing, the individual particles are still partially agglomerated together due to high surface energy. Individual particles are not being measured, just smaller agglomerates[27]. It is important to note that without the sonication step, the NanoClusters remained as agglomerated nanoparticles above the limits of DLS. Even in a dilute surfactant solution, the NanoClusters need to be subjected to intense 'shear' (sonication) to disrupt the agglomerated microparticles to generate the individual nanoparticles. Another less likely explanation is the crystals of the drug are fractured to generate the decreased particle size, and over time crystal healing or Ostwald ripening occurs increasing the particle size[9,27]. This hypothesis was not supported, however, by SEM observations. SEM micrographs do give information about the morphology of the NanoClusters. The NanoClusters have voids between the nanoparticles (Fig 2.1 and 2.2), due to the agglomeration process which forms the particles. These voids are part of the reason for the increase in surface area facilitating an increased dissolution rate.

2.3.2. Increase in Surface Area and Not a Change in Drug Properties Enhanced Dissolution

The increased dissolution rate was a direct result of the increase in surface area of the NanoCluster samples. The micronized stock materials had surface areas around 3 to 4 m^2/g, while the NanoCluster samples had surface areas of 8 times more for budesonide and even 10 to 15 times more for danazol (Table 2.1 and 2.2). There was no discernible trend for the increased surface area for budesonide as the milled NanoCluster samples all had approximately 33 m^2/g (Table 2.1). Danazol, however, showed a considerable trend with longer mill times. There was an increase of approximately 11 m^2/g for each 5 hour increase in mill time (Table 2.2) corresponding to an 8, 11, and 14 fold increase for the NanoCluster samples milled for 5, 10, and 15 hours, respectively.

The nanoparticle suspension for both compounds when run through BET surface area analysis gave a measured value of approximately 10 m^2/g. This value does not agree with the surface area of 35 m^2/g calculated from measured particle hydrodynamic radius suggesting that the Pluronic® stabilizer may have caused an anomalous reading. Comparing the calculated value with the milled NanoCluster samples shows that the surface area of the nanoparticle samples would match the respective budesonide NanoCluster samples and the 10 hour milled danazol NanoCluster sample. A calculation of nanoparticle suspension surface area (from dissolution data) is similar to the surface area of NanoClusters determined by BET (Table 2.1 and 2.2), which also supports the similar dissolution kinetics observed[47].

The increase in surface area would account for the increase in dissolution, but there were some observed differences in the trends. For budesonide, the surface area of all the milled NanoCluster samples and the nanoparticle suspension, were similar yet there were some small differences in the dissolution profiles. For danazol, there was a marketed difference in surface area between the milled NanoCluster samples, yet there was no discernible difference

in the dissolution profiles. It is possible that attaining a 'threshold' surface area is important. In other words, increasing surface area by at least 7 times compared to the micronized stock diminishes differences for these particular drugs as the surface area is further increased. Another explanation could be local saturation. After a 7 to 8 fold increase in surface area, dissolution may not increase due to a lack of local sink conditions (i.e. within the NanoCluster) or some other factor specific to these two compounds. As mentioned before, concentration gradients from the surface of the individual nanoparticles may impinge (darker regions in Fig 2.12 as dissolution profiles overlap) yielding a more complicated dissolution profile than predicted by changes in surface area alone[30]. An enhancement would still be seen in dissolution, but that enhancement may not be as extensive as expected. Finally, it is also possible that these two compounds may not exhibit a strict surface area correlation[43].

HPLC-UV analysis of NanoClusters showed that there was relatively little degradation even at extended milling times (Table 2.1 and 2.2)[43]. The percent degradation increased from 0.18% to 0.81% for budesonide and 0.21% to 1.29% for danazol as milling time progressed from 5 – 15 hours. The degradation products were determined by comparing the HPLC curves of the micronized stock and the milled products (Fig 2.3 and 2.4). Peaks were clearly separated allowing use of this approach. Previous literature results suggest the expected degradant products for budesonide to include 16α-hydroxyprednisolone and 6β-hydroxybudesonide[36] and for danazol ethisterone and 2-hydroxymethyl ethisterone[37]. These compounds are formed as hydrophobic portions of the parent compound are removed thereby decreasing hydrophobicity. The removal of these hydrophobic regions increases the exposure of more polar heteroatoms. These two chemical differences explain why the new peaks associated with degradation products have eluted earlier in the reverse phase[36,37].

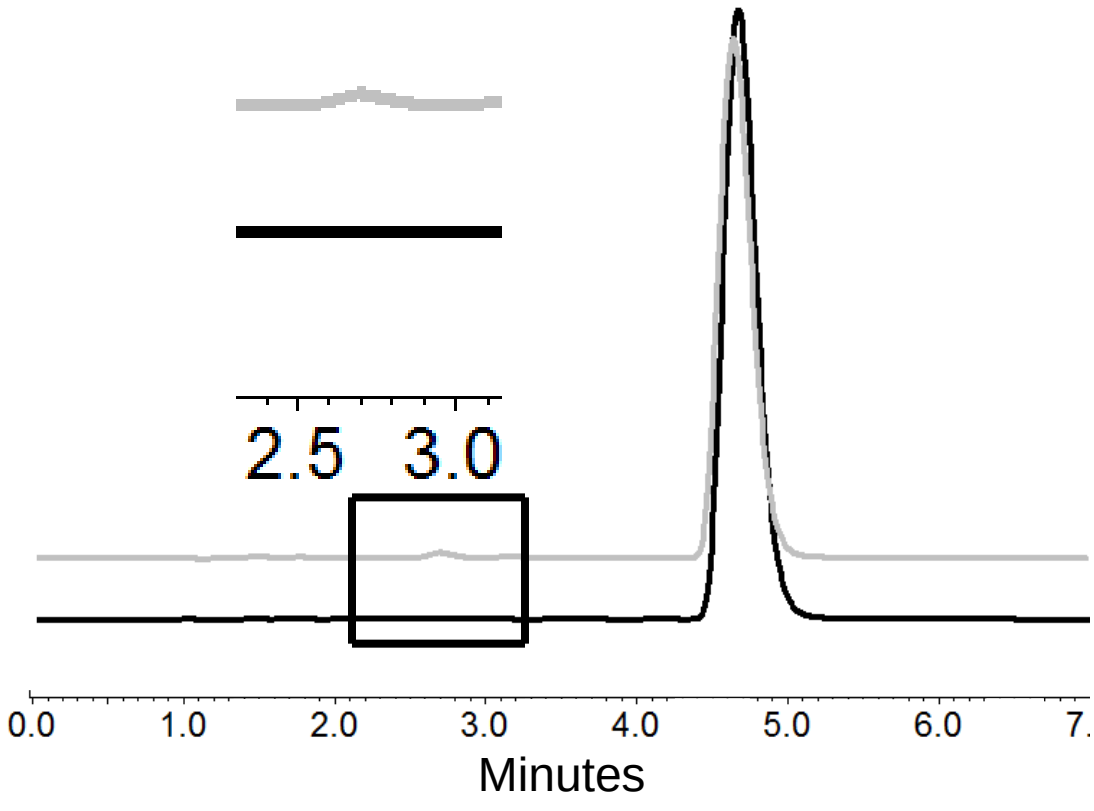

Figure 2.3: Chromatogram of budesonide. The gray trace shows the 10 hour milled NanoCluster chromatogram while the black trace shows the micronized stock form. The inset is the chromatogram portion from the black box magnified to illustrate the degradant peak.

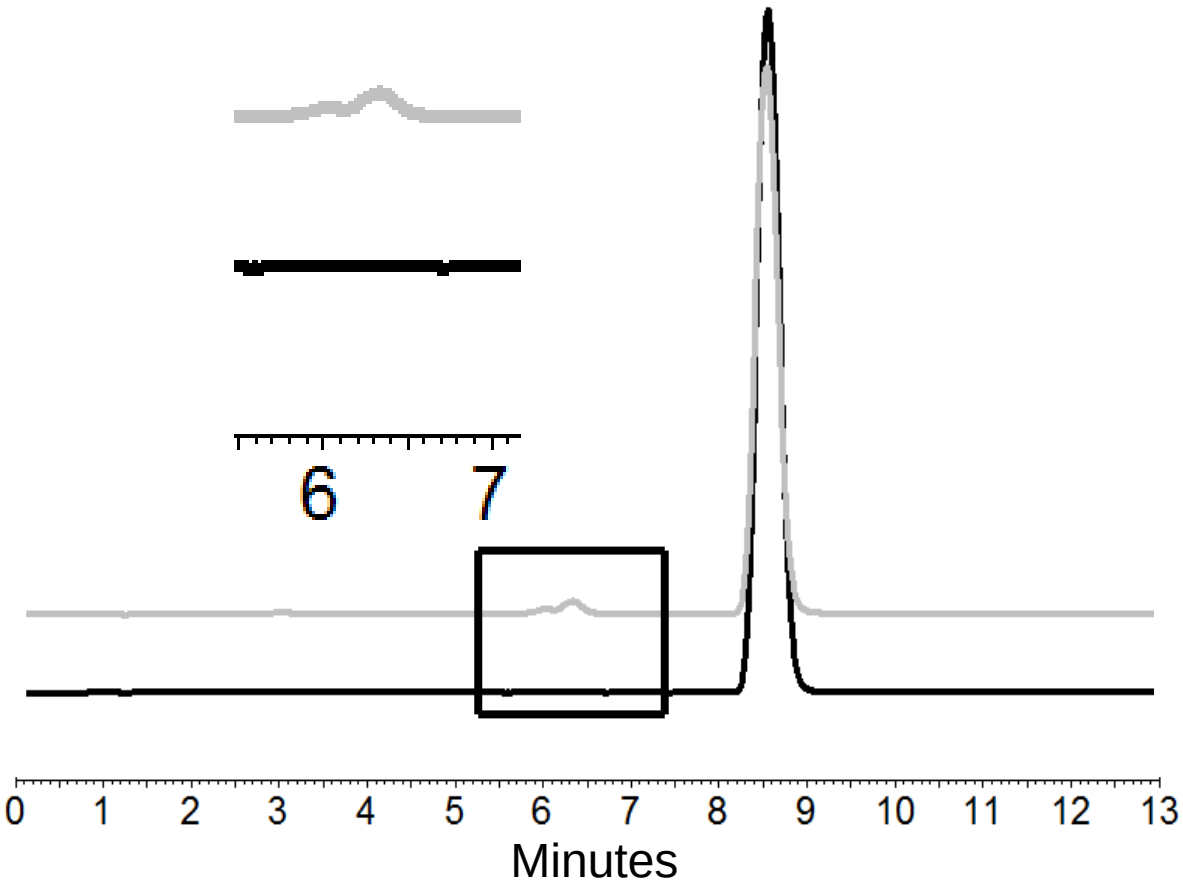

Figure 2.4: Chromatogram of danazol. The gray trace shows the 10 hour milled NanoCluster chromatogram while the black trace shows the micronized stock form. The inset is the chromatogram portion from the black box magnified to illustrate the degradant peak.

DSC thermograms illustrate the samples maintained the same relative crystallinity[43]. A decrease was seen in the melting temperature of both danazol and budesonide NanoCluster samples compared to the micronized stock material (Table 2.1 and 2.2). A decrease in melting temperature is commonly observed as particle size decreases. Since the NanoCluster samples are composed of nanoparticle agglomerates and each agglomerated microparticle has multiple crystals, heat is transported quickly in individual nanoparticles resulting in the decreased melting temperature as milling time increased. The nanoparticle powders also had decreased melting temperatures compared to the micronized stock material and had a similar melting temperature to the NanoCluster samples milled for 5 hours. The fact that the nanoparticle powder had a similar melting temperature to the NanoCluster samples and that the nanoparticle samples were

milled for a short time is further evidence that the samples have not changed crystalline form to either an amorphous solid or different polymorph. The shape of the DSC curves provided further evidence as well. The curves have a very definitive and sharp peak expected for crystalline drugs (Fig 2.5 and 2.6).

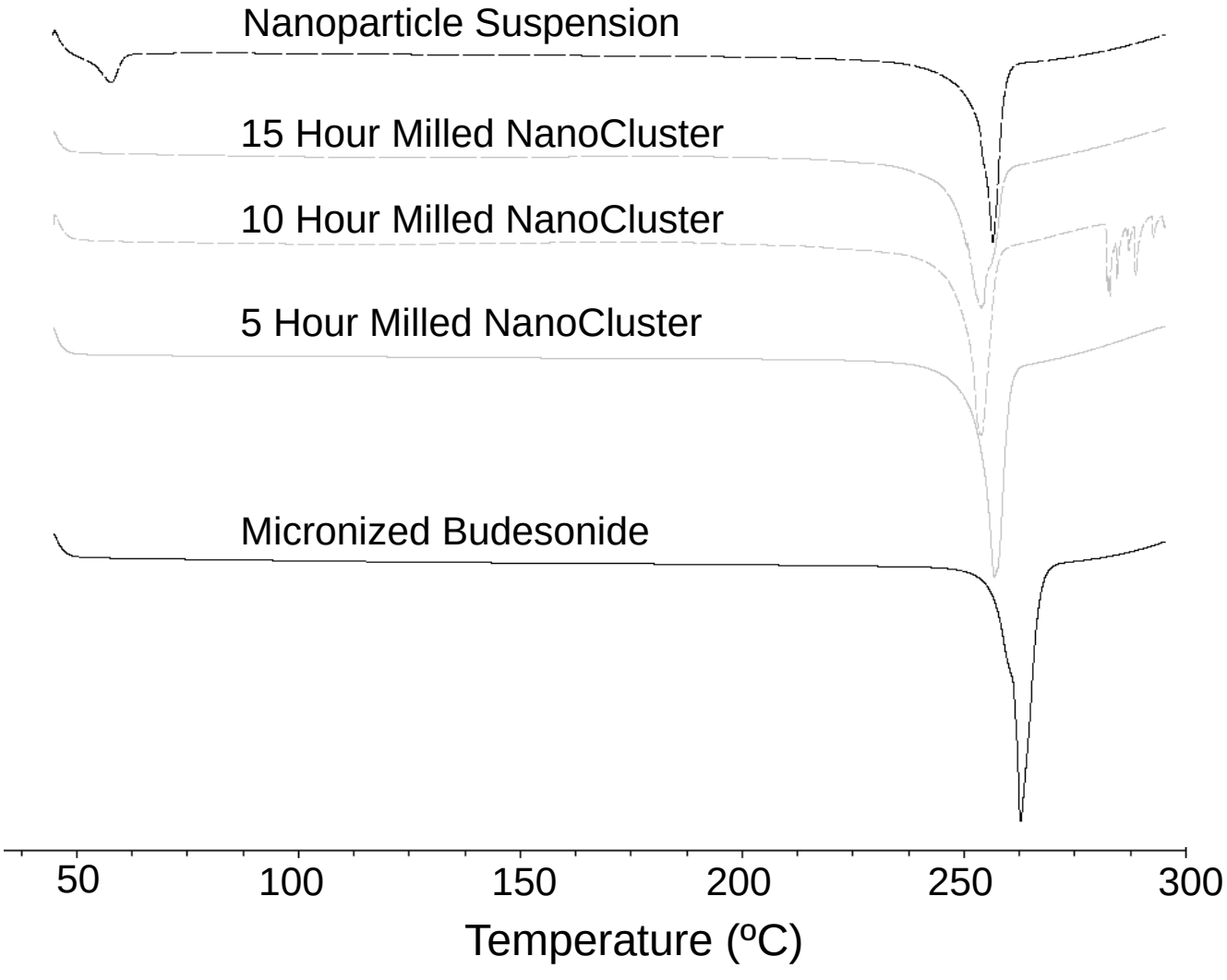

Figure 2.5: DSC of budesonide. Black solid line is the micronized stock budesonide, gray solid line is NanoCluster milled for 5 hours, gray short dash line is NanoCluster milled for 10 hours, gray long dash line is NanoCluster milled for 15 hours, and the black dash line is the nanoparticle suspension powder milled in 0.1% (w/v) Pluronic® F-68 solution.

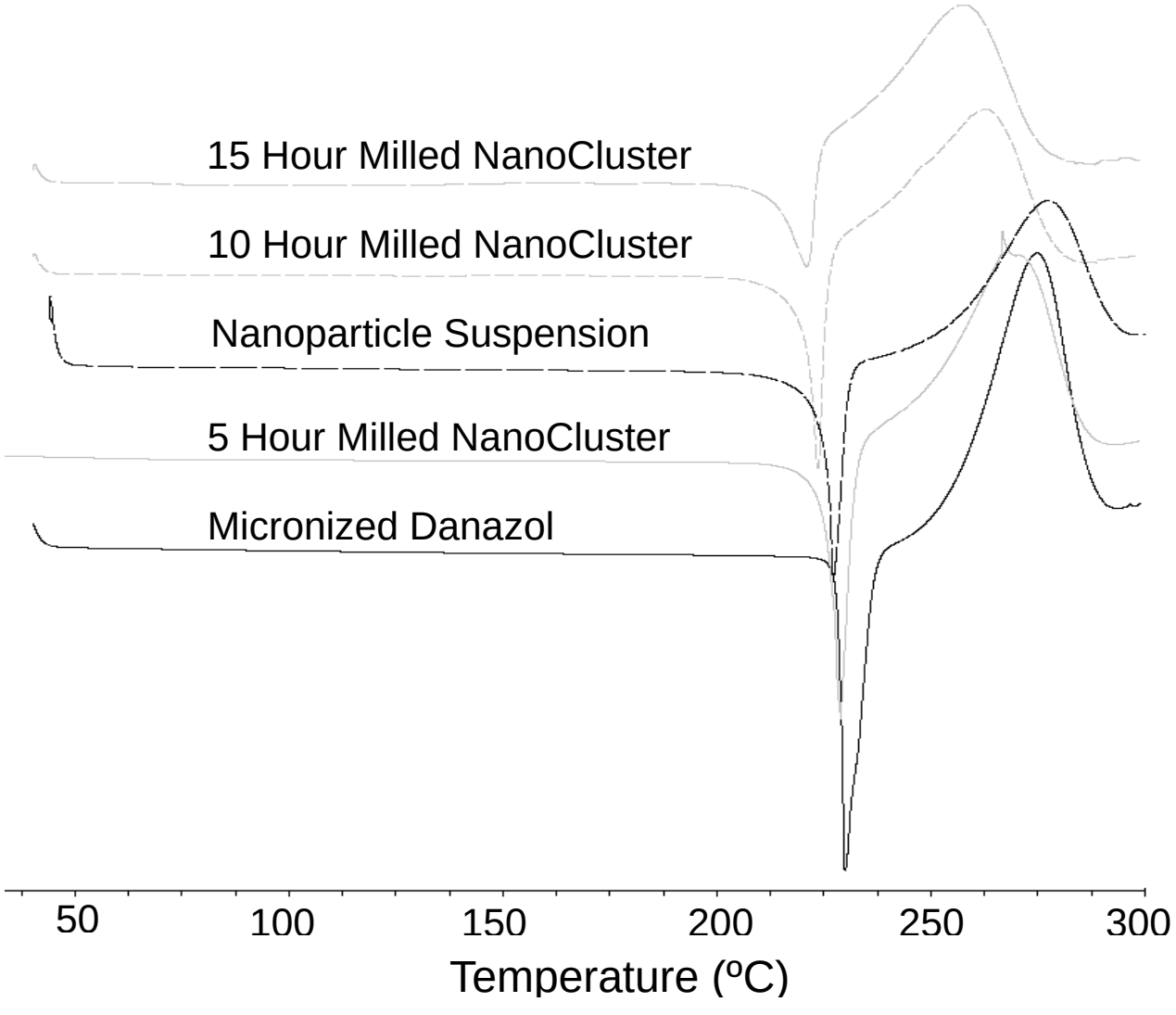

Figure 2.6: DSC of danazol. Black solid line is the micronized stock danazol, gray solid line is NanoCluster milled for 5 hours, the black dash line is the nanoparticle suspension powder milled in 0.1% (w/v) Pluronic® F-68 solution, gray short dash line is NanoCluster milled for 10 hours, and the gray long dash line is NanoCluster milled for 15 hours.

The PXRD data complements the DSC data and lends further credence to the idea that there was no change in crystallinity that caused the increase in dissolution rate (Fig 2.7 and 2.8)[43]. For budesonide, there was a decrease in peak intensity of the NanoCluster samples compared to the micronized stock budesonide. There was a small decrease in resolution from the micronized material as well compared to the NanoClusters, but the NanoClusters had a higher peak intensity compared to the nanoparticle sample. There was no trend in peak intensity that correlated to increases in mill time for the budesonide NanoClusters. The decrease in peak intensity seen particularly in Fig 2.8 can potentially be due to the nanosizing of the drug crystals. Nanosizing can produce differences in the xray scattering so the agglomerated particles can have subtle differences in scattering that may decrease intensity but peak position is more determinant. Differences due to nanosizing were also seen in the DSC thermograms, which provide further evidence that the decrease in signal intensity was not due to a change from crystalline to amorphous.

The danazol samples had a slight difference from the budesonide samples. Similar to budesonide, the micronized danazol sample had a higher peak intensity and resolution as compared to the NanoClusters. The peak height in danazol NanoCluster samples did appear to decrease in intensity with increased mill time. The 5 hour milled NanoCluster sample had a higher intensity than the nanoparticle suspension sample but the 10 hour and 15 hour milled samples had a lower peak intensity on average.

There was an interesting repeating theme as the nanoparticle samples had very similar properties to the 5 hour milled NanoCluster samples or between the 5 and 10 hour milled NanoCluster samples. For example, even though the nanoparticle samples were milled for less than half the time of the 5 hour milled NanoCluster sample, all the samples had similar melting temperatures and PXRD patterns for both budesonide and danazol. Practically speaking, shorter mill times facilitate scaling to larger amounts.

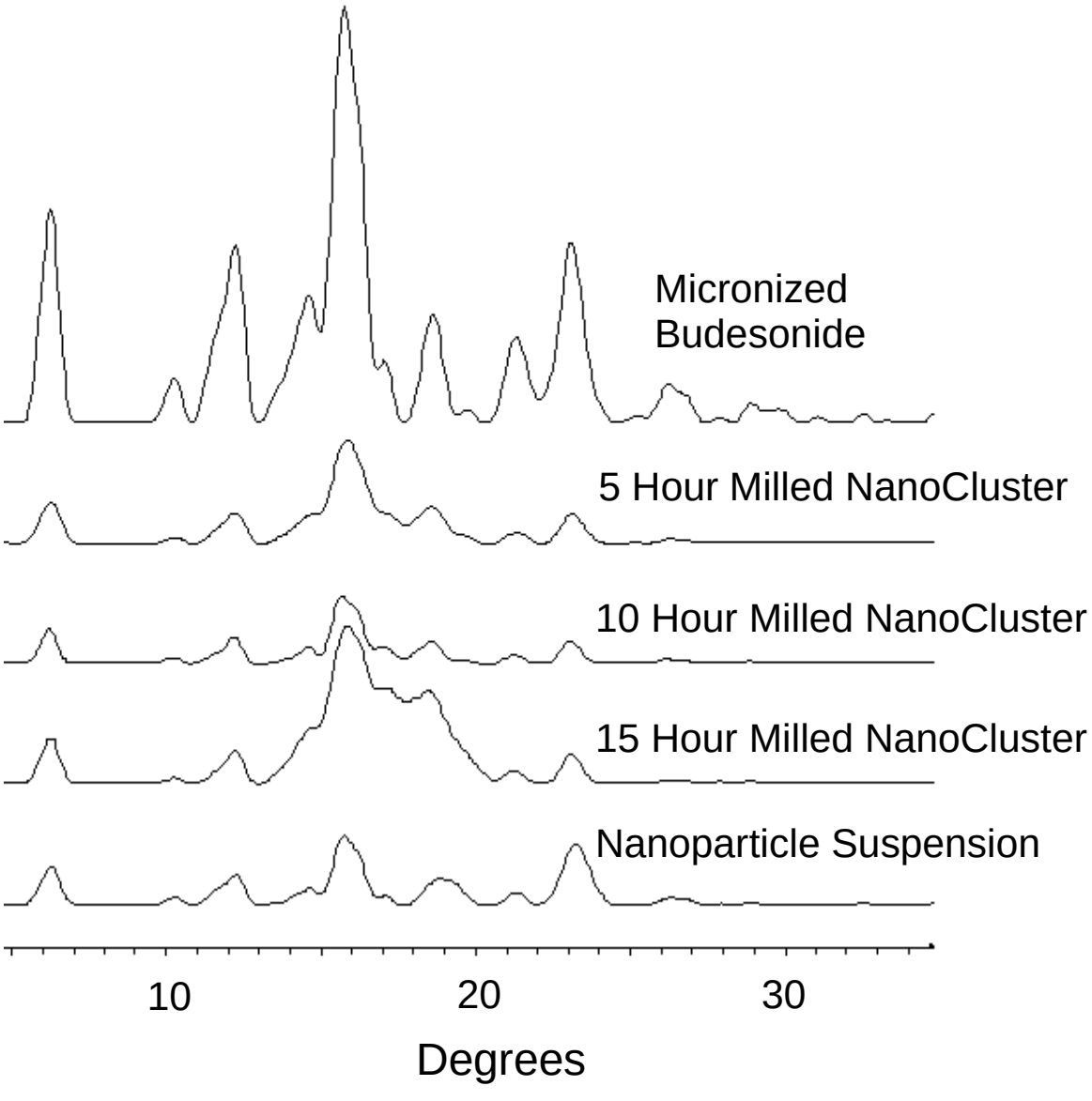

Figure 2.7: PXRD of budesonide. Micronized budesonide is the top trace followed by 5 hour milled NanoCluster, 10 hour milled NanoCluster, 15 hour milled NanoCluster, and nanoparticle suspension in descending order.

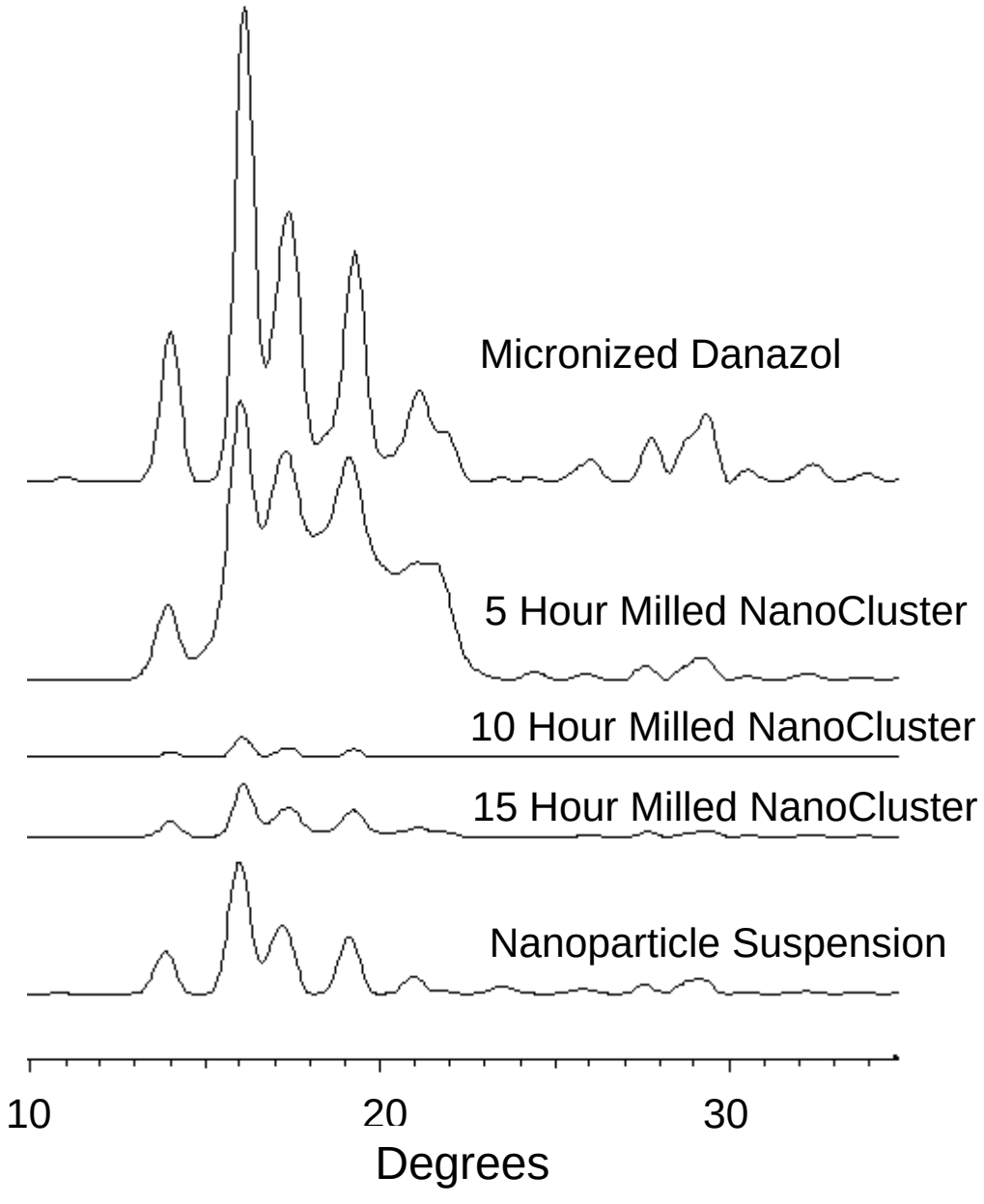

Figure 2.8: PXRD of danazol. Micronized danazol is the top trace followed by 5 hour milled NanoCluster, 10 hour milled NanoCluster, 15 hour milled NanoCluster, and nanoparticle suspension in descending order.

2.3.3. NanoClusters Enhanced Dissolution Rate

NanoCluster samples had increased dissolution rates as compared to the micronized stock drugs (Fig 2.9 and 2.10). Both budesonide and danazol micronized material gradually dissolved over the one hour study. Approximately 55% to 70% of the micronized drugs were dissolved in the first 5 minutes. Micronized budesonide and danazol samples required approximately 30 and 45 minutes, respectively, to dissolve completely. The nanoparticle suspension powder almost instantaneously dissolved and maintained a constant level over the course of the one hour study for both drugs. The NanoCluster samples had dissolution kinetics in between the two controls but were statistically more similar to the nanoparticle suspensions.

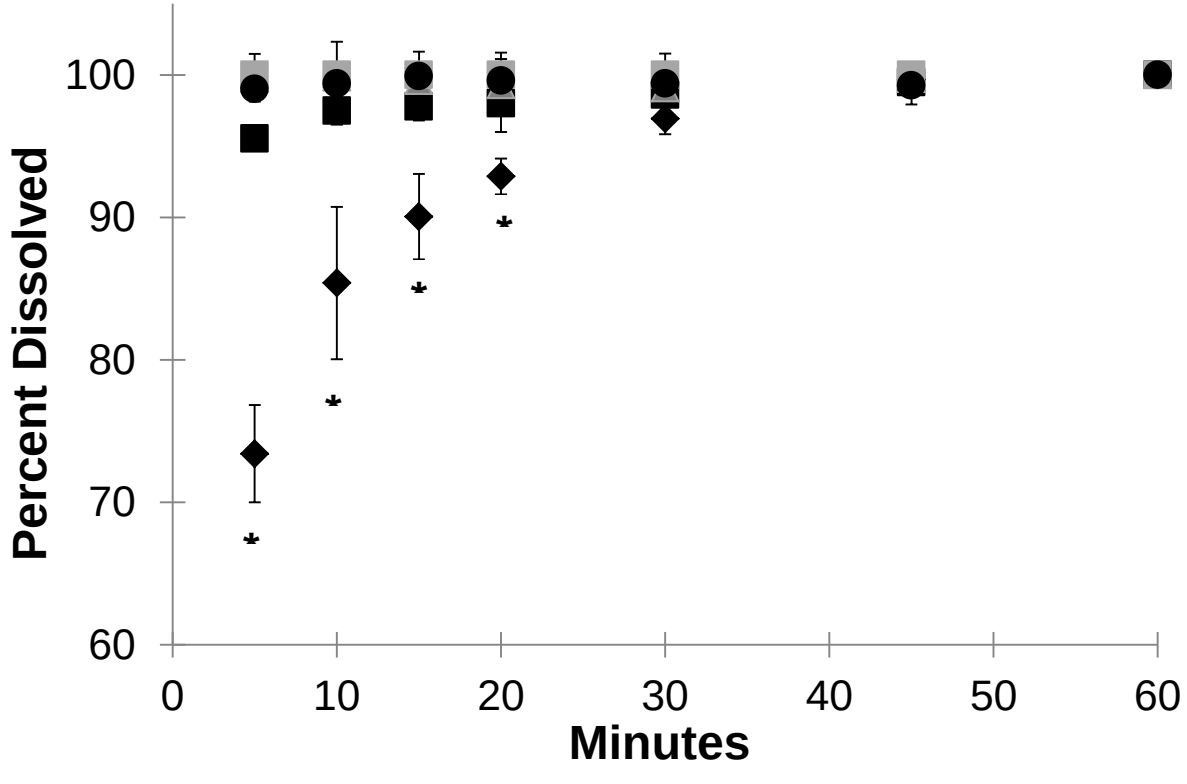

Figure 2.9: Dissolution of budesonide. Diamonds show the micronized stock while the dark squares, triangles and light squares show the NanoCluster powder milled for 5, 10, and 15 hours respectively. The circles represent the nanoparticle sample. All error bars are the standard deviations of 3 runs. Stars denote a P value < 0.05 between the micronized stock and other samples.

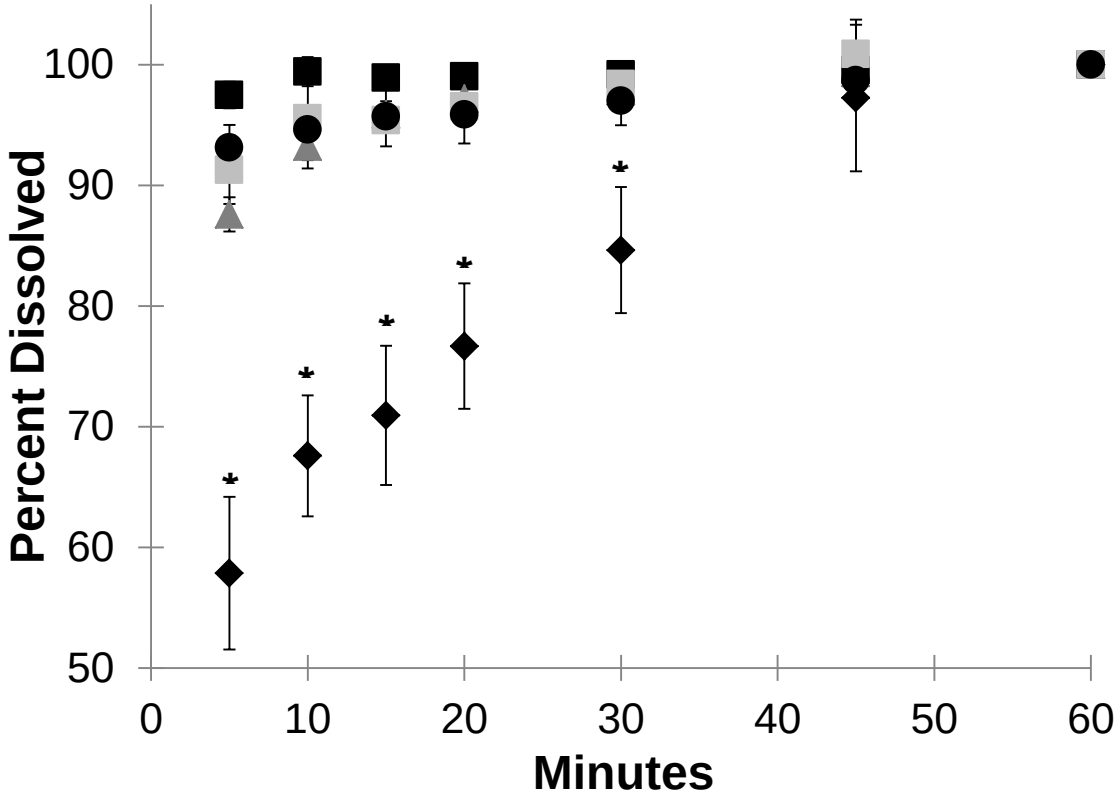

Figure 2.10: Dissolution of danazol. Diamonds show the micronized stock while the dark squares, triangles and light squares show the NanoCluster powder milled for 5, 10, and 15 hours respectively. The circles represent the nanoparticle sample. All error bars are the standard deviations of 3 runs. Stars denote a P value < 0.05 between the micronized stock and other samples.

For budesonide, there appeared to be a minor correlation between NanoCluster milling time and dissolution rate. The NanoCluster sample milled for 5 hours appeared to have less drug dissolved in the first 15 minutes compared to the NanoCluster sample milled for 10 hours, which was lower than the NanoCluster sample milled for 15 hours by a similar margin. Differences in these dissolution rates, however, were not statistically significant according to a paired T-test. NanoCluster samples milled for 15 hours had a higher dissolution rate than 5 hour milled NanoClusters up to 30 minutes. For danazol, there did not appear to be any differences between the milled NanoCluster samples. There was a small gradual increase (about 10%) in concentration with the NanoCluster samples milled for 10 and 15 hours showing a similar trend to the increase seen in comparison to the micronized stock. These differences again were not significant. Overall, the NanoCluster samples had faster dissolution rates compared to the micronized stock and similar to the nanoparticle suspension, but differences between the different NanoCluster mill times were not significant.

The next step was to model the dissolution profiles to see if they followed any previous models (Table 2.3 and Fig 2.11). The Higuchi model is the classical standard and follows a $\sqrt{t}$ dissolution model as seen in Eqn 2.1, but it was originally developed to describe the transport from a thin film into the skin. The Higuchi model is a macroscopic model that does not apply to our microscopic system and does not have the same geometry as our system. Thus the predicted dissolution profile is far below the observed dissolution profiles (Fig 2.11)[45].

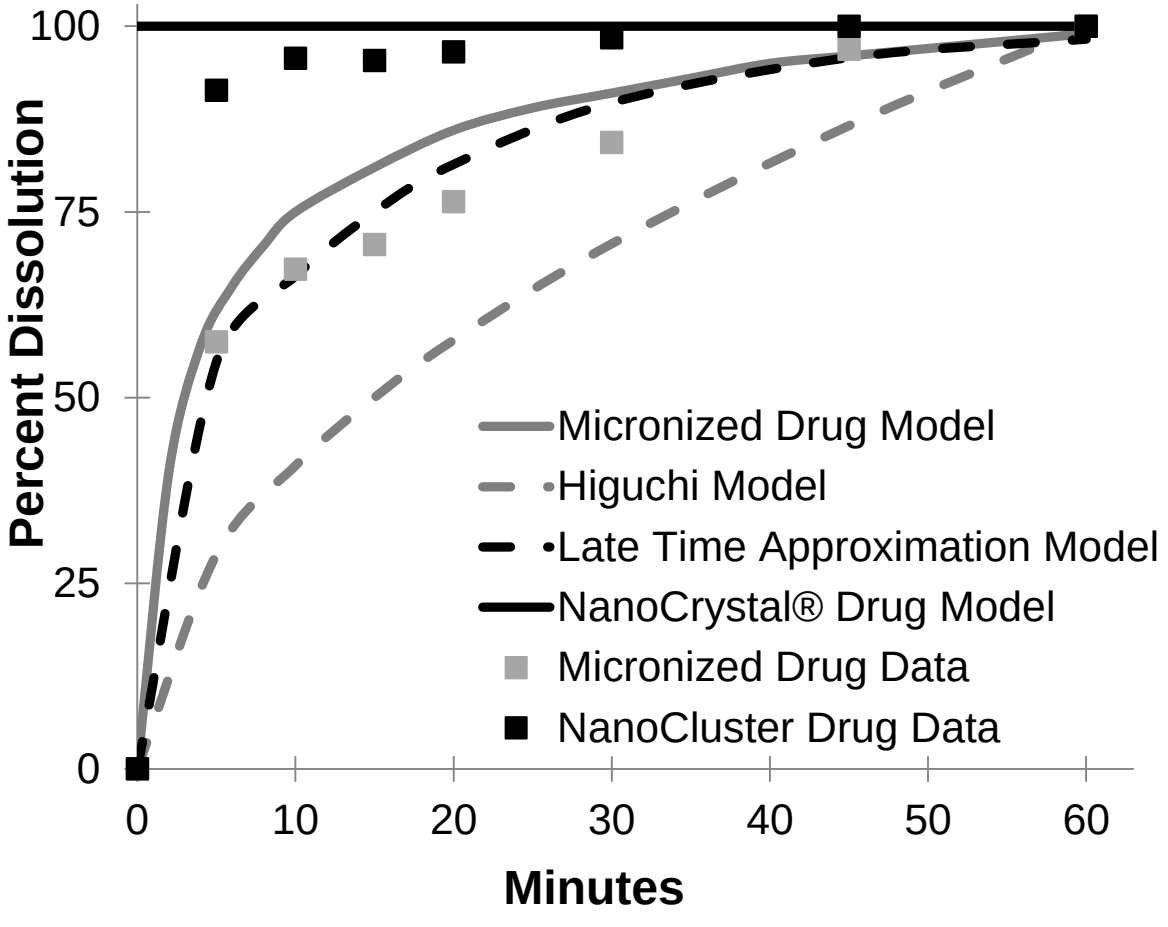

Figure 2.11: Dissolution models to represent micronized stock and NanoCluster dissolution profiles. Four models are included – two macroscopic models (Higuchi and Late Time Approximation) and two microscopic models (Micronized Drug and NanoCrystal® Drug). The two microscopic models better represent the data.

Further refinements of the Higuchi dissolution model were made by Peppas, who included multiple geometries including spheres and cylinders as drug release systems. Peppas solved for the dissolution from a sphere (Eqn 2.3)[42]. This equation was developed for tablets and formulations on a macroscopic scale, and when applied to the microparticles or nanoparticles used here, fails in part due to the smaller scale and irregular surface area of the NanoCluster system[42]. The last model used here was developed by Siepmann[48]. This model

was developed to describe release from several different drug carrier systems including drug reservoirs, monolithic solutions, or monolithic dispersions. The monolithic solution, which more closely resembles our NanoClusters samples as it is a sphere of homogenously dispersed drug with no exterior coating. The full model is the same as the system developed by Peppas (Eqn 2.3). The Siepmann model, however, provides a short time (less than 40% of drug released – Eqn 2.4) and a late time (more than 60% of drug released – Eqn 2.6) approximation for drug release. Again, using this model of late time approximation as the lowest amount of drug measured was 57% released, did not properly model NanoCluster dissolution kinetics. The major issue with this model, as with the previous two, is that this model targets macroscopic systems such as a tablet or capsule containing drug. As the system becomes smaller for micro and nanoparticles, the decreased radius skews the equations leading to inaccurate results[42]. In Fig 2.11, the Siepmann model is shown to have a good fit but that requires falsely inflating of the size of the particle, increasing it by 1000 fold to achieve this close fit.

Other models offer a better fit that can provide further explanation of this data. There are several models with NanoCrystal® technology which is similar to the nanoparticle suspension. A model based on two different processing methods: jet milled and NanoCrystal® was previously reported[45]. The reported jet milled product is very similar to the micronized stock used here with a median particle size of 3 µm and a distribution where 90% of the product is between 2 – 10 µm. The jet milled product has a similar size range as well to our milled NanoCluster providing a reasonable starting point to model dissolution of both the micronized stock and NanoClusters. The reported NanoCrystal® model has almost constant dissolution throughout time in the model. The difference in surface areas between the jet milled and NanoCrystal® was 8-9 fold. The jet milled model very closely traces our micronized stock profile with a slight overestimation but stays within 5% throughout the length of the study and model.

The more interesting observation occurs with the milled NanoClusters. Even though the NanoClusters have a similar geometric size to the jet milled product they have a similar dissolution profile to NanoCrystal® throughout most of the model. The NanoClusters have a similar increase in surface area compared to the micronized stock when contrasting the reported modeling of NanoCrystal® compared to the jet milled product. The only difference is in the early time frame which may be due to several factors.

Table 2.3: Dissolution models and governing equations

Model	Main Dissolution Equation	Other Equations	Variables	Assumptions
Classical Higuchi[45]	$Mt = k\sqrt{t}$ Eqn 2.1	$k = A\sqrt{2CiDCs}$ Eqn 2.2	Ci = initial concentration Cs = drug solubility A = surface area D = diffusion coefficient t = time Mt = released drug	1. Thin polymer film 2. Constant D 3. Minimal edge effects 4. Higher drug concentration than solubility 5. Homogenous drug dispersion
Higuchi – Peppas Derivation [42]	$Mt = 1 - \frac{6}{\pi^2}\sum_{n=1}^{\infty}\frac{1}{n^2}exp^{\frac{-Dn^2\pi^2t}{a^2}}$ Eqn 2.3	$Mt = 6\sqrt{\frac{Dt}{\pi a^2}} - 3\frac{Dt}{a^2}$ Eqn 2.4 (short time approximation)	a = radius of sphere D = diffusion coefficient t = time n = diffusional exponent characteristic of release mechanism Mt = released drug	1. Constant D 2. 1 dimensional radial release 3. Sink boundary conditions 4. Short term approx. only for first 40% of drug released
Siepmann [48]	$Mt = 1 - \frac{6}{\pi^2}\sum_{n=1}^{\infty}\frac{1}{n^2}exp^{\frac{-Dn^2\pi^2t}{a^2}}$ Monolithic solution $Mt = -\frac{3D}{R^2}\frac{Cs}{Ci}t$ Eqn 2.5 Monolithic Dispersion	$Mt = 1 - \frac{6}{\pi^2}exp\frac{-Dt\pi^2}{R^2}$ Eqn 2.6 (late time approximation)	Ci = initial concentration Cs = drug solubility a = radius of sphere D = diffusion coefficient R = radius of sphere t = time Mt = released drug	1. Sink conditions 2. Constant D 3. Drug transport in system is rate limiting 4. Homogenous drug distribution 5. Late time after 60% of drug released

One cause that could be simply not enough data points were collected during the early time phase (the first ten minutes). Another factor could be the NanoCluster microenvironment as illustrated in Fig 2.12. With the micronized stock and nanoparticle suspension, there may be well defined water contact with the free surface of drug particles allowing an approximation that sink conditions are maintained at all free surfaces. Because sink conditions can be maintained, the concentration profiles in gray are maintained allowing for simple modeling of dissolution from the particle surface (Fig 2.12A and 2.12C). Since NanoClusters are comprised of agglomerated nanoparticles, the space between the nanoparticles could experience a high local concentration that approaches or exceeds saturation. Due to the interplay of dissolution from adjacent surfaces, local concentration gradients could be affected. This complexity is difficult to model and may help explain the differences seen in the early time frame. As the particles continue to dissolve, the particles shrink providing a larger space between the individual particles thus reducing the impact of impinging concentration profiles allowing the model to capture the dissolution more accurately[30].

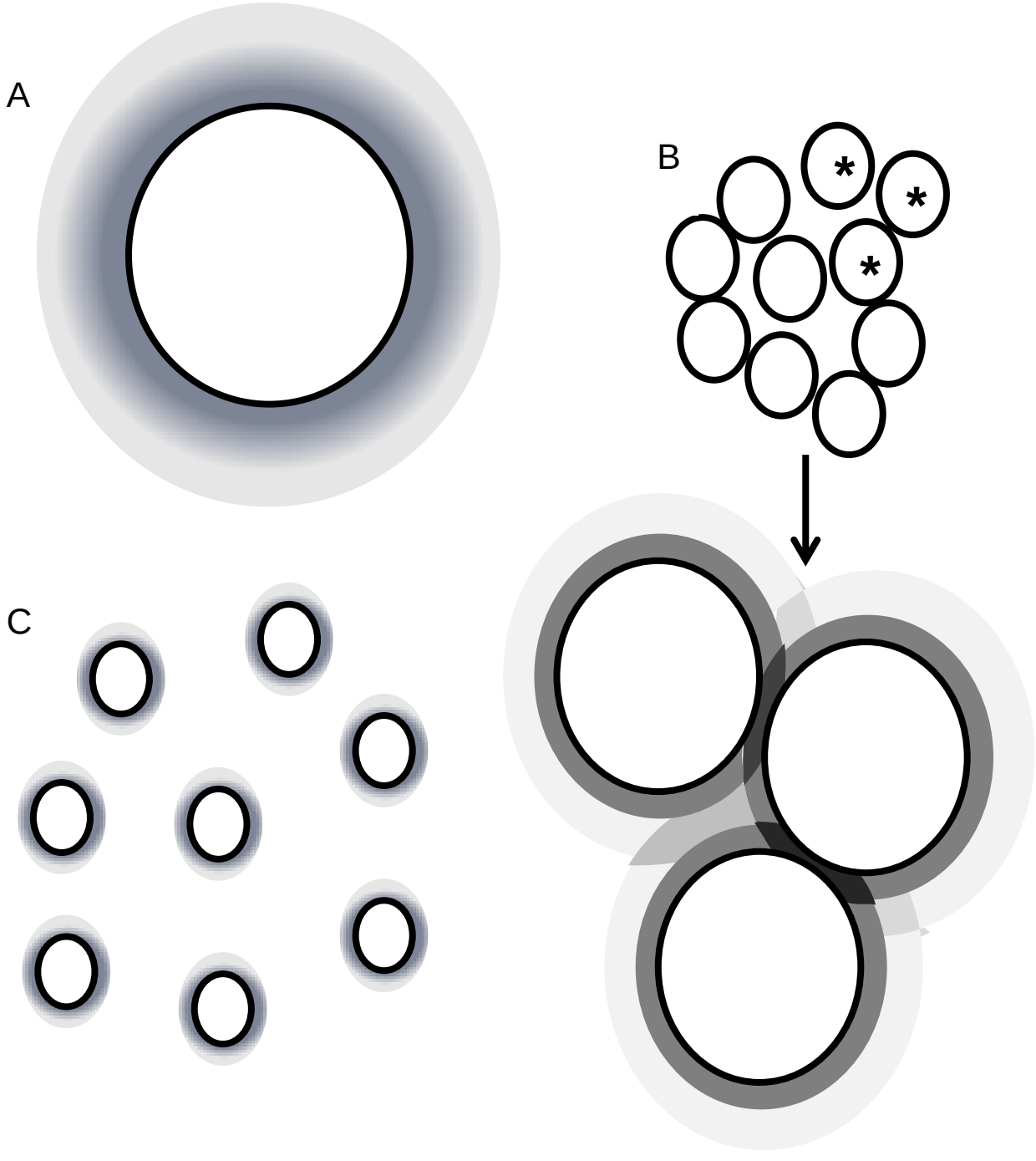

Figure 2.12: Models in black of A) micronized stock drug, B) milled NanoCluster, and C) nanoparticle suspension. Grey represents dissolution gradients from particles. Micronized stock in A and nanoparticle suspension in C have well defined concentration profiles. NanoCluster sample in B shows in the inset (enlargement of the three starred particles) that due to the individual particles proximity, the concentration gradient can overlap making an unknown internal concentration complicating the profile.

2.4. Conclusion

Corticosteroids are the standard treatment for asthma, but there are several challenges with their formulations. DPI formulations are gaining in popularity but have their own delivery difficulties associated with particle size deposition and delivering the formulation to the lung, as typically only 20% enters into the lung. Multiple particle engineering strategies have been employed to address these issues including wet milling, which was utilized to create nanoparticle agglomerates called NanoClusters. By increasing the dissolution rate of these typically poorly water soluble compounds, they are more likely to enter solution before they can be cleared by any of the multiple transport mechanisms in the lungs. NanoClusters yielded faster and more complete dissolution compared to micronized drug and had dissolution kinetics similar to nanoparticle suspension samples. The increased dissolution kinetics was theorized to be from an increase in surface area and not due to a change in crystalline form as demonstrated by DSC and PXRD analysis. By processing poorly water soluble drugs into NanoClusters, increased dissolution kinetics can be achieved using these high surface area micron-sized drug particles without the need for excipients.

References

1. Masoli, M. “Global Initiative for Asthma (GINA) program: the global burden of asthma: executive summary of the GINA Dissemination Committee report.” Allergy. 59(5):469-478. 2004

2. “Asthma in the US." Center for Disease Control and Prevention. U.S. Department of Health and Human Services. May 2011.

3. Center for Disease Control. “National Surveillance of Asthma: United States, 2001–2010.” Series 3, Number 35. 2012

4. Kleinstreuer, C, Z. Zhang, and J.F. Donohue. “Targeted Drug-Aerosol Delivery in the Human Respiratory System.” Annual Review of Biomedical Engineering. 10:195–220. 2008

5. Lipworth and Jackson. Safety of Inhaled and Intranasal Corticosteroids. Drug Safety. 23(1):11-33. 2000

6. Deshmukh CT. “Minimizing side effects of systemic corticosteroids in children.” Indian Journal of Dermatology, Venereology and Leprology. 73(4):218-221. 2007

7. Patton, John and Peter Byron. “Inhaling medicines: delivering drugs to the body through the lungs.” Nature Reviews: Drug Discovery. 6(1):67-74. 2007

8. Chow, Albert, Henry Tong, Pratibhash Chattopadhyay, and Boris Shekunov. “Particle Engineering for Pulmonary Drug Delivery.” Pharmaceutical Research. 24(3):411-437. 2007

9. Burapapadh, Kanokporn, Hirofumi Takeuchi, Pornsak Sriamornsak. “Novel pectin-based nanoparticles prepared from nanoemulsion templates for improving in vitro dissolution and in vivo absorption of poorly water-soluble drug.” European Journal of Pharmaceutics and Biopharmaceutics. 82(2):250-261. 2012

10. Raseneck and Muller. “Dissolution Rate Enhancement by in Situ Micronization of Poorly Water Soluble Drugs.” Pharmaceutical Research. 19(12):1894-1900. 2002

11. Vogt, Markus, Klaus Kunath, Jennifer B. Dressman. “Dissolution improvement of four poorly water soluble drugs by cogrinding with commonly used excipients.” International Journal of Pharmaceutics and Biopharmaceutics. 68(2):330-338. 2008

12. Edlund, U, A.-C. Albertsson. “Degradable Polymer Microspheres for Controlled Drug Delivery.” Advances in Polymer Science. 157:67-112. 2002

13. Maulvi, Furqan A., Sonali J. Dalwadi, Vaishali T. Thakkar, Tejal G. Soni, Mukesh C. Gohel, Tejal R. Gandhi. “Improvement of dissolution rate of aceclofenac by solid dispersion technique.” Powder Technology. 207(1-3):47-54. 2011

14. Hu, Jiahui, Keith P. Johnston, Robert O. Williams, III. “Rapid dissolving high potency danazol powders produced by spray freezing into liquid process.” International Journal of Pharmaceutics. 271(1-2):145-154. 2004

15. Chen, Xiaoxia, Jason Vaughn, Miguel Yacaman, Robert Williams III, Keith Johnston. “Rapid Dissolution of High-Potency Danazol Particles Produced by Evaporative Precipitation into Aqueous Solution.” Journal of Pharmaceutical Sciences. 93(7):1867-1878. 2004

16. Rogers, True, Keith P. Johnston, and Robert O. Williams III. “Physical Stability of Micronized Powders Produced by Spray-Freezing into Liquid (SFL) to Enhance the Dissolution of an Insoluble Drug.” Pharmaceutical Development and Technology. 8(2):187-197. 2003.

17. Hu, Jiahui, True L. Rogers, Judith Brown, Tim Young, Keith P. Johnston, and Robert O. Williams III “Improvement of Dissolution Rates of Poorly Water Soluble APIs Using Novel Spray Freezing into Liquid Technology.” Pharmaceutical Research. 19(9):1278-1284. 2002

18. Li, Chan, Caixia Li, Yuan Le, Jian-Feng Chen. “Formation of bicalutamide nanodispersion for dissolution rate enhancement.” International Journal of Pharmaceutics. 404(1-2):257-263. 2011

19. True L. Rogers, Andrew C. Nelsen, Marazban Sarkari, Timothy J. Young, Keith P. Johnston, and Robert O. Williams, III. Enhanced Aqueous Dissolution of a Poorly Water Soluble Drug by Novel Particle Engineering Technology: Spray-Freezing into Liquid with Atmospheric Freeze-Drying.” Pharmaceutical Research. 20(3):485-493. 2003

20. Pilcer, Gabrielle, Karim Amighi. “Formulation strategy and use of excipients in pulmonary drug delivery.” International Journal of Pharmaceutics. 392(1-2):1-19. 2010

21. Jan Möschwitzer. “Nanotechnology:Particle Size Reduction Technologies in the Pharmaceutical Development Process.” Particle Sizing. April 2010 54-59

22. Peng Liu, Xinyu Rong, Johanna Laru, Bert van Veen, Juha Kiesvaara, Jouni Hirvonen, Timo Laaksonen, Leena Peltonen. “Nanosuspensions of poorly soluble drugs: Preparation and development by wet milling.” International Journal of Pharmaceutics. 411(1-2):215-222. 2011

23. Carr, Adam G., Raffaella Mammucari, Neil R. Foster. “Particle formation of budesonide from alcohol-modified subcritical water solutions.” International Journal of Pharmaceutics. 405(1-2):169-180. 2011

24. Javadzadeh, Yousef, Leila Musaalrezaei, Ali Nokhodchi. “Liquisolid technique as a new approach to sustain propranolol hydrochloride release from tablet matrices.” International Journal of Pharmaceutics. 362(1-2):102-108. 2008

25. Jinno, Jun-ichi, Naoki Kamada, Masateru Miyake, Keigo Yamada, Tadashi Mukai, Masaaki Odomi, Hajime Toguchi, Gary G. Liversidge, Kazutaka Higaki, Toshikiro Kimura. “In vitro–in vivo correlation for wet-milled tablet of poorly water-soluble cilostazol.” Journal of Controlled Release. 130(1-2):29-37. 2008

26. Sugimoto, Shohei, Toshiyuki Niwa, Yasuo Nakanishi, and Kazumi Danjo. “Novel Ultra-Cryo Milling and Co-grinding Technique in Liquid Nitrogen to Produce Dissolution-Enhanced Nanoparticles for Poorly Water-Soluble Drugs.” Chemical and Pharmaceutical Bulletin. 60(3):325-333. 2012

27. Merisko-Liversidge, Elaine, Gary G. Liversidge. “Nanosizing for oral and parenteral drug delivery: A perspective on formulating poorly-water soluble compounds using wet media milling technology.” Advanced Drug Delivery Reviews. 63(6): 427-440. 2011

28. Liversidge, Gary G., Kenneth C. Cundy. “Particle size reduction for improvement of oral bioavailability of hydrophobic drugs: I. Absolute oral bioavailability of nanocrystalline danazol in beagle dogs.” International Journal of Pharmaceutics. 125(1):91-97. 1995

29. Khan, K A and C T Rhodes. “Water-sorption Properties of Tablet Disintegrants.” Journal of Pharmaceutical Sciences. 64(3):447-451. 1975

30. Merisko-Liversidge, Elaine, Gary G. Liversidge. “Drug Nanoparticles: Formulating Poorly Water-Soluble Compounds.”Toxicologic Pathology. 36(1):43-48. 2008

31. Tanaka, Yusuke, Mitsugi Inkyo, Ryoko Yumoto, Junya Nagai, Mikihisa Takano, and Shunji Nagata. “Evaluation of In Vitro Dissolution and In Vivo Oral Absorption of Drug Nanopowders Prepared by Novel Wet-Milling Equipment.” Current Nanoscience. 6(6):571-576. 2010

32. Baba, Koichi and Kohji Nishida. “Calpain inhibitor nanocrystals prepared using Nano Spray Dryer B-90.” Nanoscale Research Letters. 7(436). 2012

33. Bailey, Mark, Cory Berkland. “Nanoparticle Formulations in Pulmonary Drug Delivery.” Medicinal Research Reviews. 29(1):196-212. 2008

34. Smyth, H.D.C. and A.J. Hickey. Controlled Pulmonary Drug Delivery. Springer Publishing, New York, New York. 2011

35. Patton, John, C. Simone Fishburn, and Jeffry G. Weers. “The Lungs as a Portal of Entry for Systemic Drug Delivery.” Proceedings of the American Thoracic Society. 1:338-334. 2004

36. Szefler, Stanley. “Pharmacodynamics and pharmacokinetics of budesonide: A new nebulized corticosteroid.” Journal of Allergy and Clinical Immunology. 104(4 Pt 2):175-83. 1999

37. Potts, GO, HP Schane, and J Edelson. “Pharmacology and Pharmackinetics of Danazol.” Drugs. 19(5):321-330. 1980

38. Aillon, Kristin L., Nashwa El-Gendy, Connor Dennis, Jeffrey P. Norenberg, Jacob McDonald, and Cory Berkland. Iodinated NanoClusters as an Inhaled Computed Tomography Contrast Agent for Lung Visualization.” Molecular Pharmaceutics. 7(4):1274-1282. 2010

39. El-Gendy, Nashwa, Shan Huang, Parthiban Selvam, Pravin Soni, Cory Berkland. “Development of Budesonide NanoCluster Dry Powder Aerosols: Formulation and Stability.” Journal of Pharmaceutical Sciences. 101(9):3445-3455. 2012

40. El-Gendy, Nashwa, Shan Huang, Parthiban Selvam, Pravin Soni, Cory Berkland. Development of Budesonide NanoCluster Dry Powder Aerosols: Processing.” Journal of Pharmaceutical Sciences. 101(9):3425-3433. 2012

41. Tanaka, Yusuke, Mitsugi Inkyo, Ryoko Yumoto, Junya Nagai, Mikihisa Takano, and Shunji Nagata. “Nanoparticulation of poorly water soluble drugs using a wet-mill process and physiochemical properties of the Nanopowders.” Chemical and pharmaceutical Bulletin. 57(10):1050-1057. 2009

42. Siepmann, Juergen and Florence Siepmann. “Modeling of diffusion controlled drug delivery.” Journal of Controlled Release. 161(2):351-362. 2012

43. Jinno, Jun-ichi, Naoki Kamada, Masateru Miyake, Keigo Yamada, Tadashi Mukai, Masaaki Odomi, Hajime Toguchi, Gary G. Liversidge, Kazutaka Higaki, Toshikiro Kimura. “Effect of particle size reduction on dissolution and oral absorption of a poorly water-soluble drug, cilostazol, in beagle dogs.” Journal of Controlled Release. 111(1-2):56-64. 2006

44. Javadzadeh, Yousef, Baharak Jafari-Navimipour, Ali Nokhodchi. “Liquisolid technique for dissolution rate enhancement of a high dose water-insoluble drug (carbamazepine).” International Journal of Pharmaceutics. 341(1-2):26-34. 2007

45. Siepmann, Juergen, Nicholas A. Peppas. “Higuchi equation: Derivation, applications, use and misuse.” International Journal of Pharmaceutics. 418(1):6-12. 2011

46. Thiele, G., M. Poston, R. Brown. “A Case Study in Sizing Nanoparticles.” Micromeritics Analytical Services. Sizing Nanoparticles Press Release

47. Diedrich, Tamara, Agnieszka Dybowska, Jacques Schott, Eugenia Valsami-Jones, and Eric H. Oelkers. “The Dissolution Rates of SiO2 Nanoparticles As a Function of Particle Size.” Environmental Science and Technology. 46(9):4909-4915. 2012

48. Ritger, Philip, Nikolaos Peppas. “A simple equation for description of solute release 1. Fickian and non-fickian release from non-swellable devices in the form of slabs, spheres, cylinders or discs.” Journal of Controlled Release. 5(1):23-36. 1987

Chapter 3

Hyaluronic Acid Molecular Weight Determines Lung Clearance and Biodistribution after Instillation

3.1. Introduction

Hyaluronic acid (HA), is a linear biopolymer component of multiple approved products and exhibits versatility for drug delivery, since it is available in a wide range of molecular weights and offers multiple sites for chemical modification[1-6]. In the human body, HA is prevalent in cartilage, skin, and synovial fluid and is typically present as a very high molecular weight (up to 20 MDa) polymer, providing elasticity to tissues. As HA degrades, it drains away from these tissues, percolating with interstitial fluid into and through lymph nodes with a portion passing into the systemic circulation[7-13]. Thus, HA serves as an interesting polymer to carry drugs. Absorption of HA after subcutaneous[14-18] , intraperitoneal[19], oral[20,21], and intravenous injection[22-24] has been reported, but the fate of HA after pulmonary administration is not well understood. Recent work suggesting HA may be useful for inhaled drug delivery motivates a better understanding of HA fate after pulmonary administration[25-29].

The lungs eliminate materials using active transport processes including mucociliary and macrophage clearance, as well as passive diffusion to the bloodstream or lymph[30]. Mucociliary clearance occurs in the upper airways as ciliated cells sweep mucus up the trachea and into the oropharyngeal cavity where it is typically swallowed. HA residence time in the upper airways, therefore, depends on the distance from the site of deposition to the oropharyngeal cavity. The rate of mucociliary clearance can also depend on mucus viscosity. Slower and/or incomplete clearance of thick mucus is observed clinically while expectorants facilitate better mucus clearance. Further down the airways in the terminal bronchioles and alveoli, macrophages can recognize molecules or particles. Macrophages that have bound or phagocytosed HA can then actively traffic to the lymphatics draining the pulmonary bed. Finally, HA molecules may dissolve into the fluid layer lining the lung epithelium and then passively diffuse into the bloodstream[30-33]. This mode of systemic absorption is usually fastest in the alveolar region, where the tissue barriers are as thin as a few hundred nanometers[32,34]. Passive diffusion into

the lymphatic network draining the lungs may also be possible, although this clearance mechanism might be expected to be slower compared to absorption into the bloodstream[30, 32, 33].

In general, endogenous HA present in tissues has several different elimination routes as it is degraded to lower molecular weight chains through enzymatic and non-enzymatic mechanisms[7-13]. Endogenous HA that is part of the extracellular matrix or synovial fluid is on the order of 4-20 MDa in size. Enzymatic reactions that degrade HA occur in the interstitial space, in lymph, or in the blood by enzymes such as hyaluronidase. Non-enzymatic degradation of HA can occur by non-specific chemical reactions including acidic or alkaline hydrolysis or oxidation. These degradation pathways yield smaller HA fragments (100s of kDa in size), which then drain with interstitial fluid[7-13].

The interstitial fluid is collected into the lymphatics, where the majority of HA fragments smaller than 450 kDa are removed from the lymph fluid during filtration through lymph nodes before the fluid is passed back into the blood[35,36]. These HA fragments are then further degraded into even smaller fragments in the lymph nodes since the majority of HA turnover occurs in the lymphatics, thereby eliminating the HA fragments before they enter the blood circulation[6-8]. Lymphatic drainage of HA can be facilitated by active transport by binding to CD44 expressed on the surface of macrophages or lymphocytes[37,38]. Some HA fragments can reach systemic circulation from the interstitial fluid. In the blood, larger HA fragments (hundreds of kDa in size), circulate until reaching the liver where endothelial cells remove HA from circulation[5,39,40]. HA plasma clearance is rapid (half-life as low as 2 minutes)[22]. Alternatively, smaller molecular weight HA fragments can be eliminated by the kidneys since where the molecular weight cut off for efficient urinary excretion is approximately 25 kDa[4,5,22].

The lungs offer a route of administration that can facilitate local therapy, access to systemic circulation, and perhaps even delivery to pulmonary lymph nodes. HA is likely to be well-tolerated in the lungs as evidenced by studies where HA has been delivered by inhalation

to dogs[41] or nebulized into humans to treat lung inflammation[25-29]. In addition, HA is emerging as an important carrier molecule for drug delivery. In the present study, HAs of discrete molecular weights were administered to the lungs of mice via intratracheal instillation to determine how HA molecular weight dictates persistence in the lung, systemic absorption, and access to lymph nodes draining the pulmonary bed. HA molecular weights, of 7, 30, 67, 215, and 741 kDa were studied, and biodistribution was assessed by using fluorescent or radiolabeled HA[3,42-44].

3.2. Materials and Methods

3.2.1. Materials

The different molecular weights (7.5, 29/31, 67, 215, and 741 kDa) of hyaluronic acid (HA) were obtained from Lifecore Biomedical (Chaska, Minnesota). The 29/31 kDa HA (herein referred to as 30 kDa HA) was received in two different lots, with average molecular weights of 29 kDa and 31 kDa. The near infrared dye, HiLyte Fluor^{TM} 750 hydrazide, was obtained from AnaSpec (Fremont, California). DMTMM (4-(4,6-Dimethoxy-1,3,5-triazin-2-yl)-4-methylmorpholinium chloride) was obtained from ChemPep Inc (Wellington, Florida). Pierce iodination beads were purchased from Thermo Scientific (Rockport, Illinois) and $Na^{125}I$ from PerkinElmer (Waltham, Massachusetts). The mouse laryngoscope was obtained from Penn-Century (Wyndmoor, Pennsylvania). All water used was deionized (DI) water from a Labconco Pro PS system. All other chemicals and materials including tyrosine, EDC (1-Ethyl-3-(3-dimethylaminopropyl) carbodiimide), 3500 Da, 20000 Da, and 50000 Da molecular weight cutoff dialysis tubing, PD-10 columns, bent fine dissecting forceps, glacial acetic acid, sodium acetate, sodium phosphate monobasic

monohydrate, sodium phosphate dibasic, Fisherbrand disposable culture tubes (12x75mm), and phosphate buffered saline were purchased from Fisher Scientific (Pittsburgh, Pennsylvania).

3.2.2. Near Infrared Dye labeling of HA

A 1 mg vial of HiLyte Fluor 750 hydrazide dye was dissolved in 1 mL of 50 mM acetate buffer, pH 5.0. HA (7.5 mg) was dissolved in 4 mL of 50 mM acetate buffer, pH 5.0, with 0.5 equivalents of EDC to which the 1 mg/mL of dye was added[2,44-49]. The reaction was allowed to proceed for approximately 16 hours at room temperature and stirred at 450 rpm protected from light. After 16 hours, the reaction mixture was dialyzed using 3500 Da molecular weight cutoff dialysis tubing for 7.5 kDa HA, 20000 Da molecular weight cutoff dialysis tubing for 30 kDa HA, and 50000 Da molecular weight cutoff dialysis tubing for 67, 215, and 741 kDa HA; the dialysate was replaced every 6 hours for 24 hours. The HA-IR dye conjugate was removed from the tubing and then frozen at -20°C. Samples were lyophilized for 72 hours at a temperature of -72 °C at a vacuum of <300 millitorr (VirTis Feezemobile-12XL, The Virtis Company, NY). Samples were reconstituted using DI water to a concentration of 1 mg/mL prior to instillation.

Conjugation of the dye to HA was confirmed using HPLC (Figure 3.1). The conjugation efficiency of the dye was determined by taking a sample of the reaction mixture and comparing the intensity of the fluorescent peak before and after dialysis. The HPLC-fluorescence system consisted of a Shimadzu CBM-20A system controller, a LC-20SB solvent delivery pump, a RF-10A XL Shimadzu Fluorescent detector, and a SIL-20 AC HT autosampler (Shimadzu Corp, Kyoto, Japan). Chromatograms were acquired and analyzed using LC Solutions software. An isocratic system with a mobile phase of 50 mM acetic acid, pH 5.0, was used with a Vydac HPLC protein and peptide C18 column (5 µm particles, 4.6 mm x 250 mm). The flow rate was 0.5 mL/min, the injection volume was 20 µL, and the excitation and emission wavelengths were

753/782 nm respectively. The HA samples were diluted to a concentration of approximately 1 mg/mL using the mobile phase and had a retention time of 20.75 minutes.

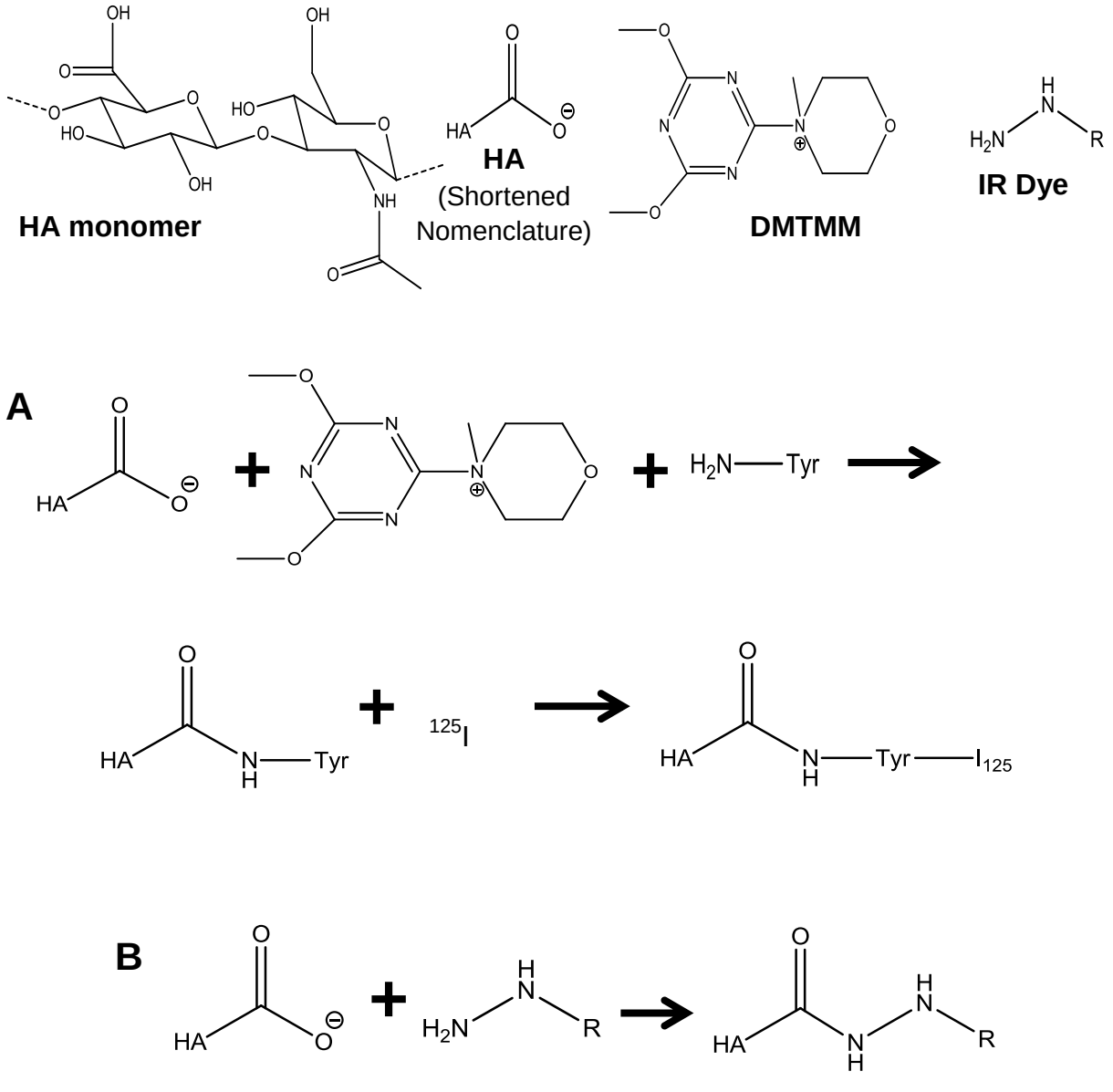

Figure 3.1: Depiction of full HA monomer unit, abbreviated HA, DMTMM molecule, and IR dye as a hydrazine group. A shows chemical reaction of HA with DMTMM and tyrosine for tyrosine conjugation followed by addition of ^{125}I for radiolabeled HA. B shows hydrazine IR dye reaction leading to conjugation on HA.

3.2.3. Radiolabeling of HA

For radiolabeling of HA, 60 mg HA was dissolved in 3 mL of 1 mM phosphate buffer pH 6.0 with 13.5 mg of tyrosine (0.5 equivalents). The pH was adjusted back to 6.0 using 1.0 M HCl after which 20.7 mg of DMTMM was added (0.5 equivalents). The reaction mixture was stirred at 175 rpm for approximately 16 hours at room temperature. Afterwards, samples were dialyzed, lyophilized, and reconstituted as necessary as described previously[3,24,42-44,50-52].

Conjugation of tyrosine to HA was confirmed by 1D proton NMR. The NMR was run using a scan rate of 16 scans and 2 dummy scans using deuterium oxide as the solvent at a concentration of 10 mg/mL. The NMR was a 400 MHz Bruker (Billerica, MA) AV spectrometer equipped with a X-channel observe probe. Conjugation efficiency was calculated by comparing the integration of HA peaks to the integration of tyrosine peaks. The conjugation efficiency of tyrosine to 741 kDa HA was unable to be determined due to viscosity issues limiting the concentration of the sample.

Iodine labeling was performed using iodination beads (Figure 3.1). Two iodination beads were used per HA molecular weight sample and were rinsed with 10X PBS for 3 minutes. The beads were then dried on filter paper and added to 200 µL of $Na^{125}I$ (1 mCi) in 10X PBS and incubated for 5 minutes at room temperature. HA-tyrosine (150 µL of 1 mg/mL) was added to the $Na^{125}I$ and bead solution was incubated overnight at room temperature. The reaction mixture was then transferred to an equilibrated PD-10 column. To elute the HA-^{125}I, 6 mL of PBS was added, and 500 µL fractions were collected in Eppendorf tubes. From each fraction, 10 µL was taken and transferred to a new Eppendorf tube and counted using a Canberra model 2000 NIM BIN with Canberra model 802-4W NaI Well (3” by 3” well) detector gamma counter. The amplifier was a Canberra model 814A with a Ortec model 775 counter, Ortec model 719 timer, Ortec model 495 power supply, and a Canberra model 2030 single channel analyzer (SCA). The settings used were an amplifier coarse gain of 8 and fine gain of 8.8 with the power

supply set at 875, SCA of Delta E: 10 and a lower level discriminator of 0.06. To determine conjugation efficiency of ^{125}I to HA-tyrosine, an ethanol precipitation method was used. The highest intensity vial from the 10 µL aliquot of HA-tyrosine-^{125}I (from now on HA-^{125}I) PD-10 eluents had 20 µL of 20 mg/mL HA added followed by the addition of 200 µL of cold ethanol. The mixture was put on dry ice for 20 minutes then was centrifuged at 2000 rpm for 20 minutes on a Biofuge A centrifuge by American Scientific Products. The supernatant was then separated from the pellet and both were recounted on the scintillation counter. Eqn. 3.1 was used to determine the conjugation efficiency from the scintillation data. All radiolabeling was conducted under the supervision of the University of Kansas Radiation Safety Committee.

$$Eqn\ 3.1: \quad \frac{Pellet\ Radioactivity\ (cpm)}{Pellet\ Radioactivity\ (cpm) + Supernatant\ Radioactivity\ (cpm)} * 100\%$$

To prepare the HA-^{125}I for intratracheal instillation, a similar ethanol precipitation procedure was used. Approximately 22-25 mg of HA was dissolved in 500 µL of water then a 500 µL fraction of HA-^{125}I collected from the PD-10 column was added. The HA-^{125}I / HA solution was precipitated with approximately 12 mL of cold ethanol and after sitting on dry ice for 10 minutes, the sample was centrifuged for 10 minutes at 12000 rpm using a Dynac 2 centrifuge from Becton Dickinson. The supernatant was removed and the pellet was dissolved in 2 mL of DI water (for HAs <700 kDa) or 3 mL of DI water for the 741 kDa HA.

3.2.4. Sizing of HA

Size exclusion chromatography (SEC) was employed to determine the difference in molecular weight between HA and HA-tyrosine. Samples were analyzed at a concentration of 5 mg/mL. The system used was a Waters e2695 separation module, Waters 2414 refractive index detector, and Waters 2489 UV/Vis detector with two columns in series: a PL Aquagel-OH

60 Analytical SEC (300 x 7.5 mm) then a PL Aquagel-OH 40 Analytical SEC (300 x 7.5 mm) (Santa Clara, California). Samples (80 µL of 5 mg/mL) were dissolved and run using an isocratic 0.5 mL/min mobile phase of 0.1 M ammonium acetate with 0.136 M sodium chloride at pH 5. Chromatograms were analyzed using EMPower 3.

Dynamic light scattering (DLS) of HA was executed to determine the approximate physical size of the HA in solution. DLS was performed using a ZetaPALS (Brookhaven Instruments Corp., ZetaPALS, Holtsville, NY). HA was dissolved in 1X PBS at a concentration of 1 mg/mL and filtered through a 0.45 µm filter. Measurements were performed in a glass cuvette using ZetaPALS software (Holtsville, NY).

3.2.5. Animals

BALB/C mice (female, 4 weeks old at 13 – 16 grams) were supplied by Monash Animal Research Services (Victoria, Australia) for the near infrared dye imaging and by Harlan Laboratories (Indianapolis, IN) for the radiolabeling. One group of Harlan mice were used in a crossover study of near infrared dye imaging to confirm similar pharmacokinetic behavior between the different suppliers. Mice were maintained on a 12 hour light/dark cycle and were fed standard rodent pellets with no dietary restrictions nor withheld food. Water was freely available at all times. All animal experiments were approved by the Monash Institute of Pharmaceutical or the University of Kansas Institutional Animal Care and Use Committee (IACUC).

3.2.6. Intratracheal Instillation of HA

For lung administration via intratracheal instillation, each animal was anesthetized with 2% isoflurane in an induction chamber for approximately 4 minutes. The unconscious mouse was positioned in dorsal recumbency using a dosing board at approximately 60° to a supine position suspended by incisor teeth using a thin wire. A nose cone was used to maintain anesthesia[53]. The mouth was opened and the tongue was gently pulled out and to the side of the mouth. A laryngoscope was then positioned to depress the tongue and visualize the vocal cords at the top of the trachea. A 50 µL solution of labeled HA was then pipetted at the top of the trachea. The tongue was withheld for at least 3 breaths, after which time the mouse was maintained under anesthesia for an additional 3 minutes on the dosing board. The mouse was then removed from the dosing board and allowed to recover from the anesthesia by being held vertically until movement was regained. For the near infrared dye, 1 mg/mL of HA-IR dye was instilled and for the radiolabeled HA, approximately 11-12 mg/mL HA for 7, 30, and 67 kDa HA, 2.8 mg/mL for 215 kDa HA and 1.6 mg/mL for 741 kDa HA was instilled according to Table 3.1.

3.2.7. Near Infrared Dye Ex Vivo Imaging

At 1, 8, or 24 hours after intratracheal instillation, mice were euthanized via an i.p. injection of sodium pentobarbital (>100 mg/kg body weight), and death was confirmed by the absence of a heartbeat. The lungs, trachea, heart, spleen, liver, kidney, stomach, intestine, and bladder were then excised to evaluate the relative distribution of HA in mice at the different time points. Fluorescent images were collected on a Caliper life sciences IVIS Lumina II from Thermo Fisher Sciences (Victoria, Australia) using living image V 4.3.1 software from Caliper Life Sciences, Massachusetts. A 745 nm wavelength bandpass filter was used for excitation and 780 nm as the emission filter. All points included at least 3 mice. Fluorescent images that

were repeated and collected at the University of Kansas were performed on a Cambridge Research and Instrumentation Maestro multi-spectrum imager (Woburn, Massachusetts) with an excitation filter of 710–760 nm and long pass emission filter of 800–950 nm.

3.2.8. Counting of Signal from Radiolabeled Tissue

At 1, 2, 4, 6, and 8 hours after intratracheal instillation, mice were euthanized via isoflurane overdose in an inhalation chamber in a hood and death was confirmed by cessation of breathing for 5 minutes. The tissues of interest were then surgically removed including the right axillary and brachial lymph nodes, the left axillary and brachial lymph nodes, trachea, heart, right and left lung lobes, spleen, liver, stomach, intestine, kidneys, bladder, and final fecal pellet in the GI tract. Each tissue sample was suspended in approximately 2-3 mL of 1X PBS in 12 by 75 mm glass Fisherbrand tubes. Samples were scintillated on a Beckman Gamma 5500B system with a 3” by 3” NaI detector. Counts were taken for 1 minute, and the average of 3 or more readings was used. All bladders were assayed without urine to keep the measurements consistent. Samples were corrected for dose and radiolabeling efficiencies. All time points for all test articles exhibited <5% error for the measurement except for the intestine 7 kDa HA at 1 hour and 741 kDa at 1 and 2 hours.

3.2.9. PK Analysis of Radiolabeled Tissue

Pharmacokinetic (PK) analysis of the radiolabeled HA data was performed using WinNonlin 6.3 software. Non-compartmental modeling analysis was performed assuming first order input with uniform weighing using extravascular dosing, plasma type model for tracking, and trapezoid linear interpolation to calculate PK parameters.

3.3. Results

3.3.1. Size Characterization of HA

The selection of the molecular weights of HA (7, 30, 67, 215, and 741 kDa) provided a size range representative of endogenous median to low molecular weight HA with regular size intervals. Theoretical radii of gyration and theoretical hydrodynamic radii were calculated utilizing Eqn 3.2 and Eqn 3.3 respectively[54,55]. Theoretical radii of gyration ranged from 7 nm to 100 nm across the molecular weights of HA studied and theoretical hydrodynamic radii ranged from 3 nm to 54 nm (Table 3.1).

$$Eqn\ 3.2: Rg = 2.35\ [MW\ in\ kDa]^{0.57} \qquad Eqn\ 3.3:\ Rh = 0.87[MW\ in\ kDa]^{0.63}$$

DLS was performed on the different molecular weights of HA to compare the measured hydrodynamic radii of HA molecules to the calculated values. As expected, the measured size increased with molecular weight (Table 3.1). The size of HA increased from 6 to 55 nm, which corresponded relatively well to the theoretical estimates of the radius of gyration and hydrodynamic radius.

Table 3.1: Calculated and experimental sizes of different molecular weights of HA.

Molecular Weight (kDa)	***Calculated Radius of Gyration (Rg) (nm)***	***Calculated Hydrodynamic Radius (Rh) (nm)***	***DLS Measurements (nm)***	***Size Based on SEC Data (kDa)*****	***SEC HA-Tyrosine (kDa)*****	***Calculated Viscosity (dL/g)***
7	7.1	3.0	6.1 ± 0.2	14 ± 3	13 ± 2	14.8
*30**	16.3	7.4	12.2 ± 1.3	68 ± 7	59 ± 4	68.9
67	25.8	12.3	22.1 ± 1.2	155 ± 14	127 ± 9	161.0
215	50.2	25.6	33.3 ± 0.2	557 ± 28	435 ± 18	477.3
741	101.6	53.9	55.0 ± 0.7	1646 ± 51	451 ± 25	1250.0

*Calculations based on an estimate molecular weight of 30 kDa HA. Lots were 29 kDa and 31 kDa. DLS and SEC data were performed for the 29 kDa HA lot. **Standard Deviations were based on running the same samples for three different runs.

3.3.2. HA-Fluorescent Dye Conjugation Efficiency

In general, the conjugation efficiency of the IR hydrazine dye decreased with increasing molecular weight (Table 3.2). The smaller HA molecules (7 and 30 kDa) had similar conjugation efficiencies that were nearly double the conjugation efficiencies observed for larger HAs (215 and 741 kDa). The 67 kDa HA had a conjugation efficiency intermediate to the smaller and larger HA.

Table 3.2: Conjugation efficiency of HA in the different reactions to IR dye, tyrosine, and HA-tyrosine to ^{125}I.

Molecular Weight (kDa)	***Conjugation Efficiency of IR Dye (%)***	***Conjugation Efficiency of Tyrosine (%)***	***Conjugation Efficiency of ^{125}I (%)***	***Concentration of HA in Intratracheal Instillation Solution (mg/mL)***
7	72.3	1.6	32.7	12.1
*30**	69.7	2.4	83.3	11.1
67	50.5	2.3	83.6	11.5
215	38.3	2.3	88.9	2.8
741	36.6	NA	41.1	1.6

* Lots were 29 kDa and 31 kDa. Conjugation efficiency of IR dye was performed on the 31 kDa HA lot, while conjugation efficiency of tyrosine, conjugation efficiency of ^{125}I, and concentration of HA in intratracheal instillation solution data were performed for the 29 kDa HA lot. NA represents not available.

3.3.3. Lung Distribution and Clearance of HA-IR Dye Conjugates

HA-IR dye conjugates were used in a pilot study to help determine HA residence in the lung and to guide the selection of optimal time points and duration for the radiolabeled HA studies. Each mouse received 1 mg/mL of HA-IR instilled at the top of the trachea. Tissue samples were imaged at 1, 8, and 24 hours. Each polymer was detected in all five lobes of the lungs for all three time points (Figure 3.2). The distribution of HA with different molecular weights appeared to be relatively equivalent throughout all the lung lobes for both lungs.

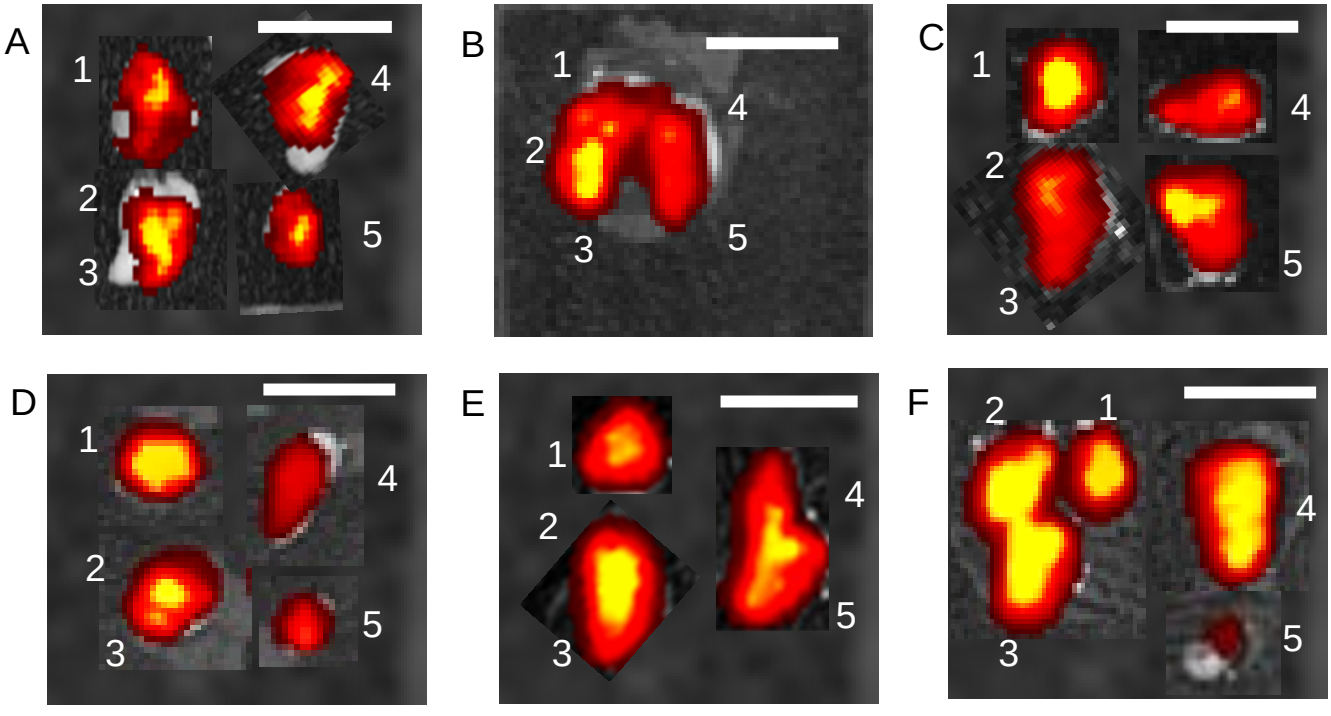

Figure 3.2: Fluorescent images of lungs injected with HA-IR showing distribution though out all lung lobes with all five different molecular weights. A: lungs injected with 5 µL of 7 kDa HA solution, B: 7 kDa HA 8 hour, C: 30 kDa HA 8 hour, D: 67 kDa HA 8 hour, E: 215 kDa HA 8 hour, F: 741 kDa 8 hour. White scale bar is 1 cm. The white numbers represent lobes of the lungs with 1, 2, and 3 representing mouse anatomical right lung lobes and 4 and 5 representing mouse anatomical left lung lobes.

The highest molecular weight HA exhibited the highest level of fluorescence at 1 hour (Figure 3.3). As HA molecular weight decreased from 741 kDa to 30 kDa, fluorescence in the lungs correspondingly decreased. The 215 and 741 kDa HA had significantly higher levels at one hour compared to the other three HA molecular weights while the two smallest HAs, 7 kDa and 30 kDa, were not significantly different at 1 hour. All five molecular weights of HA had minimal fluorescence at 8 and 24 hours, suggesting subsequent studies should last no longer than 8 hours.

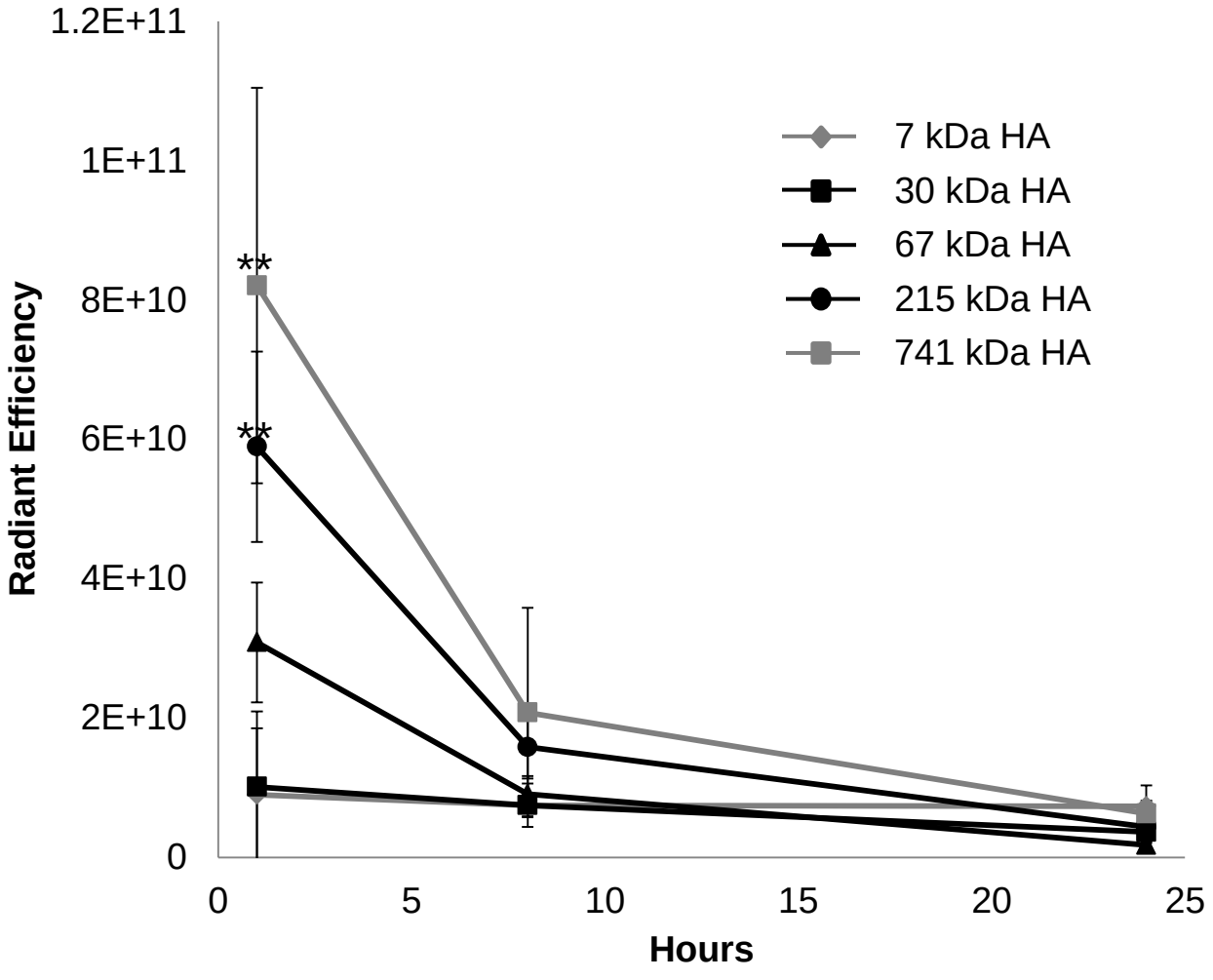

Figure 3.3: Analysis of lungs instilled with HA-IR dye. The largest molecular weight of HA had the longest persistence in the lungs which decreased with molecular weight. ** Signifies statistical difference from 7, 30, and 67 kDa HA and each point is the average of at least three animals.

3.3.4. Radiolabeled HA Physiochemical Properties

HA molecular weight was determined experimentally to compare HA as received to the HA conjugated with tyrosine, which was used for the radiolabeled HA biodistribution studies[24]. The molecular weight of HA molecules measured using SEC were at least 2-fold (and up to 10-fold) higher than the molecular weight reported for these stock HAs (Table 3.1). Tyrosine

conjugation resulted in an apparent decrease in molecular weight compared to stock HA for all five molecular weights though the differences were relatively minor for 7, 30, and 67 kDa HA. The tyrosine conjugation efficiency was similar throughout the different molecular weights ranging from 1.6% for the 7 kDa HA to ~2.3% for the next three highest molecular weights (Table 3.2). Subsequent ^{125}I conjugation was straightforward. The three middle molecular weights of HA (30, 67, and 215 kDa) had similar levels ranging from 83 to 89%. The 7 kDa and 741 kDa had lower levels of ^{125}I conjugation, 32 and 41% respectively (Table 3.2).

3.3.5. Distribution and Clearance of HA–^{125}I Conjugates

Animals were instilled with different concentrations of radiolabeled HA into the lungs due to viscosity constraints of the test articles. The three lowest molecular weights, 7, 30, and 67 kDa were instilled at 11 to 12 mg/mL, while the 215 kDa HA was dosed at 2.8 mg/mL and 741 kDa at 1.6 mg/mL (Table 3.2). The 7, 30, and 67 kDa HAs had minimal viscosity when instilled into the animals, whereas viscosity increased dramatically for the 215 and 741 kDa HAs (Table 1) [56]. Viscosity increased ~3 fold between each molecular weight studied and increased 30 fold and 100 fold when comparing 7 kDa to 215 and 741 kDa HA, respectively.

After instillation, high levels of HA were found in the left and right lung lobes and in the GI tract including the stomach and intestine (Figures 3.4-3.6 and Supplemental Figure S3.1). The shape of the lung exposure profiles over time was similar for all HA molecular weights with HA exposure peaking at an early time point and steadily declining thereafter. The magnitude of peak HA exposure to the lungs (1 to 2 hours) depended on HA molecular weight (Figure 3.4). The 7 kDa HA had the lowest peak levels, with 30 and 741 kDa having the next highest, and 67 and 215 kDa HA having the highest levels in the lungs (Figure 3.4). At eight hours, 7 and 741 kDa HA displayed the most rapid lung clearance with (approximately 75% and 50% of the initial

dose cleared, respectively). In contrast, only approximately 20% of the initial dose of 30, 67, and 215 kDa HA that reached the lungs after intratracheal instillation had been cleared by 8 hours post dose.

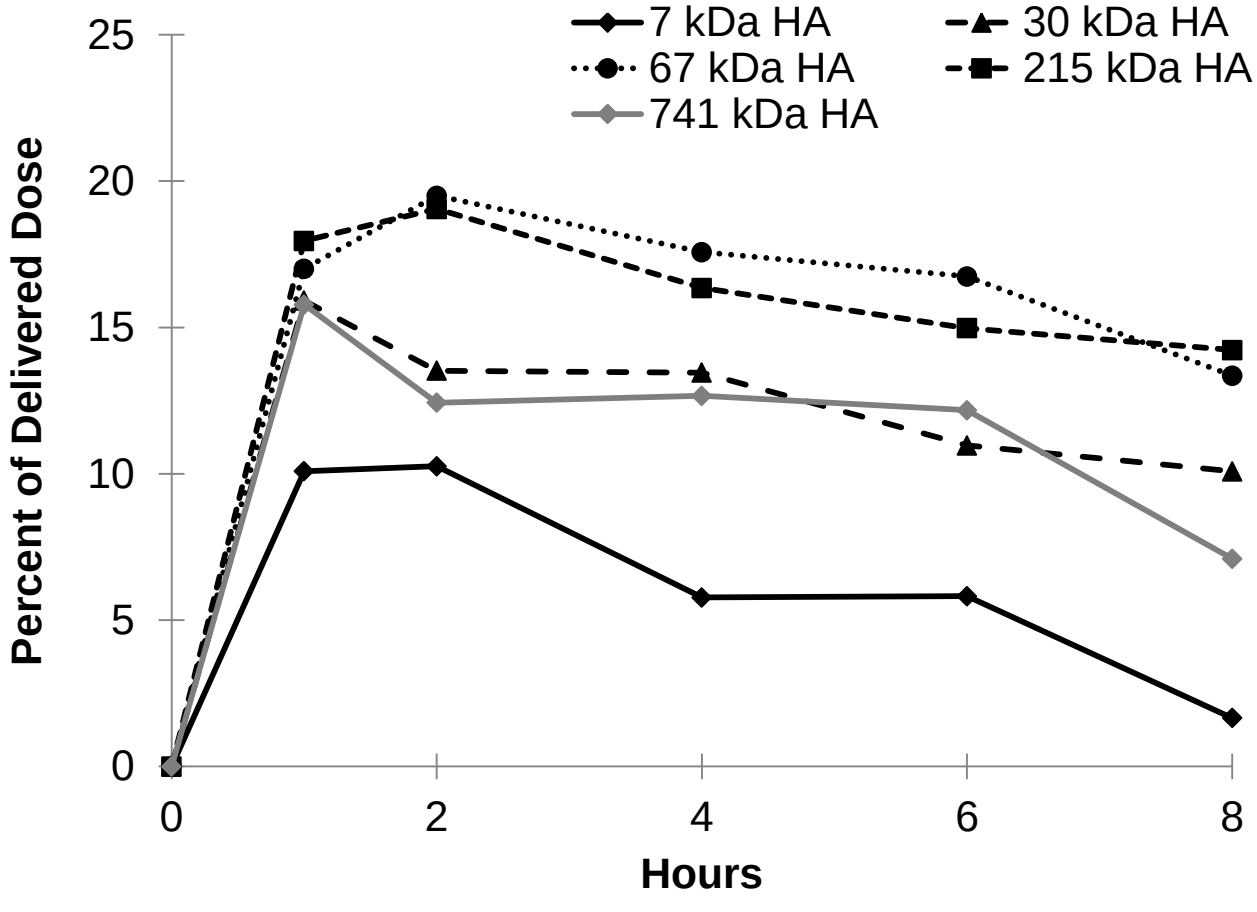

Figure 3.4: Exposure levels of HA in the lungs averaged across both right and left lung lobes as a percentage of delivered dose over time for each of the five HA molecular weights. Each point is an average of at least five animals with the error on each point <5% of the measurement.

The GI tract also showed significant levels of HA (Figures 3.5-3.6) after intratracheal instillation as expected. In the stomach, the exposure profiles of 7, 30, and 67 kDa HA peaked

at one hour and decreased over the remaining time of the study, while 215 and 741 kDa HA peaked at two hours. At the final time point of the study (8 hours), all five molecular weights of HA had similar levels in the stomach with approximately 5% of the initial dose remaining. In the intestines, the profiles mirror the stomach but all five molecular weights peaked at one hour and had approximately 5% of the initial dose remaining at eight hours.

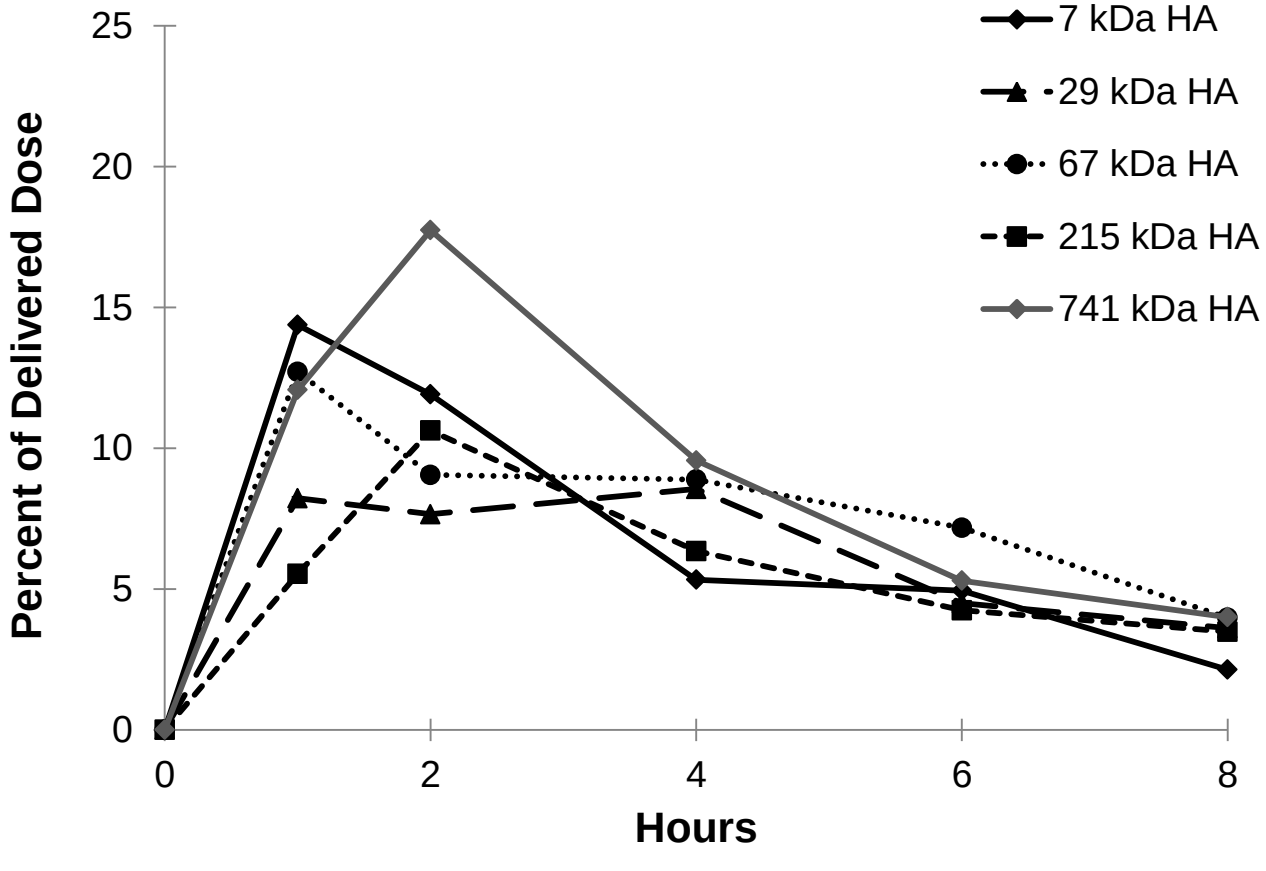

Figure 3.5: Exposure levels of HA in the stomach as a percentage of delivered dose over time for each of the five HA molecular weights. Each point is an average of at least five animals with the error on each point <5% of the measurement.

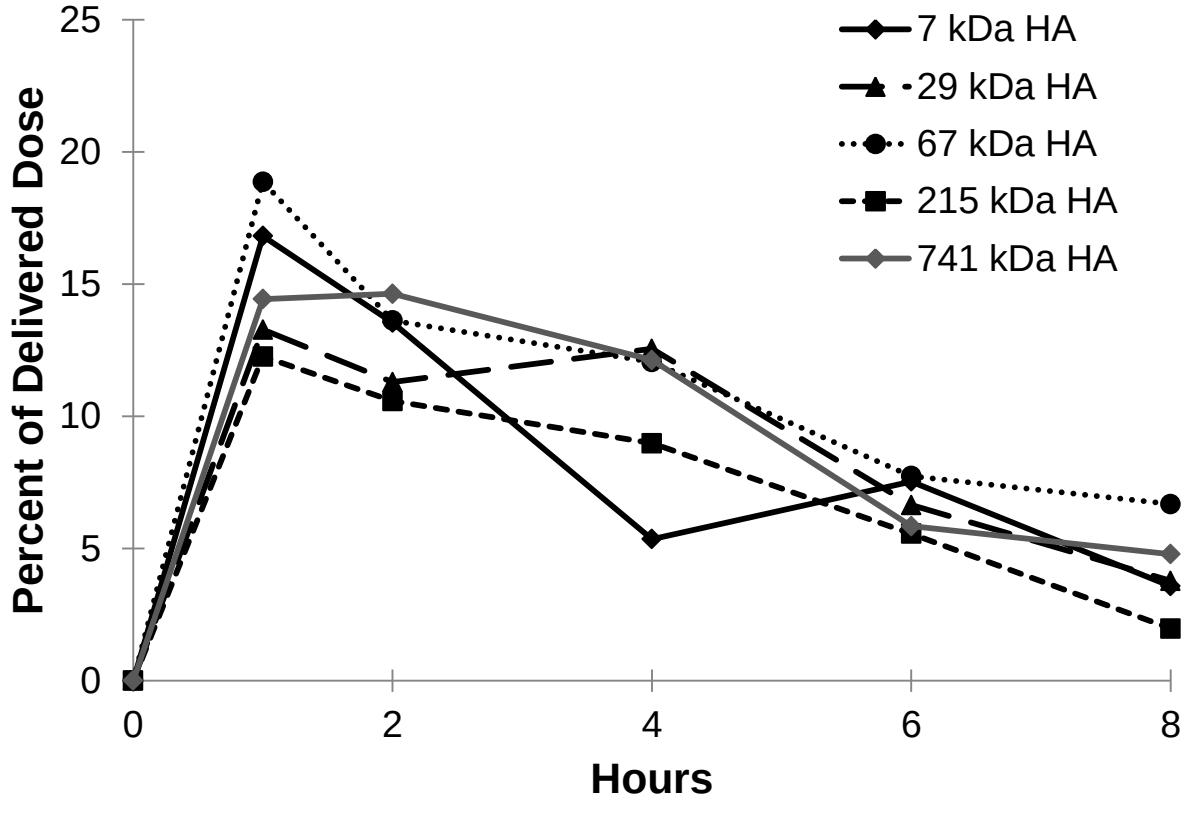

Figure 3.6: Exposure levels of HA in the intestine as a percentage of delivered dose over time for each of the five HA molecular weights. Each point is an average of at least five animals with the error on each point <5% of the measurement.

The distribution and pharmacokinetics of HA was assessed for other organs and tissues (Figure 3.7). The liver and trachea had HA exposure levels of approximately 1 to 4% of the initial dose, while the heart, spleen, kidneys, and bladder contained only a fraction of a percent of the initial dose. Interestingly, the level of HA in the trachea increased over time for all five molecular weights of HA.

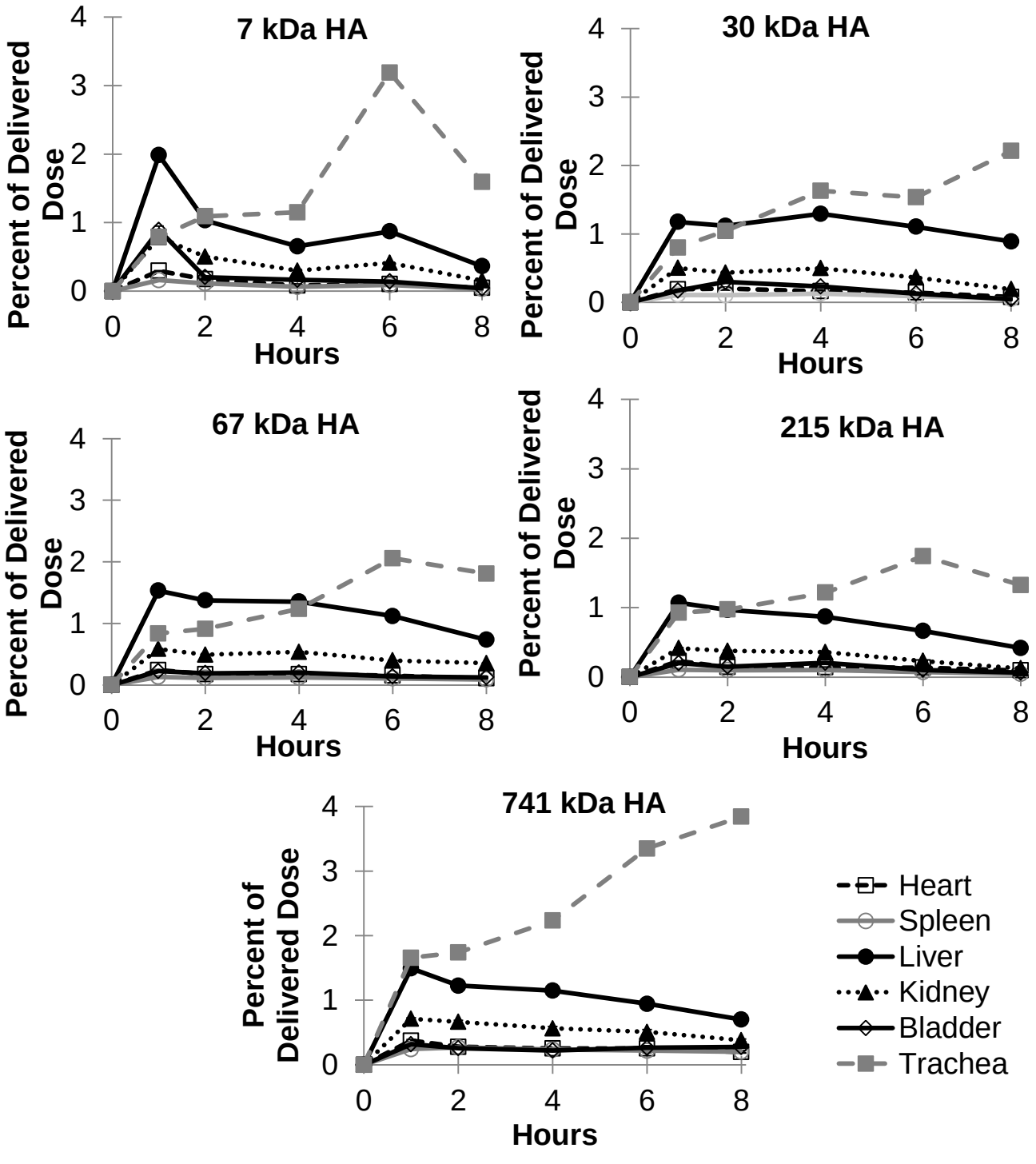

Figure 3.7: Exposure levels of HA in the heart, spleen, liver, kidney, bladder, and trachea based on molecular weight with 7 and 29 kDa HA on top, 67 and 215 kDa HA in the middle, and 741 kDa HA on the bottom as a percentage of delivered dose over time for each of the five HA molecular weights. Each point is an average of at least five animals with the error on each point <5% of the measurement.

Pharmacokinetic parameters were modeled to determine HA exposure and elimination from organs. HA half-life in the lungs and heart generally increased as HA molecular weight increased (Table 3.3). As HA molecular weight increased from 7 kDa to 215 kDa, half-life increased in the lungs from 2 hours to nearly 15 hours, but 741 kDa HA had a short half-life (4.9 – 7.5 hours) in the lungs. Half-lives for the other organs appeared relatively consistent across the various HA molecular weights with the exception of the heart (Table 3.3). The heart half-life increased from 3.7 hours to 13.5 hours as HA molecular weight increased from 7 kDa HA to 741 kDa HA; however, this calculation was based on less than 1% exposure to the heart tissue.

Table 3.3: Organ half-life in hours for each tissue based on molecular weight.

Molecular Weight (kDa)	***Right Lung Lobes***	***Left Lung Lobes***	***Heart***	***Spleen***	***Liver***	***Stomach***	***Intestine***	***Kidney***	***Bladder***
7	2.5	2.1	3.7	4.0	4.9	2.7	3.8	4.3	2.8
*30**	9.8	11.0	3.9	2.8	7.4	3.2	2.3	2.9	1.7
67	9.5	10.8	5.5	9.0	4.5	3.5	5.4	6.7	5.7
215	29.8	14.7	7.4	3.4	3.8	4.6	1.8	2.6	2.4
741	4.9	7.5	13.5	17.8	5.6	3.2	3.0	7.8	ND

*HA molecular weight of 30 kDa was comprised of lots of 29 and 31 kDa. ND – not determined.

Area under the curve (AUC)[31] trended similarly to the half-lives calculated for the different HA molecular weights (Table 3.4). AUCs increased as HA molecular weight increased from 7 to 215 kDa HA, but sharply declined for the 741 kDa HA. The low levels of HA exposure to the heart increased as HA molecular weight increased. Other organs exhibited relatively consistent AUC values across the HA sizes studied. Organ clearance rates were also calculated to describe how quickly the HA was removed from each tissue based on the extent of exposure of HA in each organ over time (Supplemental Table S3.1). Clearance rates from the lungs decreased as molecular weight increased from 7 to 215 kDa HA, but the 741 kDa HA had

a higher clearance rate from the lungs, which follows earlier elimination half-life trends. The heart clearance rate decreased as molecular weight increased, while the majority of the other organs (liver, stomach, intestine, and kidney) had clearance rates that remained relatively consistent as HA molecular weight increased.

Table 3.4: Area under the curve (AUC) in hours*µg/mL for each tissue based on molecular weight.

Molecular Weight (kDa)	***Right Lung Lobes***	***Left Lung Lobes***	***Heart***	***Spleen***	***Liver***	***Stomach***	***Intestine***	***Kidney***	***Bladder***
7	328.2	344.4	7.42	5.15	57.3	380.1	518.5	24.7	12.12
*30**	1370.1	1363	9.11	5.31	100.2	367.8	471.9	21.6	8.38
67	1913.3	1797.0	12.09	11.59	80.8	471.7	788.0	40.0	13.31
215	4471.2	2305.3	12.19	5.01	47.6	398.8	370.1	15.9	7.67
741	917.3	850.2	33.95	40.33	80.6	526.0	566.0	49.2	ND

*HA molecular weight of 30 kDa was comprised of lots of 29 and 31 kDa. ND – not determined.

3.4. Discussion

3.4.1. Characterization of HA and Labeled HA

HA is known to self-associate, a phenomenon which can occur within the same polymer chain or between different HA polymer chains. As a result, HA has the potential to form secondary structures within only 6 monomer units, while tertiary structures can occur in polymers as small as 16 monomer units[11,61,62]. These interactions can yield high viscosity solutions, especially for high molecular weight HA (>100 kDa). Careful selection of high salinity mobile phases and dilution of samples is required to accurately analyze HA, since many analytical techniques for polymers are based on mobility. For example, DLS measurements assume diffusion of a sphere as calculated using the Stokes-Einstein equation; however, changes in viscosity can result in differences in apparent size[63,64]. DLS measurements reported

here corresponded relatively well to theoretical predictions of radii for the different HA molecular weights studied. Molecular weight approximations of HA were higher than expected, but the trends followed as predicted from the stock HAs.

Similarly, HA self-association has the potential to block reactive sites when attempting to conjugate functional groups. The conjugation of tyrosine was quite low (~2%), while IR dye conjugation was much higher, suggesting poor reactivity of the tyrosine more than simple steric hindrance. ^{125}I labeling, on the other hand, was quite efficient with conjugation exceeding 50%, which is typical for HA. In addition, ^{125}I labeling maintained HA molecular weight by avoiding reducing agents such as cyanoborohydride, which can degrade HA into smaller fragments as was observed with carbon-14 or tritium[24,42]. Overall, conjugated HAs provided a wide range of molecular weights and hydrodynamic sizes for quantitatively tracking pulmonary deposition and subsequent distribution.

3.4.2. Current Pulmonary HA Studies

HA has been administered via several routes in a number of species to determine its local and systemic transport. Most reports have focused on higher molecular weight HA (≥500 kDa) delivered by intravenous, subcutaneous, or intrasynovial injections since these are used in dermal fillers and viscosupplements[5,7,39]. Recently, HA has been incorporated into pulmonary formulations primarily as an excipient to increase dose tolerability when treating inflammation. Nebulized HA (300 to 500 kDa) has been administered to mice at a concentration of ~3 mg/mL with a total dose of 6 mg to treat lung inflammation. HA treatment controlled inflammation by decreasing multiple cytokines including TNF-α and macrophage inflammatory protein-2[25]. Nebulized HA formulations employing molecular weights of 300 to 500 kDa (0.1% HA) were given twice daily in humans to treat lung inflammation[25-29]. Inclusion of HA in the nebulized

formulation decreased the length of hospital stay, increased tolerability of the formulation, and reduced lung secretions[25-29]. HA has also been incorporated into drug delivery strategies to improve formulation characteristics. For example, pulmonary administration utilizing spray dried 2 MDa HA with recombinant insulin was administered to beagle dogs. HA increased the mean residence time and terminal half-life of insulin in the lung[41].

Pulmonary administration includes the possibility of swallowing a portion of the dose directly or after mucociliary clearance. The fate of HA after swallowing is therefore an important consideration when interpreting studies reported here. Oral administration has been studied in both rats (100 kDa to 1 MDa HA) and dogs (1 MDa HA)[20,21]. A majority of the orally administered HA remained in the GI tract. There was minimal difference between molecular weights of HA in terms of distribution with only a slightly higher percentage observed in the stomach at 1 hour with 0.1 MDa HA compared to 1 MDa. One study found that less than 10% and typically 1-3% of the administered dose of HA was absorbed and detected in peripheral tissues[21]. A second study reported slightly contradictory results where only a trace amount (less than 0.1% of the dose/gram) of orally dosed HA entered systemic circulation[20]. Both studies showed the vast majority of HA was eliminated in the feces (~85-95%)[20,21].

3.4.3. Distribution and Clearance of Labeled HA

A pilot study was first conducted using HA-IR to determine the approximate length of time HA may persist in lung tissue. After instillation, HA-IR appeared to disperse evenly throughout all lung lobes for all HA molecular weights. The instilled solutions exhibited similar low viscosities, which may have facilitated exposure throughout the lungs due to gravity since mice were suspended in an upright position. Previous studies indicated the HA-IR conjugate is unlikely to dissociate especially in innocuous conditions in the lungs[8,34,65,66]. The highest

molecular weight HAs showed significantly higher lung exposure at 1 hour when compared to the two smallest sizes of HA. The low lung exposures suggested that 7 and 30 kDa HA were rapidly cleared from the lung, since all animals received similar doses. Molecules of this size are expected to be rapidly absorbed into systemic circulation[32,33,67]. These pronounced differences compelled a more quantitative investigation of rapid HA elimination from mouse lungs (<8 hours) and subsequent biodistribution.

Intratracheal instillation of HA-^{125}I showed the vast majority of HA persisted in the lungs with some clear differences between different HA molecular weights. The 7 kDa HA may have exhibited increased mucociliary clearance due to its high mobility and low viscosity but data from the trachea suggests this is unlikely. Increased clearance for the 7 kDa HA may be attributed to increased systemic absorption as seen by the lowest half-life in the heart, which led to the highest elimination constant as well as possible urinary elimination since it is below the renal clearance cutoff of 25 kDa. As seen with the increasing half-life in the heart, there is more systemic absorption clearance with the lower molecular weights of HA, which decreases as molecular weight increases. Data showed mucociliary clearance was relatively constant for 7, 30, 67, and 215 kDa HA suggesting macrophage uptake and passive diffusion accounted for the increased clearance. As passive diffusion decreased with increasing molecular weight, macrophage uptake would dominate the observed clearance. The increased persistence seen with 67 and 215 kDa HA could be due to saturated macrophage clearance and minimal clearance from the other two clearance mechanisms. Conversely, high molecular weight and high viscosity of 741 kDa potentially led to retention in upper airways, thus shortening the distance to clear this material into the oropharyngeal cavity. The three middle molecular weights of HA (30, 67, and 215 kDa) had a higher portion of HA retained in the lungs, indicating these doses penetrated the lungs well.

HA exposure to the GI tract likely resulted from a portion of the administered dose being swallowed or from mucociliary clearance out of the lungs followed by ingestion. Previous studies have shown limited absorption of 100 kDa to 1 MDa HA and little distribution after oral administration with the majority of the dose being excreted in the feces or remaining in the GI tract[20,21]. The higher level in the intestines compared to the stomach suggested gastric emptying over the first hour, which could be detected in future studies by more frequent sampling at early time points. The profile shapes can be explained by continuous mucociliary clearance and swallowing followed by gastric emptying contributing to this extended GI accumulation period. The trachea levels increased over time for all 5 molecular weight HAs, which agrees with mucociliary clearance bringing HA from the lungs continuously, independent of polymer size[68,69]. The gastric emptying and GI motility were also expected to be independent of molecular weight for the entirety of the GI tract, thus providing a likely explanation for the similar profiles[70,71].

The distribution and pharmacokinetics of radiolabeled HA was assessed for other organs and tissues (Figure 3.7). The heart had very low levels for all molecular weights, which is in agreement with the short circulation half-life reported for HA. The liver specifically eliminates endogenous HA, therefore rapid and continuous elimination of HA from the circulation by the liver was expected[13,15,19]. The kidneys had lower levels than the liver but more than the heart, spleen, and bladder suggesting that urinary excretion may be another potential route for eliminating small amounts of HA absorbed systemically from the lung[12-14]. HA content in the bladder tissue was low at all time points. The radiolabel content of urine was not assessed due to difficulties in consistently collecting all urine excreted by mice without the use of metabolic caging.

The 67 kDa and 215 kDa HA may provide the optimal range of size and viscosity for persisting in the lungs (Table 3.1). For comparison, studies with dendrimers have shown that

lung persistence incrementally increased as molecular weight increased from 11 to 22 to 78 kDa. By increasing the size of the dendrimer, researchers observed decreased degradation with lower systemic exposure and greater lung retention[27]. These observations correlate with the hydrodynamic radii observed for HAs that persisted in the lungs. The relative hydrophobic character of HA may also contribute to differences in lung persistence, until HA solution viscosity limited penetration of the instilled dose. The hydrophobicity of HA increases as molecular weight increases[63]. Increasing hydrophobicity of drug delivery systems is known to increase clearance by macrophages, which patrol the deep lung[72]. The 67 and 215 kDa HA may exhibit the most favorable proportion of hydrophobic character to escape significant macrophage clearance while retaining enough hydrophilicity for dissolution in the lung fluid and reduce mucociliary clearance along with mucus gel. In contrast, the 741 kDa HA may not have enough hydrophilic character to facilitate dissolution in the lung fluid thus promoting accelerated mucociliary clearance. The increase in size from 67 to 215 kDa could also be advantageous for facilitating dissolution into lung fluid, while remaining small enough to avoid macrophage clearance.

3.4.4. Lymphatic Transport of HA

HA naturally clears from tissue spaces through the lymphatics and has been studied as a vehicle to passively target drug delivery to lymph nodes. Properties including molecular size, hydrophobicity[57], charge[58], and injection site[58] affect lymphatic delivery[57]. Because of its molecular properties, HA has the potential to traffic to the lymphatics after instillation into the lungs. Here, HA exposure to lymph nodes associated with the lungs was also assessed. Brachial nodes draining the upper thoracic exhibited higher levels of HA compared to axillary nodes, but the HA levels were only ~0.02% of the initial delivered dose (Supplementary Figure S3.2). There was no difference between right or left lymph node packets which correlated to the

similar HA levels observed in both the right and left lungs (Supplemental Figure S3.1). It is noteworthy that 741 kDa HA content in the spleen was higher than other molecular weights of HA. HA can bind to CD44 on immune cells, which could explain the increase. The 741 kDa HA may have shown this as many endogenous HA lymphatic clearance mechanisms are for molecular weights larger than 100 kDa.

Previous studies have investigated the transport of high molecular weights of HA (4.3 to 5.5 MDA) as well as a low molecular weight HA (150 kDa) injected directly into lymph vessels of sheep[35]. A large percentage of HA was degraded (between 48-75%) with a clearance rate of 43 µg/hour and no HA ≥1 MDa detected in the blood. HA of various sizes (6.4 to 697 kDa HA) has also been injected into the footpads of mice and the fluorescently labeled HA molecules were tracked[54]. This study determined that HA ~30 to 50 nm in size (~75 kDa HA) had the optimal size to access the lymphatics[54]. Similarly, 67 and 215 kDa HA were found here to persist in lung tissues, suggesting lymphatic transport may be augmented by persistence of the HA in tissues supplying the regional lymphatic network.

3.5. Conclusion

HA is a natural biopolymer that has been used in dermal fillers and viscosupplements, and more recently as an anti-inflammatory therapy and delivery vehicle for therapeutics. The lungs of several animal models and even humans have been treated with HA, thus compelling an improved understanding of HA exposure and elimination from lungs. HAs of different molecular weight (7, 30, 67, 215, and 741 kDa HA) were instilled into the lungs of mice and tracked using a fluorescent label or a radiolabel. HA was predominately found in the lungs and the GI tract. The trachea and liver exhibited the next highest HA exposure, but these tissues had significantly lower amounts of HA compared to the lungs and the GI tract. In the lungs, 7

kDa HA exhibited the lowest exposure levels, 30 and 741 kDa HA showed modest exposure, while 67 and 215 kDa exhibited the highest. Pharmacokinetic modeling indicated 67 kDa and 215 kDa HA offered the longest half-life in the lungs. Also, HA was detectable in mouse lymph nodes draining the lungs and in spleens, suggesting radiolabeled HA may be interesting to study in animal models of inflammatory lung diseases. Understanding the biodistribution and pharmacokinetics of different molecular weights of HA delivered to the lungs may enable approaches to increase lung persistence or to preferentially access selected tissue compartments to increase therapeutic efficacy.

References

1. Kuo, JW. Practical Aspects of Hyaluronan Based Medical Products. Crc Press, Boca Raton, Florida. 2006

2. Schanté, Carole, Guy Zuber, Corinne Herlin, Thierry Vandamme. "Chemical modifications of hyaluronic acid for the synthesis of derivatives for a broad range of biomedical applications." Carbohydrate Polymers. 85(3):469-489. 2011

3. Sugiura, Grant, Helen Kühn, Max Sauter, Uwe Haberkorn and Walter Mier. "Radiolabeling Strategies for Tumor-Targeting Proteinaceous Drugs." Molecules. 19(2):2135-2165. 2014

4. Motokawa, Keiko, Sei Kwang Hahn, Teruo Nakamura, Hajime Miyamoto, Tsuyoshi Shimoboji. "Selectively crosslinked hyaluronic acid hydrogels for sustained release formulation of erythropoietin." Journal of Biomedical Materials Part A. 78(3):459-465. 2006

5. Fakhari, Amir. "Biomedical Application of Hyaluronic Acid Nanoparticles." Dissertation from University of Kansas. 2012

6. Allison DD, Grande-Allen KJ. "Hyaluronan: a powerful tissue engineering tool." Tissue Engineering. 12(8):2131-2140. 2006

7. Necas, J, L Bartosikova, P Brauner, J Kolar. "Hyaluronic Acid (Hyaluronan): a Review." Veterinarni Medicina. 53(8): 397-411. 2008

8. Jiang, Dianhua, Jiurong Liang, Paul Noble. "Hyaluronan as an Immune Regulator in Human Diseases." Physiological Reviews. 91(1):221-264. 2011

9. Jiang, Dianhua, Jiurong Liang, and Pau lW. Noble. "Hyaluronan in Tissue Injury and Repair." Annual Review of Cell and Developmental Biology. 23:435-461. 2007

10. Laurent, Torvard, Ulla BG Laurent, J Robert Fraser. "The Structure and Function of Hyaluronan: an Overview." Immunology and Cell Biology. 74(2):A1-A7. 1996

11. Laurent, Torvard and J Robert Fraser. "Hyaluronan." The Journal of the Federation of American Societies for Experiental Biology." 6(7):2397-2404. 1992

12. Laurent, Torvard. "Biochemistry of Hyaluronan." Acta Oto-laryngologica. 104(s442):7-24. 1987

13. Hascall, Vincent. "Hyaluronan, a common thread." Glycoconjugate Journal. 17(7-9):607-616. 2000

14. Brown, MB, SA Jones. "Hyaluronic acid: a unique topical vehicle for the localized delivery of drugs to the skin." *Journal* of the European Academy of Dermatology and Venereology. 19(3):308-318. 2005

15. Burdick, Jason A. and Glenn D. Prestwich. “Hyaluronic Acid Hydrogels for Biomedical Applications.” Advanced Materials. 23(12):H41-H56. 2011

16. Reed, R, U Laurent, S King, J Fraser, T Laurent. “Effect of Increased Interstitial Fluid Flux on Fractional Catabolic rate of High Molecular Weight [3H]Hyaluronan Injected in Rabbit Skin.” Acta Physiologica Scandinavica. 156(2):93-98. 1996

17. Reed, Rolf and Ulla Laurent. “Removal rate of [3H] hyaluronan injected subcutaneously in rabbits.” American Journal of Physiology. 259(2 Pt 2):H532-5. 1990

18. Laurent, Ulla, Lauritz Dahl, and Rolf Reed. “Catabolism of Hyaluronan in Rabbit Skin Takes Place Locally, in Lymph Nodes and Liver.” Experimental Physiology. 76(5):695-703. 1991

19. Allen, Steven, Robert Fraser, Ulla Laurent, Rolf Reed, and Torvard Laurent. “Turnover of hyaluronan in the rabbit pleural space.” Journal of Applied Physiology. 73(4):1457-1460. 1992

20. Laznicek, Milan, Alice Laznickova, Dagmar Cozikova, Vladimir Velebny. “Preclinical pharmacokinetics of radiolabelled hyaluronan.” Pharmacological Reports. 64(2):428-437. 2012

21. Balogh, Lajos, Andras Polyak, Domokos Mathe, Reka Kiraly, Juliana Thuroczy, Marian Terez, Gyozo Janoki, Yaoting Ting, Luke Bucci, Alexander Schauss. “Absorption, Uptake and Tissue Affinity of High-Molecular-Weight Hyaluronan after Oral Administration in Rats and Dogs.” Journal of Agricultural and Food Chemistry. 56(2):10582-10593. 2008

22. Fraser, R, T Laurent, A Engstrom-Laurent, and U Laurent. “Elimination of Hyaluronic Acid From the Blood Stream in the Human.” Clinical and Experimental Pharmacology and Physiology. 11(1): 17-25. 1984

23. Fraser, Robert, Torvard Laurent, Hakan Pertoft, and Elsmaree Baxter. “Plasma clearance, tissue distribution and metabolism of hyaluronic acid injected intravenously in the rabbit.” Biochemical Journal. 200(2):415-424. 1981

24. Gustafson, Stefan, Tomas Bjorkman, Jan-Erik Westlin. “Labelling of high molecular weight hyaluronan with 1251-tyrosine: studies in vitro and in vivo in the rat.” Glycoconjugate Journal. 11(6):608-613. 1994

25. Gavina, Manuela, Alessandro Luciani, Valeria R. Villella, Speranza Esposito, Eleonora Ferrari, Ilaria Bressani, Alida Casale, Emanuela M. Bruscia, Luigi Maiuri, and Valeria Raia. “Nebulized Hyaluronan Ameliorates Lung Inflammation in Cystic Fibrosis Mice.” Pediatric Pulmonology. 48(8):761–771. 2013

26. Buonpensiero, Paolo, Fabiola De Gregorio, Angela Sepe, Antonio Di Pasqua, Pasqualina Ferri, Maria Siano, Vito Terlizzi, and Valeria Raia “Hyaluronic Acid Improves “Pleasantness” and Tolerability of Nebulized Hypertonic Saline in a Cohort of Patients with Cystic Fibrosis.” Advanced Therapeutics. 27(11):870-878. 2010

27. Casale, Manuele, Lorenzo Sabatino, Valeria Frari, Francesco Mazzola, Rosa Dell’Aquila,

Peter Baptista, Ranko Mladina, Fabrizio Salvinelli. "The potential role of hyaluronan in minimizing symptoms and preventing exacerbations of chronic rhinosinusitis." American Journal of Rhinology and Allergy. 28(4):345-348. 2014

28. Furnari, Maria Lucia, Lisa Termini, Gabriella Traverso, Stefania Barrale, Maria Rita Bonaccorso, Giuseppina Damiani, Caterina Lo Piparo and Mirella Collura. "Nebulized hypertonic saline containing hyaluronic acid improves tolerability in patients with cystic fibrosis and lung disease compared with nebulized hypertonic saline alone: a prospective, randomized, double-blind, controlled study." Therapeutic Advances in Respiratory Disease. 6(6):315-322. 2012

29. Nenna, Raffaella, Paola Papoff, Corrado Moretti, Daniela De Angelis, Massimo Battaglia, Stefano Papasso, Mariangela Bernabucci, Giulia Cangiano, Laura Petrarca, Serena Salvadei, Ambra Nicolai, Marianna Ferrara, Enea Bonci, and Fabio Midulla. "Seven Percent Hypertonic Saline—0.1% Hyaluronic Acid in Infants With Mild-To-Moderate Bronchiolitis." Pediatric Pulmonology. 49(9):919-925. 2014

30. Smyth, H.D.C. and A.J. Hickey. Controlled Pulmonary Drug Delivery. Springer Publishing, New York, New York. 2011

31. Winkler, Julia, Guenther Hochhaus, and Hartmut Derendorf. "How the Lung Handles Drugs Pharmacokinetics and Pharmacodynamics of Inhaled Corticosteroids." Proceedings of the American Thoracic Society. 1:356-363. 2004

32. Patton, John and Peter Byron. "Inhaling medicines: delivering drugs to the body through the lungs." Nature Reviews: Drug Discovery. 6(1):67-74. 2007

33. Patton, John, C. Simone Fishburn, and Jeffry G. Weers. "The Lungs as a Portal of Entry for Systemic Drug Delivery." Proceedings of the American Thoracic Society. 1:338-334. 2004

34. Bailey Mark and Cory Berkland. "Nanoparticle Formulations in Pulmonary Drug Delivery. Medical Research Reviews. 29(1):196–212. 2008

35. Fraser, J, W Kimpton, T Laurent, R Cahill, and N Vakakis. "Uptake and degradation of hyaluronan in lymphatic tissue." Biochemical Journal. 256(1):153-158. 1988

36. Reed, Rolf, Torvard Laurent and Aubrey Taylor. "Hyaluronan in prenodal lymph from skin: changes with lymph flow." American Journal of Physiology - Heart and Circulatory Physiology. 259(4):1097-1100. 1990

37. Kim, Youngmi, Yun-Sil Lee, Jang-Hee Hahn, Jongseon Choe, Hyung Joo Kwon, Jai Youl Ro, Dooil Jeoung. "Hyaluronic acid targets CD44 and inhibits FcRI signaling involving PKC, Rac1, ROS, and MAPK to exert anti-allergic effect." Molecular Immunology. 45(9):2537-2547. 2008

38. Casalino-Matsuda, S. Marina, Maria E. Monzon, Anthony J. Day, and Rosanna M. Forteza. "Hyaluronan Fragments/CD44 Mediate Oxidative Stress–Induced MUC5B Up-Regulation in

Airway Epithelium." American Journal of Respiratory Cell and Molecular Biology. 40(3):277-285. 2009

39. Garg, H.G. and C.A. Hales. Chemistry and Biology of Hyaluronan. Elsevier Science, Atanta, Georgia. 2004

40. Smedsrod, Bard, Hakan Pertoft, Sigbritt Eriksson, Robert Fraser, Torvard Laurent. "Studies in vitro on the uptake and degradation of sodium hyaluronate in rat liver endothelial cells." Biochemical Journal. 223(3):617-626. 1984

41. Surendrakumar, K, G.P. Martyn, E.C.M. Hodgers, M. Jansen, J.A. Blair. "Sustained release of insulin from sodium hyaluronate based dry powder formulations after pulmonary delivery to beagle dogs." Journal of Controlled Release. 91(3):385-394. 2003

42. Orlando, P, G Sanctis, C Giordano, G Valle, R la Bua, R Ghidoni. "Tritium Labeled Hyaluronic Acid Derivative." Journal of Labeled Compounds and Radiopharmaceuticals. 22(9):961-969. 1985

43. Orlando, P, L Binaglia, A De Feo, M Orlando, R Trenta, R Trevisi, "An Improved Method for Hyaluronic Acid Radioiodination." Labelled Compounds and Radiopharmaceuticals. 36(9): 855-859. 1995

44. D. Cozikova, A. Laznickova, M. Hermannova, E. Svanovsky, L. Palek, R. Buffa, P. Sedova, R. Koppova, M. Petrik, D. Smejkalova, M. Laznicek, V. Velebny. "Preparation and the kinetic stability of hyaluronan radiolabeled with 111In, 125I and 14C." Journal of Pharmaceutical and Biomedical Analysis. 52(4):517-524. 2010

45. Oh, Eun Ju, Kitae Park, Ki Su Kim, Jiseok Kim, Jeong-A Yang, Ji-Hyun Kong, Min Young Lee, Allan S. Hoffman, Sei Kwang Hahn. "Target specific and long-acting delivery of protein, peptide, and nucleotide therapeutics using hyaluronic acid derivatives." Journal of Controlled Release. 141(1):2-12. 2011

46. Moller, Lena, Andreas Krause, Ivonne Bartsch, Andreas Kirschning, Frank Witte, Gerald Drager. "Preparation and In Vivo Imaging of Lucifer Yellow Tagged Hydrogels." Macromolecular Symposia. 309/310(1): 222-228. 2011

47. Kadi, Shirin, Di Cui, Eric Bayma, Thomas Boudou, Claire Nicolas, Karine Glinel, Catherine Picart, and Rachel Auzely-Velty. "Alkylamino Hydrazide Derivatives of Hyaluronic Acid:Synthesis, Characterization in Semidilute Aqueous Solutions, and Assembly into Thin Multilayer Films." Biomacromolecules. 10(10):2875-2884. 2009

48. Ossipov, Dmitri, Sujit Kootala, Zheyi Yi, Xia Yang, and Jöns Hilborn. "Orthogonal Chemoselective Assembly of Hyaluronic Acid Networks and Nanogels for Drug Delivery." Macromolecules. 46(10):4105-4113. 2013

49. Prestwich, Glenn, Dale Marecak, James F. Marecek, Koen P. Vercruysse, Michael R. Ziebell. "Controlled chemical modification of hyaluronic acid: synthesis, applications, and biodegradation of hydrazide derivatives." Journal of Controlled Release. 53(1-3):93-103. 1998

50. Rydergren, Sara. "Chemical Modifications of Hyaluronan using DMTMM-Activated Amidation." Thesis from Uppsala University. 2013

51. D'Este, Matteo, David Eglin, Mauro Alini. "A systematic analysis of DMTMM vs EDC/NHS for ligation of amines to Hyaluronan in water." Carbohydrate Polymers. 108:239-246. 2014

52. Farkas, Pavol, Alzbeta Cízová, Slávka Bekesová, Slavomír Bystricky. "Comparison of EDC and DMTMM efficiency in glycoconjugate preparation." International Journal of Biological Macromolecules. 60:325-327. 2013

53. Rayamajhi, Manira, Elizabeth F. Redente, Tracy V. Condon, Mercedes Gonzalez-Juarrero, David W.H. Riches, and Laurel L. Lenz. "Non-surgical intratracheal instillation of mice with analysis of lungs and lung draining lymph nodes by flow cytometry." Journal of Visualized Experiments – NIH Public Access. 51:2702. 2012

54. Bagby, Taryn R., Shuang Cai, Shaofeng Duan, Sharadvi Thati, Daniel J. Aires and Laird Forrest. "Impact of Molecular Weight on Lymphatic Drainage of a Biopolymer-Based Imaging Agent." Pharmaceutics. 4(2):276-295. 2012

55. Takahashi, Ryo, Kenji Kubota, Masatoshi Kawada, Akio Okamoto. "Effect of Molecular Weight Distribution on the Solution Properties of Sodium Hyaluronate in 0.2M NaCl Solution." Biopolymers. 50(1):87-98. 1999

56. Mendichi, R, L Soltés, A Giacometti Schieroni. "Evaluation of radius of gyration and intrinsic viscosity molar mass dependence and stiffness of hyaluronan." Biomacromolecules. 4(6):1805-1810. 2003

57. Prokop, Ales. Intracellular Delivery – Fundamentals and Applications. Springer Publishing, New York, New York. 2011

58. Bagby, Taryn R., Shaofeng Duan, Shuang Cai, Qiuhong Yang, Sharadvi Thati, Cory Berkland, Daniel J. Aires, M. Laird Forrest. "Lymphatic trafficking kinetics and near-infrared imaging using star polymer architectures with controlled anionic character." European Journal of Pharmaceutical Sciences. 47(1): 287-294. 2012

59. Ryan, Gemma, Lisa M. Kaminskas, Brian D. Kelly, David J. Owen, Michelle P. McIntosh, and Christopher J. H. Porter. "Pulmonary Administration of PEGylated Polylysine Dendrimers: Absorption from the Lung versus Retention within the Lung Is Highly Size-Dependent." Molecular Pharmaceutics. 10(8):2986-2995. 2013

60. Kaminskas, Lisa M., Christopher J.H. Porter. "Targeting the lymphatics using dendritic polymers (dendrimers)." Advanced Drug Delivery Review. 63(10-11):899-900. 2011

61. Scott, John, Christine Cummings, Andy Brass, and Yuan Cheni. “Secondary and tertiary structures of hyaluronan in aqueous solution, investigated by rotary shadowing-electron microscopy and computer simulation.” Biochemical Journal. 274(3):699-705. 1991

62. Heatley, Frank and John Scott. “A water molecule participates in the secondary structure of hyaluronan.” Biochemical Journal. 254(2):489-493. 1988

63. “Size matters: Rh versus Rg.” Malvern Corporate Meet the Experts Press Release. November 15, 2012.

64. Zwanzig, Robert and Alan K. Harrison. “Modifications of the Stokes–Einstein formula.” AIP:The Journal of Chemical Physics. 83(11):5861-5862. 1985

65. Mori, Masahiko, Minako Yamaguchi, Shinichiro Sumitomo, Yoshiaki Takai. “Hyaluronan-Based Biomaterials in Tissue Engineering.” Acta Histochemica et Cytochemica. 37(1):1-5. 2004

66. Vindigni, Vincenzo, Roberta Cortivo, Laura Iacobellis, Giovanni Abatangelo and Barbara Zavan. “Hyaluronan Benzyl Ester as a Scaffold for Tissue Engineering. ”International Journal of Molecular Sciences. 10(7):2972-2985. 2009

67. Patton, John and Robert Platz. “Routes of Delivery: Case Studies: Pulmonary delivery of peptides and proteins for systemic action.” Advanced Drug Delivery Reviews. 8(2-3):179-196. 1992

68. Grubb, B. R.,J. H. Jones, and R. C. Boucher. “Mucociliary transport determined by in vivo microdialysis in the airways of normal and CF mice.” American Journal of Physiology - Lung Cellular and Molecular Physiology. 286(3):L588-L595. 2003

69. Foster, W. Michael, Dianne M. Walters, Malinda Longphre, Kristin Macri and Laura Miller. “Methodology for the measurement of mucociliary function in the mouse by scintigraphy.” Journal of Applied Physiology. 90(3):1111-1118. 2001

70. Padmanabhan, Parasuraman, Johannes Grosse, Abu Bakar Md Ali Asad, George K Radda and Xavier Golay. “Gastrointestinal transit measurements in mice with 99mTc-DTPA-labeled activated charcoal using NanoSPECT-CT.” European Journal of Nuclear Medicine and Molecular Imaging. 3(60):1-8. 2013

71. Schwarz, R, Kaspar, Seelig, Künnecke. “Gastrointestinal transit times in mice and humans measured with 27Al and 19F nuclear magnetic resonance.” Magnetic Resonance in Medicine. 48(2):255-261. 2002

72. Loira-Pastoriza, Cristina, Julie Todoroff, Rita Vanbever. “Delivery strategies for sustained drug release in the lungs.” Advanced Drug Delivery Reviews. 75:81-91. 2014

Supplemental Data

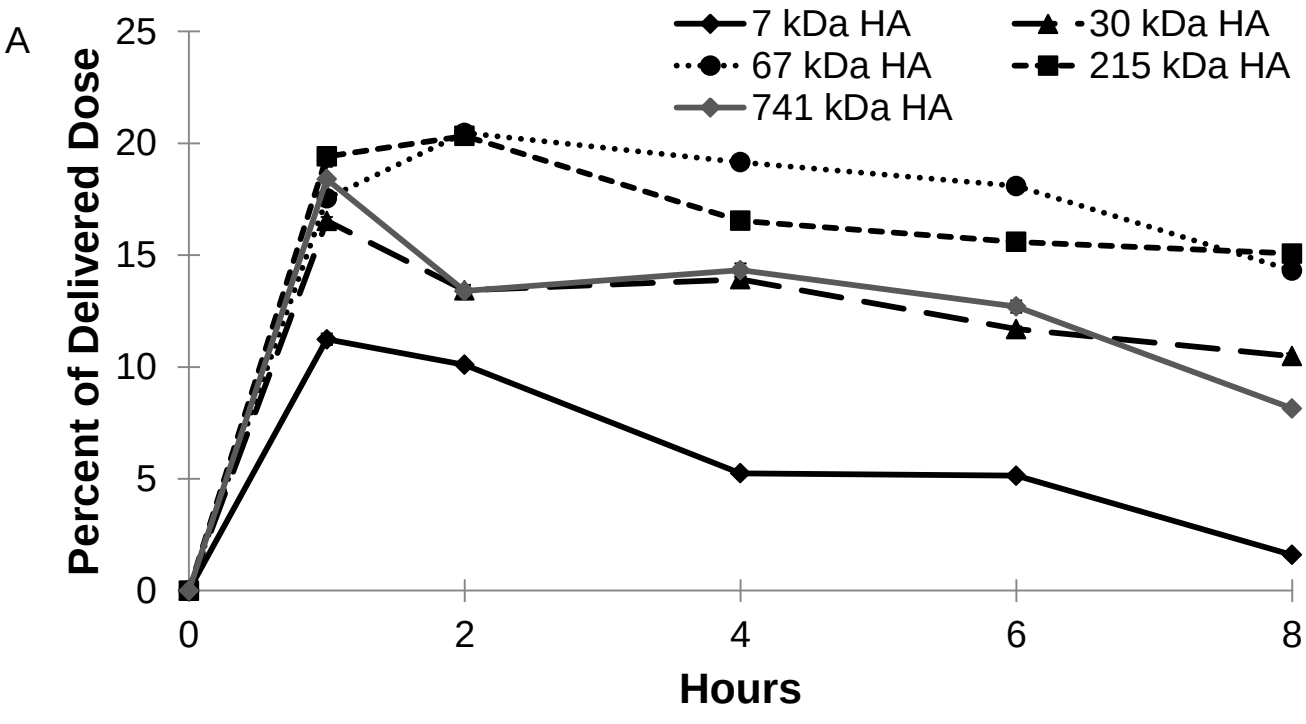

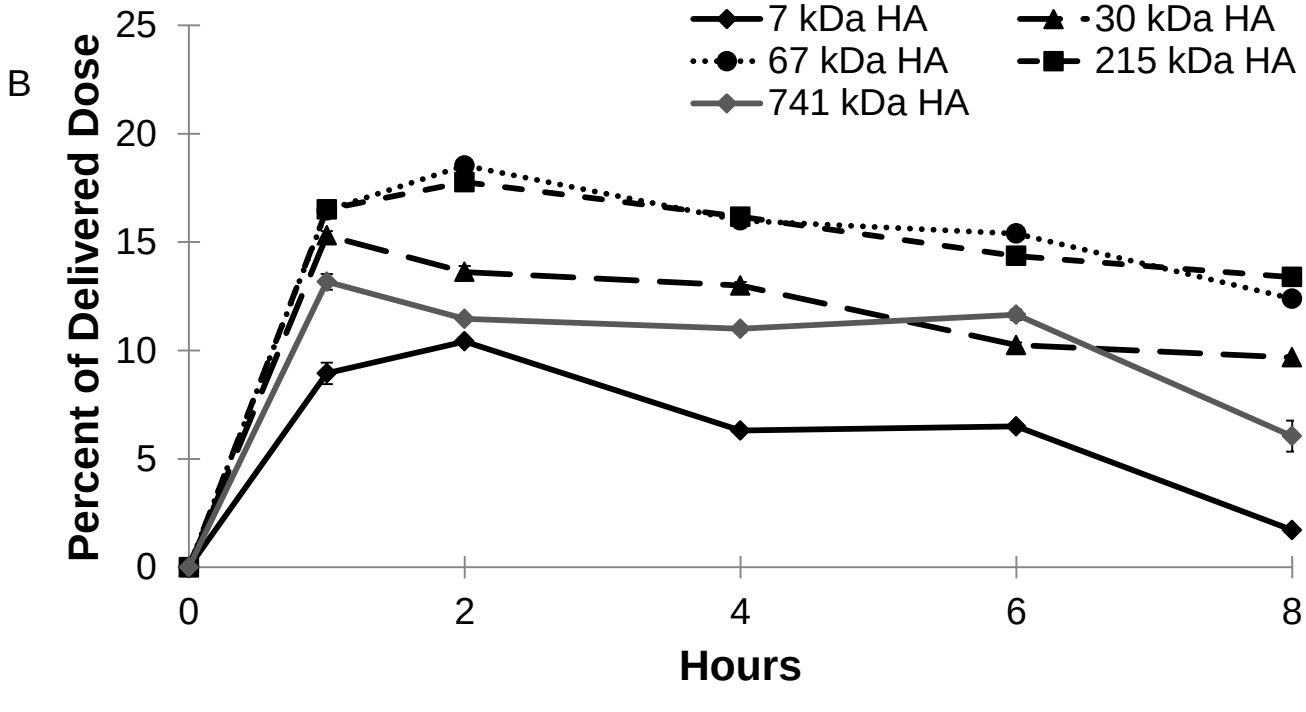

Supplemental Figure S3.1: Exposure levels of HA in the lungs as a percentage of delivered dose over time for each of the five HA molecular weights. A shows the right lungs, while B depicts the left lungs with the molecular weights displayed for each. Each point is an average of at least five animals with the error on each point <5% of the measurement.

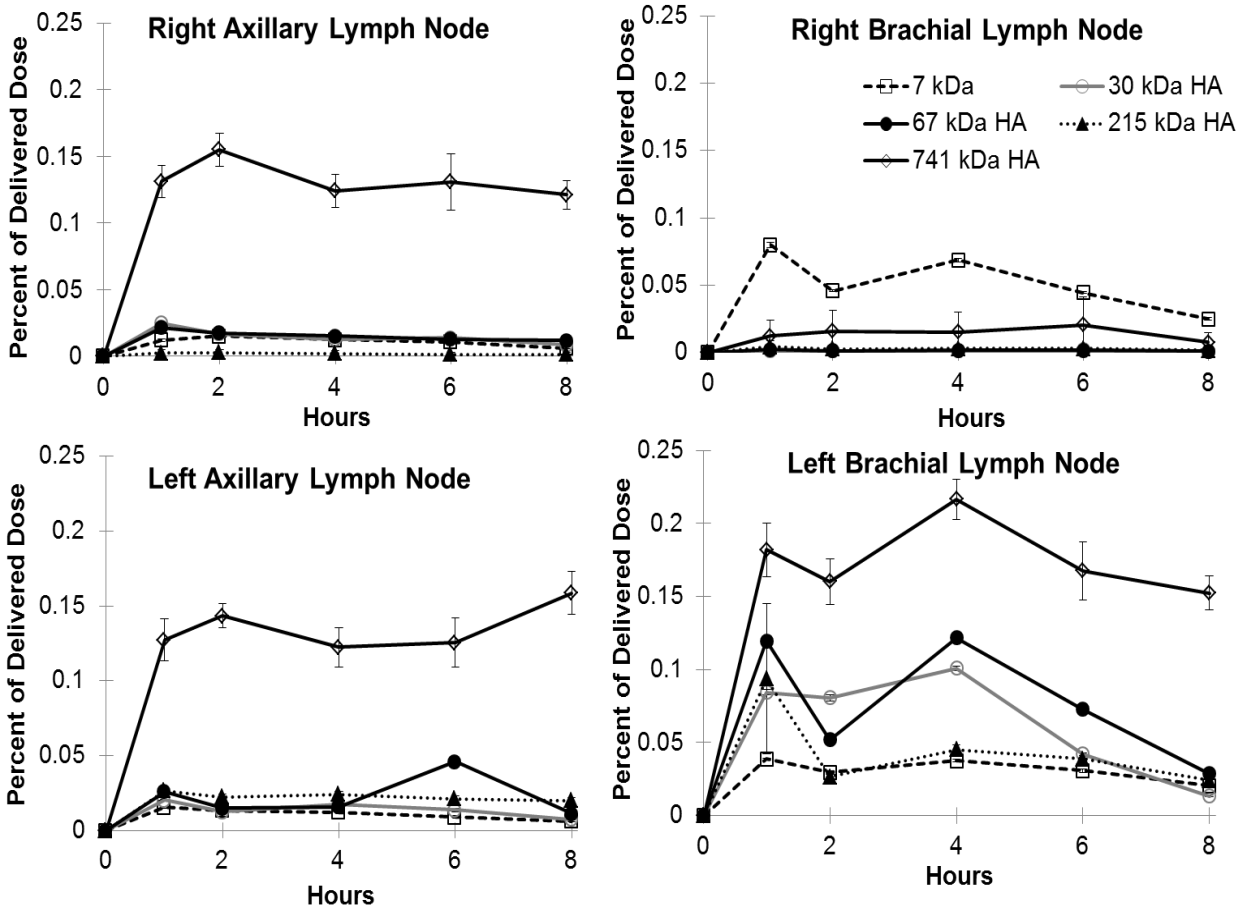

Supplemental Figure S3.2: Exposure levels of HA in the 4 extracted lymph nodes: right and left axillary and brachial, as a percentage of delivered dose over time for each of the five HA molecular weights. Each point is an average of at least five animals with the error on each point <5% of the measurement.

Table S3.1: Organ clearance rate in mL/hours^{-1} for each tissue based on molecular weight.

Molecular Weight (kDa)	***Right Lung Lobes***	***Left Lung Lobes***	***Heart***	***Spleen***	***Liver***	***Stomach***	***Intestine***	***Kidney***	***Bladder***
7	1.87	1.75	81.2	117.0	10.5	1.59	1.16	24.4	49.7
*30**	0.41	0.42	61.0	104.7	5.6	1.51	1.18	25.7	66.3
67	0.30	0.32	47.5	49.5	7.1	1.22	0.73	14.3	43.1
215	0.13	0.25	47.2	114.8	12.1	1.44	1.55	36.2	75.0
741	0.63	0.68	17.1	14.4	7.2	1.10	1.02	11.8	0

Chapter 4

Using Soluble Antigen Arrays (SAgAs) for Immune Modulation after Pulmonary Administration

4.1. Introduction

Inducing antigen specific immune tolerance is an emerging avenue of treatment of autoimmune diseases[1]. The classical approach of antigen specific immunotherapy (ASIT) has been to desensitize the immune system through a series of subcutaneous injections. This approach has generally been applied to foreign antigens (e.g. hyposensitization in the form of "allergy shots"). The treatment regimen, however, requires injections over multiple years and disease improvement is often modest[1-5]. Similar strategies have been investigated for desensitizating patients to autoantigens including proinsulin peptide for type-1 diabetes[6], splicesomal peptide for Lupus[7], and a pathogenic peptide for rheumatoid arthritis[8]. Alternative delivery approaches have appeared as strategies to improve efficacy of ASIT. Recently, new products including Ragwitek® and Grastek® that utilize sublingual administration to desensitize the immune system to foreign antigens through mucosal surfaces. Treating the mucosal surfaces, such as nasal passages or lungs, may also improve performance or reduce the timeline required for ASIT[2,5,9].

Mucosal membranes such as nasal, buccal, and pulmonary tissues offer the first line of defense against exogenous antigen insult. Mucosal barriers have multiple mechanisms to remove foreign pathogens and because of this, almost 80% of all immune cells constitute the mucosal immune system. The mucosal immune system serves multiple purposes; protection from exposure to dangerous pathogens, processing of foreign antigens, and inducing appropriate immune responses to these foreign antigens. The immune cells and surrounding tissues are part of the mucosa-associated lymphoid tissue (MALT) and are awash in foreign antigens compared to the rest of the immune system, which functions in a sterile environment[2,11]. Because of the plethora of foreign antigens, MALT must also prevent damage to surrounding cells. The MALT is a separate part of the immune system that functions independent of the systemic immune system. There are separate distinct immune cell

populations with limited cycling between regions given the highly compartmentalized nature to reduce unwanted immune responses[12-16].

Antigen presentation is not limited to foreign antigens. Typically, dendritic cells patrol the peripheral tissues including blood and lymphoid tissues taking up foreign antigens that enter the body. Dendritic cells internalize and process the foreign proteins and degrade them to their constituent peptides, which are then processed on the surface of these cells on cell surface receptors including major histocompatibility complex II (MHC II). Dendritic cells, after encountering certain signals, enter a process of maturation and become professional antigen presenting cells (pAPCs) with an increase in MHC peptide presentation[16-19] . These pAPCs are capable of inducing differentiation of naïve T cells into mature T cells that have the capability to counter the foreign pathogens by utilizing surface cell receptors for MHC I and II and intercellular adhesion molecule I (ICAM-1), for example[17,20-23]. Similarly, B cells are adept at capturing low levels of antigen using B cell receptors; subsequently processing and presenting peptide epitopes on MHC II[23]. Sometimes, however, the immune system can malfunction and attack self-antigens. Dendritic cells and B cells can process and present self-antigens, activating T cells and propagating destruction of tissues. This immune response to self-antigens is what is seen in autoimmune diseases including rheumatoid arthritis, Celiac disease, Type 1 diabetes, and multiple sclerosis[1,24].

Multiple sclerosis (MS) is an autoimmune disease, where immune cells attack and degrade the myelin sheath surrounding neurons interrupting the transmission of electrical signals[3,4,25,26]. Many of the current therapies approved for MS focus on treating inflammation or neurological symptoms including loss of balance, degrees of paralysis, and a loss of coordination. Fewer efforts have aimed to correct the underlying immune response leading to the symptoms. If this autoimmunity is uncorrected, patients can experience progressive cycles of remission and relapse, where periodic symptoms are followed by remission, but the patient

does not fully recover to the previous baseline. There are different forms of this disease: secondary progressive, primary progressive, progressive relapsing, and relapsing remitting, which affects a majority of patients, approximately 80%[4,25,26]. Experimental autoimmune encephalomyelitis (EAE) is the murine model of relapsing and remitting MS and is induced by an epitope from proteolipid protein (PLP), a component of the myelin sheath. In this model, mice exhibit a peak of disease followed by remission over the course of approximately 25 days[3,4,24].

An approved therapy for MS, Copaxone® is a random polymer of glatiramer acetate comprised of glutamic acid, lysine, alanine, and tyrosine, which are found in myelin basic protein, a component of the myelin sheath[3,27]. Copaxone® acts similarly to some aspects of conventional ASIT. Copaxone® potentially generates tolerance by inducing regulatory T cells, but the mechanism is still under investigation. One issue with Copaxone® is that it is prescribed to treat the symptoms of MS and to prevent a relapse, and reversal of the underlying cause of immune dysregulation has not been observed[27].

An alternative approach to Copaxone® is the creation of multivalent soluble antigen arrays (SAgAs) comprised of a hyaluronic acid (HA) polymer backbone with grafted epitope from proteolipid protein amino acids 139-151 (PLP) from the myelin sheath, and a grafted peptide inhibitor of cell surface receptor intracellular cell-adhesion molecule-1 (ICAM-1)[3]. Previous work has shown that pulmonary delivery of SAgAs had increased efficacy compared to subcutaneous and intravenous delivery[4]. By co-delivering these peptides, SAgAs desensitize the immune response to PLP, but further study was necessary to determine which individual components are key in eliciting the toleragenic immune response that ameliorate EAE in mice (Table 4.1).

Table 4.1: Description of each component investigated in EAE mouse studies.

Components	***Description***	***Cartoon Representation***
Phosphate Buffered Saline	Negative control	NA
HA	Delivery vehicle	
LABL	Cell surface receptor ligand (ITDGEATDSG)	
PLP	Antigenic peptide (HSLGKWLGHPDKF)	
SAgA	Multivalent therapeutic of HA, PLP, and LABL	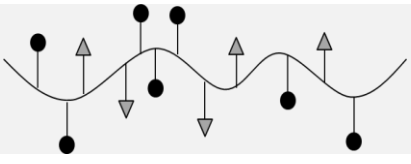
BPI	Positive control	

4.2. Materials and Methods

4.2.1. Materials

Hyaluronic acid (HA) molecular weight 16 kDa was purchased from Lifecore Biomedical (Chaska, Minnesota). Aminooxy-LABL (AoLABL) and Aminooxy-PLP (AoPLP) peptides were obtained from PolyPeptide Inc (San Diego, CA). Incomplete Freund's Adjuvant Oil and Mycobacterium tuberculosis were obtained from BD Difco Adjuvants (Franklin Lakes, New Jersey) and pertussis toxin was purchased from List Biological Laboratories, Inc. (Campbell, California). The mouse laryngoscope was purchased from Penn-Century (Wyndmoor, Pennsylvania). All water used was deionized (DI) water from a Labconco Pro PS system. All other chemicals and materials including 3500 Da molecular weight cutoff dialysis tubing, bent fine dissecting forceps, glacial acetic acid, sodium acetate, sodium phosphate monobasic

monohydrate, sodium phosphate dibasic, and phosphate buffered saline were purchased from Fisher Scientific (Pittsburgh, Pennsylvania).

4.2.2. Soluble Antigen Array (SAgA) Synthesis

The purified peptides were conjugated onto HA. In 20 mM acetate buffer pH 5.5, a concentration of 2 mg/mL of 16.9 kDa HA was made. AoLABL and AoPLP peptides were added in equal molar proportions, then were added to the 2 mg/mL HA solution using a ratio of 2 HA monomers to 1 Ao peptide. The reaction was allowed to proceed for 24 hours at room temperature. After 24 hours, the reaction mixture was added to 3500 Da molecular weight cutoff dialysis tubing using DI water as the dialysate for 24 hours with the dialysate being changed every 6 hours. Samples were then frozen ad lyophilized for 72 hours at a temperature of -72 °C at a vacuum of <300 millitorr (VirTis Feezemobile-12XL, The Virtis Company, NY).

SAgAs had their peptide loading analyzed using reverse phase high performance liquid chromatography (RP-HPLC) and size exclusion chromatography (SEC). SAgAs were dissolved in 0.1 M HCl pH 1.0 for 4 hours to hydrolyze peptides from the HA backbone. With the HPLC, a calibration curve of free peptide was employed to determine the amount of peptide that was conjugated to the HA for SAgAs, which was compared to the relative size ascertained from SEC. The HPLC method employed was performed using a Waters 2487 dual absorbance detector and a Waters 2796 bioseparation module. The HPLC method employed was a gradient system with mobile phase A comprised of 94.9% Di water, 5% acetonitrile, and 0.1% trifluoroacetic acid and mobile phase B comprised of 99.9% acetonitrile and 0.1% trifluoroacetic acid. The solvent system was 100% A from 0 to 15 minutes, 85% A/15% B at 15 minutes, 83% A/17% B at 20 minutes, 80% A/20% B at 33 minutes, 75% A/25% B at 42 minutes, 30% A/70% B at 43 minutes, and 100% A at 46 minutes until 60 minutes with a total flow rate of 1 mL/min.

A C18 Higgins Analytical Proto200, 5 µm, 200 Å, 250 × 4.6 mm^2 column was used with an injection volume of 30 µL using samples with a concentration of 1 mg/mL with wavelength detection at 220 nm.

SEC was employed to determine the increase in size of SAgA from HA due to the conjugation of peptides. The system used included a Waters e2695 separation module, Waters 2414 refractive index detector, and Waters 2489 UV/Vis detector with two columns in series: a PL Aquagel-OH 60 Analytical SEC (300 x 7.5 mm) then a PL Aquagel-OH 40 Analytical SEC (300 x 7.5 mm). The mobile phase employed for SEC was of 0.1M ammonium acetate with 0.136M sodium chloride at pH 5 using an isocratic system. Samples injected were 80 µL at a concentration of 5 mg/mL with a total flow rate of 0.5 mL/min flow. Samples were dissolved in the mobile phase at a concentration of 5 mg/ml and chromatograms were analyzed using EMPower 3.

4.2.3. Animals

SJL/J mice (female, 4 weeks old) were supplied by Harlan Laboratories (Indianapolis, IN) for the study. Mice were approximately 13-16 g and were weighed throughout the course of the experiment. The mice were housed in a pathogen-free facility at the University of Kansas approved by the Association for Assessment and Accreditation of Laboratory Animal Care (AAALAC). Mice were maintained on a 12 hour light/dark cycle and were fed standard rodent pellets with no dietary restrictions or withheld food with water always available. All animal experiments were approved by the University of Kansas Institutional Animal Care and Use Committee (IACUC).

4.2.4. Induction of Experimental Autoimmune Encephalomyelitis (EAE) and Time Course of Study

Each SJL/J mouse had EAE induced on study day 0 with 4 injections of an emulsion of Incomplete Freund's Adjuvant Oil, Mycobacterium tuberculosis, and 200 nM of PLP. Each of the 4 injections was 50 µL given subcutaneously: 2 above the shoulder blades and 2 above the rear hip haunches. Each SJL/J mouse had 100 µL of 200 ng pertussis toxin injected intraperitoneal on day 0 as well as day 2. There were 6 mice in each of the groups split into 2 cages of 3 mice.

Over the course of the 25 day study, each mouse was weighed and given a clinical score from study day 7 to 25. The clinical scoring ranged from 0 to 5 with half integer values and a higher score correlated to an increase in disease progression. The advancement of the scoring was as follows: 0 corresponded to no symptoms of disease; 1 with a limp tail and waddling gait; 2 with partial leg paralysis and increased alteration of gait; 3 with paraplegia or complete hind leg paralysis; 4 with partial front leg paralysis; and 5 with complete front leg paralysis or moribund. Half integer values corresponded with disease progression between scoring levels[3,4].

4.2.5. Treatment Schedule and Pulmonary Instillation of Compounds

Treatment was administered on study days 4, 7, and 10. Before treatment, each of the study compounds was dissolved in sterile phosphate buffered saline (PBS). The study groups were PBS, 16 kDa HA, LABL, PLP, SAgA, and bifunctional peptide inhibitor (BPI). Each animal had 50 µL of each compound corresponding to 200 nM with the exception of BPI, which was 150 nM administered via pulmonary instillation as described in detailed below[3,4]. All the

statistical analyses were performed on Prism GraphPad 5 software, using ANOVA analysis. Tukey post-hoc analysis was applied to the data.

For lung administration via pulmonary instillation, each animal was anesthetized with 2% isoflurane in an induction chamber for approximately 4 minutes. After the mouse was fully anesthetized, the mouse was positioned in dorsal recumbency using a dosing board at approximately 60° to a supine position suspended by incisor teeth using a thin wire. A nose cone was used to maintain anesthesia. The mouth was opened and the tongue was gently pulled out and to the side of the mouth. A laryngoscope was then positioned to depress the tongue and visualize the vocal cords at the top of the trachea. A 50 µL solution of HA was then pipetted at the top of the trachea. The tongue was withheld for at least 3 breaths, after which time the mouse was maintained under anesthesia for an additional 3 minutes on the dosing board. The mouse was then removed from the dosing board and allowed to recover from the anesthesia by being held vertically until movement was regained[28].

4.3. Results

4.3.1. Characterization of SAgAs

Reverse phase chromatography was utilized to determine the amount of peptide conjugated to HA. Based on the RP-HPLC results, there was approximately 5 to 6 PLP peptides and 7 to 8 LABL peptides conjugated per polymer chain. By determining the number of peptides conjugated, the approximate average molecular weight calculated using both SEC and HPLC results (Table 4.2).

Table 4.2: Characterization of SAgAs and peptide loading.

Average Number of AoPLP on SAgA	*Average Number of AoLABL on SAgA*	*Average Molecular Weight of SAgA*	*AoLABL:AoPLP*	*AoPLP:AoLABL*
5.8	7.5	33000	1.3	0.78

4.3.2. Co-Delivery of Peptides via SAgAs Offers Improved Therapeutic Efficacy

The co-delivery of peptides using SAgAs was necessary for ameliorating EAE symptoms. The mice were treated on study days 4, 7, and 10, as was previously established in earlier publications. The PBS group had high clinical scores that were similar to the group treated with LABL (Figure 4.1). Both groups had scores that increased as of day 10 with the PBS group having the highest scores between days 12-15 and peaking on 14, while LABL peaked slightly earlier at day 12. Both PBS and LABL remained high throughout the course of the study ending with scores of approximately 1.0. The HA group had a slightly delayed onset of disease as disease was observed at day 11 with a peak on day 14 and a decrease to near baseline values by day 18. The PLP group had similar scoring to the BPI group with scores remaining around 0.5 after disease onset. The SAgA group had lower scores throughout the length of the study with scoring ranging between approximately 0 and 0.25, but were not statistically different from PLP and BPI.

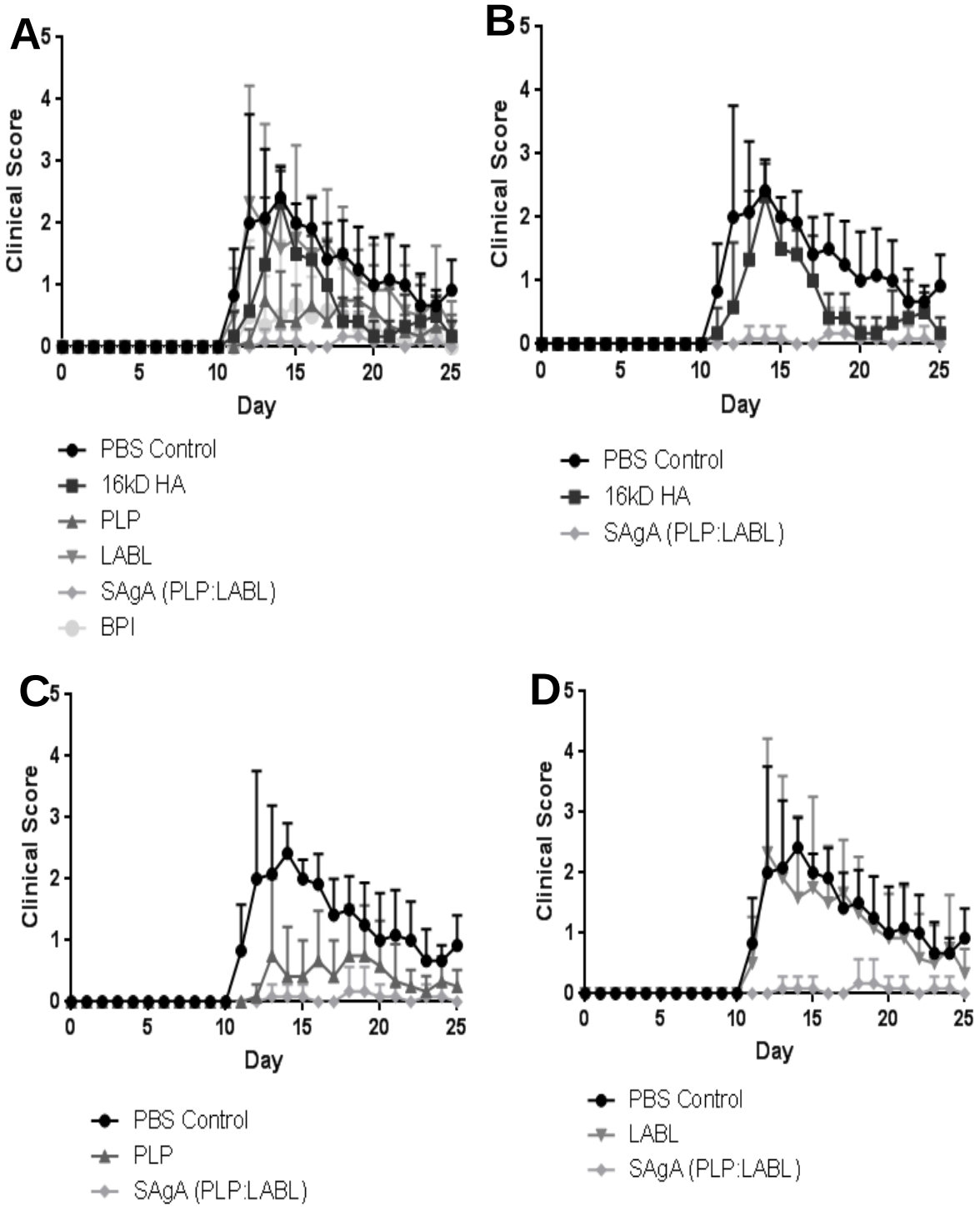

Figure 4.1: Clinical scores throughout the study from each of the 6 groups: PBS control, HA, LABL, PLP, SAgA, and BPI. Panel A depicts all 6 groups; Panel B shows PBS, HA, and SAgA; Panel C represents PBS, PLP, and SAgA; and Panel D depicts PBS, LABL, and SAgA. Each point is the average of 6 animals with the standard deviation within each group.

Table 4.3: Significance of clinical scores throughout the study from each of the 6 groups. Significance is compared between two groups with listed days showing significant difference. NS represents not statistically significant.

	PI PBS	***PI 16 kDa HA***	***PI PLP***	***PI LABL***	***PI SAgA***	***PI BPI***
PI PBS	X	Day 12, 18, 21	Days 12-17	NS	Days 12-18, 20-25	Days 12-16, 18-25
PI 16 kD HA	Day 12, 18, 21	X	Day 14, 15	Day 12, 18	Days 13-16	Days 13, 14, 16
PI PLP	Days 12-17	Day 14,15	X	Days 12-15, 17	NS	NS
PI LABL	NS	Day 12, 18	Days 12-15, 17	X	Days 12-19	Days 12-18
PI SAgA	Days 12-18, 20-25	Days 13-16	NS	Days 12-19	X	NS
PI BPI	Days 12-16, 18-25	Day 13, 14, 16	NS	Days 12-18	NS	X

The area under the curve (AUC) from clinical scores in Figure 4.1 provides a holistic view of the disease state of EAE mice (Figure 4.2). The PBS group had the highest AUC of approximately 20 with LABL being similar. HA showed a decreased AUC compared to LABL and PBS but was higher compared to both PLP and BPI. Again, BPI and PLP were quite similar, approximately 4-5, in terms of AUC. SAgA had the lowest AUC value throughout the course of the study, but was not statistically lower than the BPI treatment.

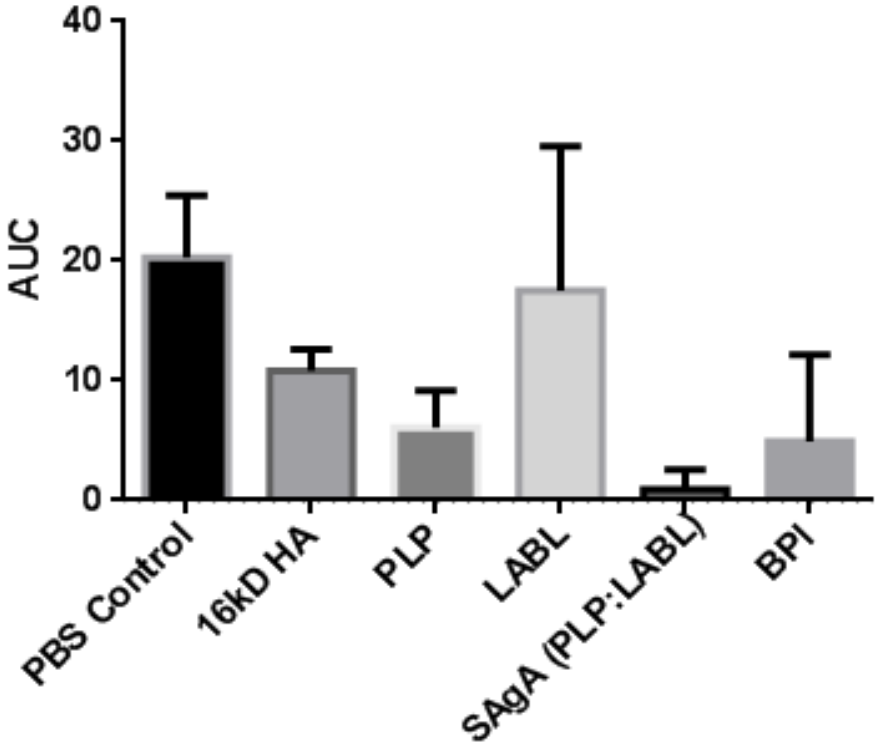

Figure 4.2: Area under the curve (AUC) of clinical scores throughout the study from each of the 6 groups. Each group is the averaged aggregate total of the scores from the individual animals over the entirety of the 25 day long study.

Table 4.4: Significance of AUC values based on accumulative clinical scores throughout the study from each of the 6 groups. Significance is compared between two groups with listed days showing significant difference. NS represents not statistically

	PI PBS	***PI 16 kDa HA***	***PI PLP***	***PI LABL***	***PI SAgA***	***PI BPI***
PI PBS	X	p<0.01	p<0.01	NS	p<0.001	p<0.01
PI 16 kD HA	p<0.01	X	p<0.05	NS	p<0.0001	NS
PI PLP	p<0.01	p<0.05	X	NS	p<0.05	NS
PI LABL	NS	NS	NS	X	p<0.05	NS
PI SAgA	p<0.001	p<0.0001	p<0.05	p<0.05	X	NS
PI BPI	p<0.01	NS	NS	NS	NS	X

The incidence of disease was also determined (Figure 4.3). Mice are considered 'diseased' when progressing to a score of 1.0 or higher, corresponding to symptoms affecting the rear legs as well as the tail. The PBS, HA, and LABL groups had a rapid progression to disease with HA and PBS showing all the animals were sick by day 14 and all LABL-treated animals by day 17. The PLP group had only 1 animal remain disease free throughout the course of the study. The BPI group had 4 of 6 animals remain disease free, while the SAgA group had 5 of the 6 animals remain disease free.

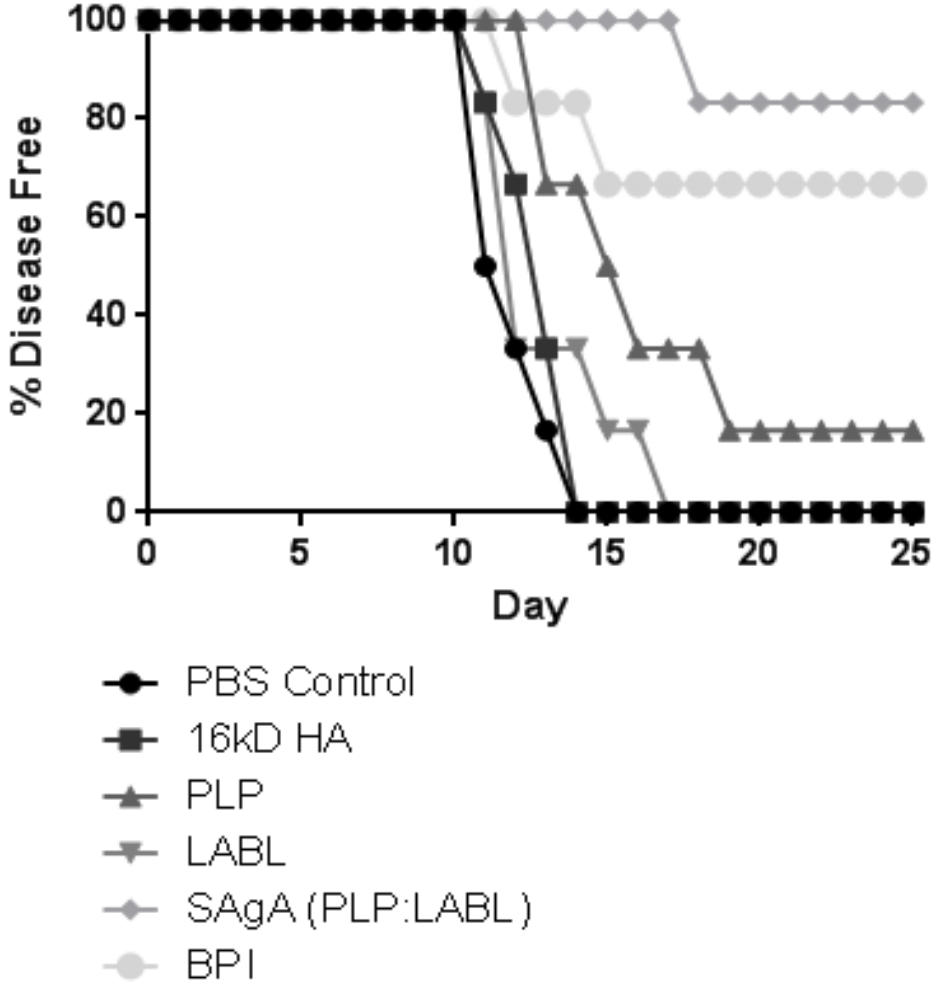

Figure 4.3: Incidence of disease, (when clinical score exceeds 1.0) throughout the study from each of the 6 groups (PBS control, HA, LABL, PLP, SAgA, and BPI). Each point is the average of 6.

Table 4.5: Significance of incidence of disease throughout the study from each of the 6 groups. Significance is compared between two groups with listed days showing significant difference. NS represents not statistically significant.

	PI PBS	***PI 16 kDa HA***	***PI PLP***	***PI LABL***	***PI SAgA***	***PI BPI***
PI PBS	X	NS	p<0.05	NS	p<0.001	p<0.01
PI 16 kD HA	NS	X	NS	NS	p<0.001	p<0.01
PI PLP	p<0.05	NS	X	NS	p<0.01	NS
PI LABL	NS	NS	NS	X	p<0.001	p<0.05
PI SAgA	p<0.001	p<0.001	p<0.01	p<0.001	X	NS
PI BPI	p<0.01	p<0.01	NS	p<0.05	NS	X

A more quantitative measurement than clinical score is assessment of weight throughout the study (Figure 4.4). The weight of the animal decreases around the onset of disease due to decreased mobility of the animal and general decrease of animal health. Typically, weight decreases starting around day 10 and as the disease resolves, will gradually increase to a similar level at the end as at the beginning of the study. By tracking change in weight, a more quantitative measurement can be utilized and normalized to the individual animals. The PBS, LABL, and HA groups had similar decreases in weight starting on day 10 with the greatest decrease in weight occurring on days 14 and 15. All three groups had similar increases with weight by the end of the study, recovering to levels similar to the starting weights. The BPI and PLP groups, again, were quite similar with decreases in weight from day 11 to 18 but with less of a decrease in weight compared to PBS, HA, and LABL. The SAgA group had almost continuous weight gain throughout the course of the study ending with almost a 10% weight gain on average.

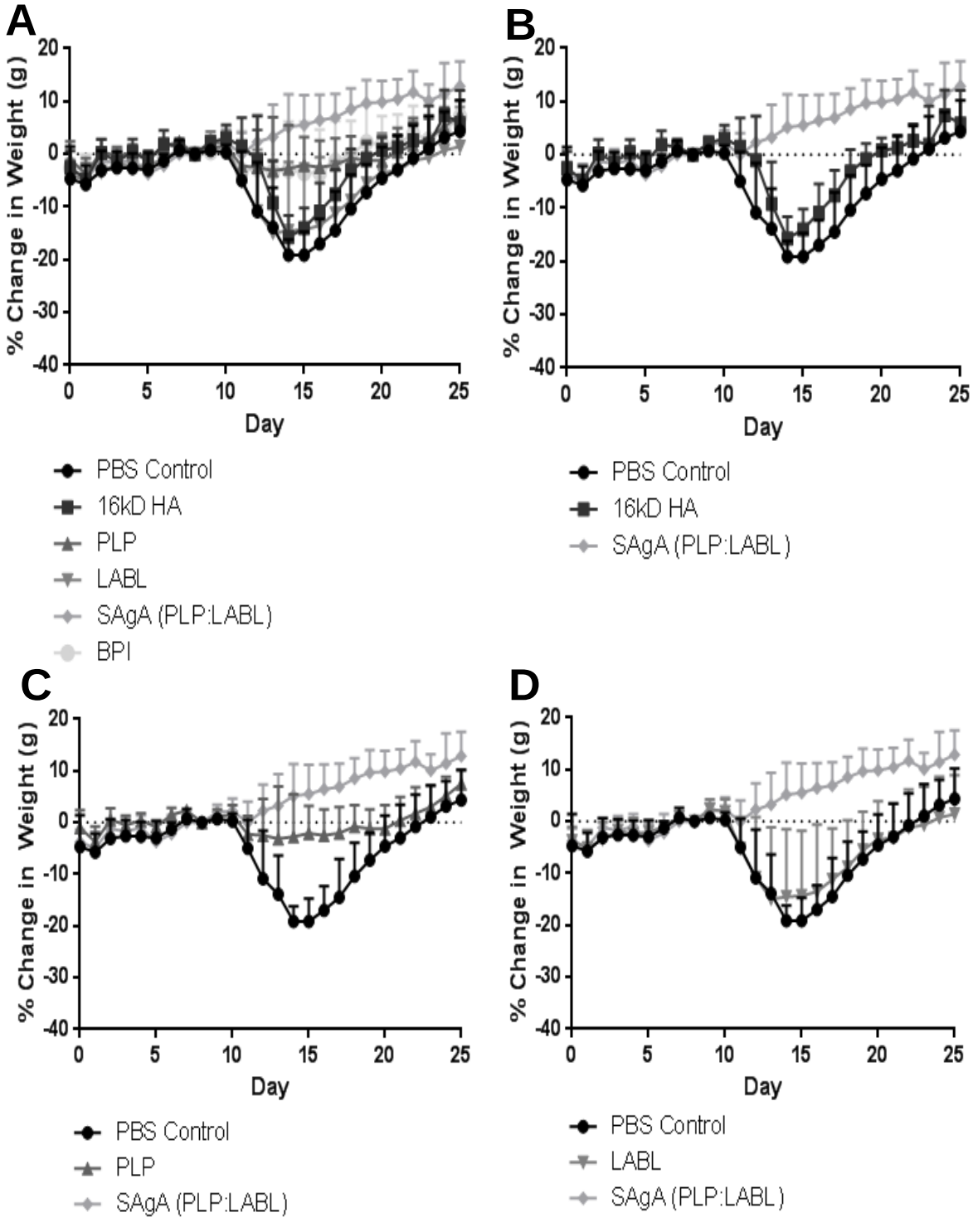

Figure 4.4: Change in weight based on normalization to the initial weight on Day 0 throughout the study with all 6 groups (PBS control, HA, LABL, PLP, SAgA, and BPI). Panel A depicts all 6 groups; Panel B shows PBS, HA, and SAgA; Panel C represents PBS, PLP, and SAgA; and Panel D depicts PBS, LABL, and SAgA. Each point is the average of 6 animals with the standard deviation within each group.

Table 4.6: Statistical significance of percentage of weight gain throughout the study from each of the 6 groups. Significance is compared between two groups with listed days showing significant difference. NS represents not statistically significant.

	PI PBS	***PI 16 kDa HA***	***PI PLP***	***PI LABL***	***PI SAgA***	***PI BPI***
PI PBS	X	Day 12	Days 13-18	NS	Days 12-23	Days 13-19
PI 16 kD HA	Day 12	X	Day 14, 15	Day 12	Days 13-22	Day 14, 15
PI PLP	Days 13-18	Day 14, 15	X	Days 13-17	Days 16-22	NS
PI LABL	NS	Day 12	Days 13-17	X	Days 12-25	Days 13-17
PI SAgA	Days 12-23	Days 13-22	Days 16-20	Days 12-25	X	Day 15, 16
PI BPI	Days 13-19	Day 14, 15	NS	Days 13-17	Day 15, 16	X

4.4. Discussion

4.4.1. The Lungs and Immune Tolerance

Antigen-specific immunotherapies are traditionally administered via subcutaneous injections. Injections of antigens can potentially transport by two mechanisms: diffusion from the injection site to enter systemic circulation where immune cells can take up the antigens and process them to generate tolerance (e.g. hyposensitization therapy) and active local uptake and cellular transport to lymph nodes[1-5]. Mucosal delivery, including buccal (e.g. Grastek®), nasal, and pulmonary delivery, offers a convenient route of administration and the potential for improved performance. Mucosal surfaces serve as the initial barrier to entry and are constantly inundated with foreign pathogens. These surfaces have their own MALT, which includes specialized epithelial cells that can take up antigens and direct the antigens to antigen presenting cells to elicit an immune response[2,5,9,10].

4.4.2. Potential Licensing of Immune Cells in the Lungs for Immune Tolerance

Recent research has shown the lungs to play a more important role in the immune system than previously thought. For example, the 'Hub and Spoke' hypothesis suggests immune cells in systemic circulation or in the secondary lymphoid organs such as the lymph nodes and spleen have to be 'licensed' to become active[29]. Immune cells gain information so they can migrate to different parts of the body after they enter the lungs, or the hub. Once these immune cells are imbued with this information, they then can pass through to the particular spoke of an autoimmune disease, such as the brain for MS, pancreas for type-1 diabetes, and the large intestine for irritable bowel disease. Research has shown that activated immune cells specific to CNS antigens do not elicit CNS symptoms until 5 days after injection when given intravenously. If these same cells are delivered into the CNS, no symptoms are seen. More interestingly is that these same cells if injected into the lungs, elicit the CNS symptoms without the delay after approximately 1 day[30,31].

The 'Hub and Spoke' hypothesis is especially important for T cells to migrate to a particular location in the body by modifying transcription and translation of necessary molecules for traversing tissue known as integrins. Tissue-specific integrins, are necessary for the immune cells to migrate, and these molecules have been pursued as potential therapeutics. The potential licensing of immune cells in the lungs of EAE mice has increasing evidence. Researchers are elucidating the cell populations involved, tracking the cells to determine if these mechanisms impact efficacy. Modification of the immune response via MALT or systemic changes in autoimmunity may hinge on the ability of cells to migrate through the lungs and to different compartments. Thus, the lungs provide an intriguing route of ASIT administration to skew immune responses throughout the body[29-31].

4.4.3. Potential Immune Modulation Mechanism for SAgAs

The pulmonary delivery of SAgA components suggested the need for co-delivery of the PLP antigen epitope with LABL peptide to the lungs of EAE mice. HA has some inherent immune activity as it can bind to CD44+ immune cells yet no therapeutic efficacy was observed with the delivery of HA. The delivery of LABL also did not change the disease state suggesting blocking ICAM-1, a known mediator of immune cell adhesion and co-stimulation, was not therapeutic. It is possible that LABL was digested quickly by peptidases in the lungs or that it was quickly eliminated from the lung tissue via clearance or absorption. Treating with PLP alone had increased efficacy based on AUC of the clinical scores, but most EAE mice treated with PLP became sick. Animals treated with PLP had a delayed onset of disease and exhibited decreased scores compared to HA and LABL hinting that PLP may function as conventional ASIT. If this is the case, PLP may reduce disease scores by acting as a 'decoy' and repeated, perhaps, escalating, doses may hyposensitize EAE to PLP. Ultimately, the co-delivery of the peptides practically eliminated disease as seen with both BPI and SAgA suggesting that co-delivery of both PLP and LABL was necessary for treatment. Although only SAgA showed statistical benefit compared to PLP alone, this was likely due to the lower dose of BPI administered.

Some of the results may be explained by looking at potential immune interactions of SAgAs compared to the results obtained for PLP alone and for BPI treatment. BPI is also composed of the PLP peptide and the LABL peptide with a short linker connecting the two peptides. When antigen presenting cells such as dendritic cells interact with T cells, they form an immunological synapse where the cell surface receptors coalesce into a distinct pattern[32,33]. An initial study with BPI showed the forming of an immunological synapse comprised of different cell surface receptors co-localizing including MHC and ICAM-1. The study with BPI showed that by blocking either of the receptors led to no response and no interaction of the BPI with the cell

receptors, but it was not certain if this was a simultaneous or sequential process. This work also suggests that a majority of the interaction is cell surface mediated providing further evidence for the use of LABL, an ICAM-1 cell surface receptor ligand[34].

Besides the cellular aspect, there is the need to consider transport. Previous work on SAgAs has reported a range of physical sizes based on the HA polymer polydispersity and the amount of peptide conjugated. The physical size has typically ranged from 3-10 nm[4]. This size range can potentially allow different physiological compartments to be accessed as the largest of these, 10 nm, can potentially be excluded from absorption into systemic circulation and passively drain to the lymphatics[35-37]. Finally, active binding to immune cells and transport to secondary lymphoid organs may be the most likely mechanism of SAgA efficacy. Future studies aim to define these potential mechanisms when comparing SAgAs to conventional ASIT.

4.5. Conclusion

Restoring immune tolerance in autoimmune diseases has been an important avenue of research especially with their increasing prevalence. ASIT has been used for decades to desensitize patients to allergens, but similar approaches applied to autoimmune disease have yet to achieve robust clinical success. Traditional allergy desensitization strategies have employed injections, while new approaches have achieved immune tolerance by applying ASIT to mucosal membranes (e.g. Grastek® and Ragwitek®), suggesting the lung may also provide a viable target tissue. SAgA molecules exhibiting grafted antigen and a grafted inhibitor of immune cell adhesion or signally may amplify the effect of traditional ASIT. SAgAs with grafted PLP and LABL delivered into the lungs of EAE mice showed increased efficacy based on clinical scoring, weight gain, and incidence of disease compared to the individual components.

SAgAs may, therefore, provide a more potent ASIT to restore immune tolerance to self-antigens when treating the distinct immunological mechanisms associated with delivery to the lungs.

References

1. Sabatos-Peyton, Catherine, Johan Verhagen, and David C Wraith. “Antigen-specific immunotherapy of autoimmune and allergic diseases.” Current Opinion in Immunology. 22(5):609–615. 2010

2. Holmgren, Jan and Ceecil Czerkinsky. “Mucosal Immunity and Vaccines.” Nature Medicine. 11(4):545-553. 2005

3. Sestak, Joshua, Bradley P Sullivan, Sharadvi Thati, Laura Northrup, Brittany Hartwell, Lorena Antunez, M Laird Forrest, Charlotte M Vines, Teruna J Siahaan, and Cory Berkland. “Codelivery of antigen and an immune cell adhesion inhibitor is necessary for efficacy of soluble antigen arrays in experimental autoimmune encephalomyelitis.” Nature Molecular Therapy — Methods & Clinical Development. 1:1-9. 2014

4. Thati, Sharadvi, Christopher Kuehl, Brittany Hartwell, Joshua Sestak, Teruna Siahaan, M Laird Forrest, and Cory Berkland. “Routes of Administration and Dose Optimization of Soluble Antigen Arrays in Mice with Experimental Autoimmune Encephalomyelitis.” Journal of Pharmaceutical Sciences. 10(2)4:714–721. 2015

5. Aasbjerg, K., V. Backer, G. Lund, J. Holm, N. C. Nielsen, M. Holse, V. R. Wagtmann, and P. A. Wurtzen. “Immunological comparison of allergen immunotherapy tablet treatment and subcutaneous immunotherapy against grass allergy.” Clinical and Experimental Allergy. 44(3):417–428. 2014

6. Thrower, SL, James L, Hall W, Green KM, Arif S, Allen JS, Van-Krinks C, Lozanoska-Ochser B, Marquesini L, Brown S et al. “Proinsulin peptide immunotherapy in type 1 diabetes: report of a first-in-man Phase I safety study.” Clinical and Experimental Immunology. 155(2):156-165. 2009

7. Muller, S, Monneaux F, Schall N, Rashkov RK, Oparanov BA, Wiesel P, Geiger JM, Zimmer R “Spliceosomal peptide P140 for immunotherapy of systemic lupus erythematosus: results of an early phase II clinical trial.” Arthritis and Rheumatology. 58(12):3873-3883. 2008

8. Koffeman EC, Genovese M, Amox D, Keogh E, Santana E, Matteson EL, Kavanaugh A, Molitor JA, Schiff MH, Posever JO et al. “Epitope-specific immunotherapy of rheumatoid arthritis: clinical responsiveness occurs with immune deviation and relies on the expression of a cluster of molecules associated with T cell tolerance in a double-blind, placebo-controlled, pilot phase II trial.” Arthritis and Rheumatology. 60(11):3207-3216. 2009

9. Ye, Yi-Ling, Ya-Hui Chuang, and Bor-Luen Chiang. “Strategies of mucosal immunotherapy for allergic Diseases.” Cellular and Molecular Immunology. 8(6):453–461. 2011

10. Wang, Zhen-hua, Xiao-han Cao, Xiao-gang Du, Hai-bo Feng, Di-Wang, He-Song, Xian-yin Zeng. “Mucosal and systemic immunity in mice after intranasal immunization with recombinant Lactococcus lactis expressing ORF6 of PRRSV.” Cellular Immunology. 287(2):69-73. 2014

11. Mestecky, J., Michael E. Lamm, Jerry R. McGhee, John Bienenstock, Lloyd Mayer and Warren Strober. Mucosal Immunology 3rd edition. Academic Press, San Diego, 2005

12. Mowat, A.M. “Anatomical basis of tolerance and immunity to intestinal antigens.” Nature Reviews Immunology. 3(4):331−341. 2003

13. Kiyono, H. and S Fukuyama. “NALT- versus Peyer's-patch-mediated mucosal immunity.” Nature Reviews Immunology. 4(9):699−710. 2004

14. Ishikawa, H, H Saito, T Suzuki, T Oida, and Y Kanamori. “New gut associated lymphoid tissue "cryptopatches" breed murine intestinal intraepithelial T cell precursors.” Immunologic Research. 20(2):243−250. 1999

15. Guy-Grand, D, O Azogui, S Celli, S Darche, MC Nussenzweig, P Kourilsky, P Vassalli. “Extrathymic T cell lymphopoiesis: ontogeny and contribution to gut intraepithelial lymphocytes in athymic and euthymic mice.” Journal of Experimental Medicine. 197(3):333−341. 2003

16. Bilsborough, J, and JL Viney. “Gastrointestinal dendritic cells play a role in immunity, tolerance, and disease.” Gastroenterology. 127(1):300−309. 2004

17. Guermonprez, Pierre, Jenny Valladeau, Laurence Zitvogel, Clotilde Thery and Sebastian Amigorena. “ Antigen Presentation and T Cell Stimulation by Dendritic Cells.” Annual Review of Immunology. 20:621–667. 2002

18. Théry, Clotilde and Sebastian Amigorena. “The cell biology of antigen presentation in dendritic cells.” Current Opinion in Immunology.13(1):45–51. 2001

19. Heath, William and Francis R. Carbone. “Cross-Presentation, Dendritic Cells, Tolerance, and Immunity.” Annual Review of Immunology. 19:47–64. 2001

20. Itano, Andrea and Marc K Jenkins. “Antigen presentation to naive CD4 T cells in the lymph node.” Nature Immunology Review. 4(8):733-739. 2003

21. Shen, Lianjun and Kenneth L Rock. “Priming of T cells by exogenous antigen cross-presented on MHC class I molecules.” Current Opinion in Immunology. 18(1):85-91. 2006

22. den Haan, Joke and Michael J Bevan. “Antigen presentation to CD8+ T cells: cross-priming in infectious diseases.” Current Opinion in Immunology. 13(4):437–441. 2001

23. Batista, Facundo and Naomi E. Harwood. “The who, how and where of antigen presentation to B cells.” Nature Reviews Immunology. 9(1):15-27. 2009

24. Kuchroo, Vijay, Ana C. Anderson, Hanspeter Waldner, Markus Munder, Estelle Bettelli, and Lindsay B. Nicholson. “T Cell Response in Experimental Autoimmune Encephalomyelitis (EAE): Role of Self and Cross-Reactive Antigens in Shaping, Tuning, and Regulating the Autopathogenic T Cell Repertoire.” Annual Review of Immunology. 20:101–123. 2002

25. Steinman, Lawrence. “A molecular trio in relapse and remission in multiple sclerosis.” Nature Reviews of Immunology. 9(6):440-447. 2009

26. Steinman, Lawrence. “Immunology of Relapse and Remission in Multiple Sclerosis.” Annual Review of Immunology. 32:257–81. 2014

27. Copaxone® Full Prescribing Information – FDA. 2009

28. Rayamajhi, Manira, Elizabeth F. Redente, Tracy V. Condon, Mercedes Gonzalez-Juarrero, David W.H. Riches, and Laurel L. Lenz. “Non-surgical intratracheal instillation of mice with analysis of lungs and lung draining lymph nodes by flow cytometry.” Journal of Visualized Experiments – NIH Public Access. 51:2702. 2012

29. Steinman, Lawrence. “‘Hub-and-spoke’ T cell traffic in autoimmunity.” Nature Medicine. 19(2):139-141. 2013

30. Odoardi, Francesca, Christopher Sie, Kristina Streyl, Vijay K. Ulaganathan, Christian Schlager, Dmitri Lodygin, Klaus Heckelsmiller, Wilfried Nietfeld, Joachim Ellwart, Wolfgang E. F. Klinkert, Claudio Lottaz, Mikhail Nosov, Volker Brinkmann, Rainer Spang, Hans Lehrach, Martin Vingron, Hartmut Wekerle, Cassandra Flugel-Koch, Alexander Flugel. “T cells become licensed in the lung to enter the central nervous system.” Nature. 488(7413):675-682. 2012

31. Ransohoff, Richard. “Licensed in the Lungs.” Nature Research News and Views. 488(7413):595-596. 2012

32. Friedl, Peter, Annemieke Th. den Boer and Matthias Gunzer. “Tuning Immune Responses: Diversity and Adaption of the Immunological Synapse.” Nature Reviews Immunology. 5(7):532-545. 2005

33. van der Merwe, Anton. “Formation and function of the immunological synapse.” Current Opinion in Immunology. 14(3):293–298. 2002

34. Murray, Joseph, Sabah Oney, Jennifer E. Page, Angela Kratochvil-Stava, Yongbo Hu, Irwan T. Makagiansar, John C. Brown, Naoki Kobayashi, and Teruna J. Siahaan. “Suppression of Type 1 Diabetes in NOD Mice by Bifunctional Peptide Inhibitor: Modulation of the Immunological Synapse Formation.” Chemical Biology and Drug Design. 70(3): 227–236. 2007

35. Rao DA, Forrest ML, Alani AW, Kwon GS, Robinson JR. 2010. “Biodegradable PLGA based nanoparticles for sustained regional lymphatic drug delivery.” Journal of Pharmaceutical Science. 99(4):2018–2031. 2010

36. Bagby TR, Cai S, Duan S, Thati S, Aires DJ, Forrest L. “Impact of molecular weight on lymphatic drainage of a biopolymer-based imaging agent.” Pharmaceutics. 4(2):276–295. 2012

37. Khan, Arshad, Jahanzeb Mudassir, Noratiqah Mohtar, Yusrida Darwis. “Advanced drug delivery to the lymphatic system: lipid-based nanoformulations.” International Journal of Nanomedicine. 8(1):2733-2744. 2013

Chapter 5:
Conclusions and Future Directions

5.1. Conclusions and Future Directions

5.1.1. Potential Opportunities for Pulmonary Drug Delivery Challenges

Classical pulmonary therapies have focused on treating local lung diseases such as asthma, COPD, and tuberculosis. Many of these therapies have utilized small molecule formulations and continued development has been employed to increase duration and efficacy of these treatments. There are still many challenges remaining with the treatments available as there is a growing prevalence of respiratory diseases complicated by poor patient compliance for some of the diseases. To improve compliance, longer duration or persistence can be utilized but the strategy to achieve this can take many forms. To increase duration, there is the potential to achieve a faster onset by increased dissolution or by modified release by employing particle engineering or incorporating polymers.

Many of these approaches have focused on local treatment and delivery for lung diseases. The lung may provide a potential systemic delivery platform. The lung interplays with several different organ systems as there is only a minimal physiological barrier between the alveoli and the cardiovascular system. The lungs have recently been identified as an important part of the immune system allowing for the potential to influence the immune response and possibly accessing the lymphatics. By delivering different therapeutics to the lungs, different systemic responses can be achieved along with the potential to modulate the immune system for autoimmune diseases.

5.1.2. Outline of Dissertation Chapters and Conclusions

Chapter 2 focused on particle engineering microparticle NanoClusters, which were comprised of nanoparticle agglomerates, and assessed their characteristics and dissolution profile. Particle engineering has been a drug delivery strategy employed in pulmonary drug

delivery to create increased deposition into the lungs or controlled release therapeutic systems. Depending on the properties of the particles, they have the potential to be cleared by lung clearance mechanisms before they can dissolve to elicit their therapeutic effect as many of the drugs are poorly water soluble. By wet milling these poorly water soluble compounds, nanoparticle agglomerate microparticles were formed called NanoClusters. MFI, DLS, and SEM confirmed that the particles were microparticles mainly between 1-5µm in size that were comprised of nanoparticles of several hundred nanometers. Characterization by DSC and PXRD showed that the NanoClusters remained crystalline even with extended milling time. BET surface area analysis showed an increase in surface area of approximately 8 times for budesonide and 10-15 times for danazol compared to the micronized stock. The increase of surface area modeled by the increased void spaces between nanoparticles in the microparticles was hypothesized as the reason for the enhanced dissolution. NanoClusters had dissolution similar to a nanoparticle suspension even though they were much larger in size. NanoClusters provide a particle engineering strategy that combines the ability to achieve a high delivery fraction into the deep lung with the capability to readily dissolve before being removed by lung clearance mechanisms. NanoClusters achieve these improved properties without the aid of excipients that could disrupt the lung surface.

Chapter 3 focused on the biodistribution and pharmacokinetics of a polymer drug carrier HA. HA, given its potential for different chemistries and availability in a multitude of molecular weights, has been utilized in many different products. Different administration routes have been investigated including intravenous and subcutaneous and the distribution has been determined. HA has been recently employed in nebulized formulations, but the distribution and other properties has yet to be determined. HA of different molecular weights (7, 30, 67, 215, and 741 kDa) was labeled with either a fluorescent or radiolabel then administered to mice via pulmonary instillation. Size characterization was performed with SEC and DLS and was shown to have a well distributed size range even with label conjugation. The fluorescent study as a pilot showed

no difference in distribution throughout the lung lobes based on molecular weight but that the two highest molecular weights had higher levels at 1 hour, which decreased at 8 hours. The radiolabel portion showed the lungs and GI tract had the highest levels of HA, much higher than the heart, spleen, trachea, lymph nodes, liver, kidneys, and bladder. In the lungs, the 7 kDa HA had the lowest levels followed by 30 and 741 kDa, while 67 and 215 kDa had the highest levels throughout the 8 hours studied. Pharmacokinetic analysis agreed with the scintillation data with 7 and 741 kDa having lower values compared to 67 and 215 kDa HA. This work provides a basis for improved persistence of pulmonary therapeutics by employing molecular weight. Polymers are being used more frequently as advanced drug delivery strategies, and by investigating how their physical size and molecular weight determine their distribution after pulmonary administration, polymer based lung therapeutics can have increased efficacy and reduced side effects.

Chapter 4 built on chapter 3 as HA had peptides conjugated and delivered into the lungs to stimulate immune modulation in EAE in mice. EAE, an animal model of MS, is caused when immune cells attack the myelin sheath. Previous treatments to induce tolerance have focused on inducing tolerance to foreign antigens, but here the approach is utilized for eliciting tolerance to self-antigens. Increased efficacy has been shown by delivering SAgAs to the lungs instead of using other administration routes possibly due to the newly determined role of the lungs in the immune system. The different components of SAgA were delivered into the lungs as were controls of PBS and BPI. SAgA showed increased efficacy in terms of clinical scoring, incidence of disease, and weight gain compared to the individual components and negative PBS control and similar to the positive BPI control. Although one component, PLP showed more efficacy than the other individual components, it was still less effective than the combined SAgA. This work further implicates the lung as an immunologically active organ. The lung serves as a delivery target that can block the progression of autoimmune diseases by co-

delivery of antigens that can be potentially harnessed for other autoimmune diseases to increase the efficacy of potential therapeutics.

5.1.3. Future Directions of Dissertation Chapters

Particle engineering can provide a multitude of opportunities in the future. Besides the current methods for increasing deposition and the fraction of dose delivered into the lungs, dissolution can be one way to modulate release. This work has focused on increasing dissolution, but by employing other drugs or the addition of excipients, the dissolution could be extended for a potential long acting/sustained release system. By increasing the duration by modifying dissolution not just in the lungs, but in other body compartments such as joints for rheumatoid arthritis, it is possible to improve patient outcomes. The next step would be testing NanoClusters, both by inhalation (and possible injection) in animals to determine the pharmacokinetic profile. Gaining this information across multiple drug classes besides corticosteroids, could validate NanoClusters as a modified release platform.

Inhaled formulations of HA, or other polymers, allow for increased possibilities in inhalation therapies. Polymers, like particle engineering, can be utilized for modified release profiles and have been to an extent in treating tuberculosis locally in the lung. The addition of polymers as a vehicle could allow for access to different body compartments allowing the lungs to be employed as a potential platform for systemic delivery. The next step in this work would be to radiolabel and track HA in real time. By using a PET scanner to follow the labeled HA in mice, particularly in the same animal over time, would provide a clearer profile of the polymer distribution with enhanced time points and power. Also, labeling other polymers including polysaccharides dextran and chondroitin, as well as classical polymers like polyacrylamide over a smaller size range from 50 to 250 kDa would better determine polymer clearance from the

lung based on molecular weight. The addition of this information could potentially provide the basis for a statistical model for polymer lung pharmacokinetics.

The final work with SAgAs was already a partial future direction of chapter 3 by making the polymer a therapeutic. The next step of this work encompasses multiple avenues. The immune system is composed of many cells types (B cells, T cells, dendritic cells, etc.) and determining which cells are involved would better elucidate the mechanism of SAgA action. A better understanding of action could provide an improve set of criteria for synthesizing the SAgA. Modifying the size of the SAgAs by varying the molecular weight of the HA backbone could provide increased efficacy at a lower dose via pulmonary instillation with further testing. Finally, by labeling the SAgAs, it could be tracked throughout the animals to determine which body compartments and tissues are important for the efficacy, which can lead to further optimization of SAgAs. Real time PET tracking with radiolabeled SAgAs would allow dose schedule optimization, which is important in advancing this therapy into humans and could provide a further understanding for the mechanism of action.

Pulmonary drug delivery has been a fairly limited space in the pharmaceutical world. Most of the current products focus on treating lung diseases with local administration from lung delivery platforms (DPI, pMDI, and nebulizers). There are only a few drug classes primarily corticosteroids, bronchodilators like β2 agonists, and antibiotics that are delivered and only a small fraction of the dose is deposited into the lung to elicit the therapeutic effect. Continued research in pulmonary drug delivery in both academic and industrial settings are necessary to expand this underutilized delivery route that has increased promise both locally as well as systemically to improve patient outcomes. My contributions as stated in this dissertation serve to enhance the sphere of delivery to the lungs by employing multiple techniques (particles and polymers). Further broadening these techniques serve as mechanisms to increase onset time by the enhanced dissolution of NanoClusters, enhance deposition into the lungs, increase

persistence and decrease accessing unwanted organs by employing the proper molecular weight of the polymer therapeutic, and employing immune modulation via SAgAs, which all further broaden how the lung can be employed as an delivery target by enhanced therapeutics.